Tomas Bata University in Zlín
Faculty of Technology

Doctoral Thesis

Vývoj a charakterizace multimodálního hydrogelu kyseliny hyaluronové s řízeným uvolňováním protizánětlivých léčiv k léčbě roztroušené sklerózy

Development and Evaluation of a Multi-Modal Hyaluronic Acid Hydrogel for Anti-Inflammatory Drug Delivery for Multiple Sclerosis Therapy

Author: **Tutut Ummul Habibah, M.Sc**

Degree programme: Chemistry and Materials Technology (P2808)

Degree course: Technology of Macromolecular Substance (2808V006)

Supervisor: doc. RNDr. Marek Ingr, Ph.D.
PharmDr. Martin Pravda, Ph.D. (Contipro)

Zlín, June 2025

Published by **Tomas Bata University in Zlín** in the Edition **Doctoral Thesis.**
The publication was issued in the year 2025

Klíčová slova*: Řízené uvolňování léčiv, hyaluronová kyselina, chondroitin sulfát, hydrogely, zánět, minocyklin, roztroušená skleróza, komplexy polyelektrolytů, syntetický preimplantační faktor*

Key words: *Controlled Drug Delivery Systems, Hyaluronic acid, Chondroitin Sulphate, Hydrogels, Inflammatory, Minocycline, Multiple Sclerosis, Polyelectrolyte Complexes, Synthetic Pre-Implantation Factor*

Full text of the doctoral thesis is available in the Library of TBU in Zlín.

ACKNOWLEDGEMENTS

The completion of this doctoral dissertation marks the culmination of an intellectually demanding yet profoundly rewarding journey, providing a unique fusion of academic rigor and industrial exposure made possible by the European Union's Horizon 2020 under the Marie Sklodowska-Curie grant (No 813263) for PMSMatTrain consortium. This work would not exist without the unwavering support, expertise, and encouragement of countless individuals and institutions.

To my academic supervisor, doc. RNDr. Marek Ingr, Ph.D: My deepest gratitude for your exceptional academic guidance, intellectual challenge, and steadfast belief in this project. Your insightful critiques, rigorous standards, and constant encouragement were indispensable in navigating complex theoretical frameworks and ensuring the scientific integrity of this research. Thank you for fostering this industrial partnership and fostering an environment where applied science meets fundamental discovery.

To Contipro, my industrial supervisor, and colleagues: I extend my immense appreciation to Contipro for providing not only essential resources and cutting-edge facilities but also a vibrant, application-driven environment that defined this industrial-based doctorate. To my primary industrial supervisor, PharmDr. Martin Pravda, Ph.D., and the entire regenerative medicine/hydrogel research group, thank you so much for welcoming me into your dynamic team. Your expertise in hydrogel applications, practical insight, and collaborative spirit were instrumental in shaping this work. I am especially grateful for the freedom to explore, the patience shown during iterative development, and the valuable insights gained from daily interactions centered on real-world application. Special thanks to the wonderful Veronika Hkrlova, my heartfelt gratitude for making each day in the lab smoother and brighter. Your kindness was a constant support, and your legendary cakes not only sweetened our breaks but also brightened my entire journey at Contipro. To my colleagues who became dear friends, Erik Jirasek and Eva Papackova, you truly are the best. Your endless patience, generous support, wonderful friendship, shared cryptic jokes, and delicious food brought joy to my days and made life in Ustí nad Orlicí not only easier, but genuinely happier and filled with memories I will always treasure.

To my cherished circle - Raches Sudirman, Danira Pattinasarany, Nella Sari, Shaviga Usman, drg. Rasda Diana, Dr. Abdullah ElGamal, Dr. Malgorzata Dabrowska, and Dr. Bhavya Ojha - thank you for walking every step of this path with me. Your boundless love, patient listening, and constant encouragement were the bedrock throughout this process, especially during the long nights and moments when focus faltered. Celebrating every tiny triumph with your genuine

smiles made the climb so much brighter and easier. And to the amazing Uni Astrid Juklickova, you have a rare kind of magic - your soul-warming Indonesian feasts and nurturing presence, conjured far from home in the midst of the Czech winter, were more than just meals; they were edible hugs that restored my spirit and sustained me through countless marathon study session.

My deepest thanks go to my wonderful Mom and Dad. Those lively dinner-table debates, and your own bright, curious minds first ignited my love for learning when I was little. Your steady, loving encouragement and unwavering belief in me did not just support my studies, they became the quiet strength behind every step I have taken, right through this PhD. Thank you for being my first and forever teachers.

Finally, to all who contributed directly or indirectly. Thank you for being part of this transformative chapter. I carry forward not only set of experiences but also profound gratitude for the community that made it possible.

ABSTRACT

Current treatments for multiple sclerosis (MS) are hindered by adherence challenges linked to frequent systemic dosing regimens, which demand active patient participation and often lead to suboptimal therapeutic outcomes. Conventional disease-modifying therapies (DMTs) administered orally or via injection, struggle to balance efficacy with patient quality of life, compounded by risks of systemic toxicity and rapid drug clearance. Recent surveys underscore a growing demand for implantable drug delivery systems (DDS) that minimize dosing frequency, reduce patient burden, and enhance long-term compliance.

This dissertation addresses these unmet needs by developing an injectable hydrogel platform based on aldehyde-functionalized hyaluronic acid (HAOX) and chondroitin sulfate (CSOX), designed for localized, sustained delivery of anti-inflammatory therapeutics. Central to this innovation is the immobilization of polyelectrolyte complexes (PECs) within the covalently crosslinked hydrogel matrix. Unlike conventional nanoparticle-based DDS, which rely on freely diffusing carriers prone to burst release and instability, immobilized PECs exploit electrostatic interactions between therapeutic agents (minocycline, MN; Fluorescein isothiocyanate-modified synthetic Preimplantation Factor, FITC-SPIF) and the anionic sulfate groups of CSOX. This strategy enhances drug retention, reduces manufacturing complexity, and eliminates the need for costly encapsulation processes.

For MN, a repurposed tetracycline antibiotic, PECs formed with Ca^{2+} and gelatin achieved sustained release over 288 hours with an 88% reduction in burst release compared to unbound formulations. Similarly, FITC-SPIF, an immunomodulatory peptide, exhibited prolonged delivery kinetics proportional to CSOX concentration, minimizing premature leakage. The hydrogel's enzymatic resistance, injectability (<185 kPa extrusion force, Dynamic Glide Force < 40 N), and mechanical adaptability (storage modulus: 125–1,083 Pa) ensure structural stability under physiological conditions, addressing key limitations of prior DDS.

In vitro validation confirmed therapeutic bioactivity: released MN suppressed pro-inflammatory IL-6 secretion by 56% in human monocytes, while FITC-SPIF promoted TGF-β expression in macrophages, indicative of anti-inflammatory polarization. By integrating immobilized PECs with a tuneable HAOX-CSOX matrix, this platform resolves the historical trade-offs between controlled release, scalability, and clinical practicality.

This work advances MS therapy by offering a patient-centric solution that aligns with preferences for minimally invasive and long-acting treatments. The

HAOX-CSOX hydrogel's cost-effective design, coupled with its capacity to deliver diverse therapeutics, positions it as an alternative tool for managing chronic neuroinflammatory diseases, bridging the gap between material innovation and patient-centred care.

ABSTRAKT

Současné terapie roztroušené sklerózy (RS) jsou limitovány problémy s dodržováním léčebných režimů založených na častém dávkování léčiv, které vyžadují aktivní účast pacientů, což vede ke snížené terapeutické účinnosti. Terapie modifikující onemocnění (DMTs), podávaná perorálně nebo injekčně, nedokáže účinně sladit klinický přínos s kvalitou života pacientů, a to zejména v důsledku systémové toxicity a rychlé eliminace léčiv. Nedávné průzkumy zdůrazňují rostoucí poptávku po implantovatelných systémech pro řízené uvolňování léčiv (DDS), které minimalizují frekvenci aplikace, snižují zátěž pacientů a zlepšují dlouhodobou adherenci.

Tato disertační práce řeší tyto nedostatky vývojem injekčně aplikovatelného hydrogelového systému na bázi aldehydem modifikované hyaluronové kyseliny (HAOX) a chondroitin sulfátu (CSOX), určeného pro lokalizované a prodloužené uvolňování protizánětlivých léčiv. Klíčovou inovací je imobilizace polyelektrolytových komplexů (PECs) v kovalentně zesíťované hydrogelové matrici. Na rozdíl od konvenčních DDS založených na nanočásticích, které využívají volně difundující nosiče náchylné k prvotnímu prudkému uvolnění (burst effect) a nestabilitě, imobilizované PECs využívají elektrostatické interakce mezi terapeutiky (minocyklin, MN; fluoresceinisothiokyanátem modifikovaný syntetický preimplantační faktor, FITC-SPIF) a aniontovými sulfátovými skupinami CSOX. Tato strategie zvyšuje retenci léčiv, snižuje výrobní náročnost a eliminuje potřebu nákladných enkapsulačních procesů.

Pro MN, repurposed antibiotikum ze skupiny tetracyklinů, dosáhly PECs s Ca^{2+} a želatinou prodlouženého uvolňování po dobu 288 hodin s 88% redukcí prudkého uvolňování efektu ve srovnání s neimobilizovanými formami. Podobně FITC-SPIF, imunomodulační peptid, vykazoval kinetiku uvolňování úměrnou koncentraci CSOX, což minimalizovalo předčasnou ztrátu účinné látky. Enzymatická odolnost hydrogelu, injekční aplikovatelnost (<185 kPa vytlačovací síla, dynamická kluzná síla <40 N) a mechanická adaptabilita (elastická složka dynamického modulu ve smyku G‘: 125–1 083 Pa) zajišťují strukturální stabilitu za fyziologických podmínek, čímž řeší hlavní omezení předchozích DDS.

In vitro testy potvrdily biologickou aktivitu uvolňovaných léčiv a kompatibilitu systému HAOX-CSOX: uvolněný MN potlačil sekreci prozánětlivého IL-6 v lidských monocytech o 56 %, zatímco FITC-SPIF

indukoval expresi TGF-β v makrofázích, což indikuje protizánětlivou polarizaci. Integrací imobilizovaných PECs do matrice HAOX-CSOX tato platforma překonává tradiční kompromisy mezi řízeným uvolňováním, škálovatelností a klinickou praktičností.

Práce přináší inovativní řešení pro léčbu RS, které odpovídá preferencím pacientů pro minimálně invazivní a dlouhodobě působící terapie. Nákladově efektivní design hydrogelu HAOX-CSOX spolu s jeho schopností dodávat různé terapeutické látky jej předurčuje jako alternativní nástroj pro léčbu chronických neurozánětlivých onemocnění, propojující materiálový výzkum s potřebami pacientů.

Table of Contents

ACKNOWLEDGEMENTS 3

ABSTRACT 5

ABSTRAKT 7

1. INTRODUCTION AND CURRENT STATE OF THE ART OF THE ISSUE DEALT WITH 12

1.1 INTRODUCTION 12
1.2 CURRENT STATE OF THE ART 13
1.2.1 PATHOETIOLOGY OF MULTIPLE SCLEROSIS 13
1.2.2 SYSTEMIC TOXICITY OF CONVENTIONAL MS TREATMENT: A HIDDEN COST OF CONVENTIONAL DELIVERY 16
1.2.3 SOCIOECONOMIC IMPLICATION OF CONVENTIONAL MULTIPLE SCLEROSIS TREATMENT AND POTENTIAL TREATMENT STRATEGY 18
1.2.4 MINOCYCLINE: FROM ANTIBIOTIC TO NEUROPROTECTANT 20
1.2.5 FROM GESTATION TO NEUROPROTECTION: REPURPOSING SYNTHETIC PREIMPLANTATION FACTOR FOR IMMUNOMODULATION IN MULTIPLE SCLEROSIS 22
1.2.6 HYDROGELS: PROMISES AND PITFALLS 23
1.2.7 POLYELECTROLYTE COMPLEXES (PEC): SCALABILITY VERSUS STABILITY 26
1.2.8 TOWARD A PARADIGM SHIFT: THE HAOX-CSOX HYDROGEL PLATFORM 29

2. AIM OF THE THESES 33

3. EXPERIMENTAL SECTIONS 35

3.1 MATERIALS AND METHODS FOR IN SITU FORMED HYALURONIC ACID HYDROGEL LOADED WITH POLYELECTROLYTE COMPLEX FOR MINOCYCLINE CONTROL RELEASE 35
3.1.1 MATERIALS 35
3.1.2 CHEMICAL MODIFICATION OF CHONDROITIN SULFATE VIA ALDEHYDE FUNCTIONALIZATION 35
3.1.3 HYDROGEL FORMULATIONS 37
3.1.4 PREPARATION OF HAOX-BASED HYDROGEL AND CSOX-BASED HYDROGEL 40
3.1.5 PREPARATION OF HAOX HYDROGEL INCORPORATING UNBOUND PEC (HAOX_PECS) 40
3.1.6 PREPARATION OF HAOX CONTAINING IMMOBILIZED PEC (HAOX_PECOX) 41
3.1.7 GELATION TIME 42
3.1.8 SWELLING RATIO 42
3.1.9 DRUG RELEASE EXPERIMENT 43
3.1.10 MESH SIZE, **Mc**, AND CROSSLINKING DENSITY 44
3.1.11 INJECTABILITY 47
3.1.12 VISCOELASTIC PROPERTIES OF THE DRUG DELIVERY SYSTEM 47

3.1.13 WHOLE BLOOD MONOCYTES ACTIVATION TEST (WB-MAT) 48
3.2 MATERIALS AND METHOD FOR IN SITU FORMING HYDROGEL FROM ALDEHYDE-MODIFIED HYALURONIC ACID AND ALDEHYDE-MODIFIED CHONDROITIN SULFATE FOR SYNTHETIC PREIMPLANTATION FACTOR DELIVERY 49
3.2.1 MATERIALS 49
3.2.2 HYDROGEL FORMULATIONS 50
3.2.3 PREPARATION OF HAOX-BASED HYDROGEL (HAOX_15, HAOX_17) 51
3.2.4 HYDROGEL PREPARATION FOR HAOX CONTAINING IMMOBILIZED CSOX 52
3.2.5 GELATION TIME 52
3.2.6 SWELLING RATIO 52
3.2.7 DRUG RELEASE EXPERIMENT 52
3.2.8 MESH SIZE, **Mc**, AND CROSS-LINKING DENSITY 53
3.2.9 INJECTABILITY 53
3.2.10 VISCOELASTIC PROPERTIES OF THE DRUG DELIVERY SYSTEM 53
3.2.11 FITC-SPIF-INDUCED MACROPHAGE POLARIZATION: AN IN VITRO BIOACTIVITY STUDY 53
3.3 DATA PROCESSING AND STATISTICAL APPROACHES 54

4. RESULT AND DISCUSSION 55

4.1 IN SITU INJECTABLE HYALURONIC ACID HYDROGEL LOADED WITH POLYELECTROLYTE COMPLEX FOR MINOCYCLINE CONTROL RELEASE 55
4.1.1 SYNTHESIS OF ALDEHYDE-MODIFIED CHONDROITIN SULFATE (CSOX) 57
4.1.2 INTERDEPENDENT PHYSICOMECHANICAL PROPERTIES: GELATION DURATION AND STRUCTURAL RESILIENCE FOR INJECTABLE HAOX-BASED DDS 58
4.1.3 MINOCYCLINE RELEASE PROFILES AND THE MECHANISM IN INJECTABLE HAOX-BASED DRUG DELIVERY SYSTEM 62
4.1.4 INTERPLAY BETWEEN CROSSLINKING DENSITY, SWELLING BEHAVIOUR, AND SUSTAINED MN RELEASE IN HYDROGEL-BASED DELIVERY SYSTEM 66
4.1.5 WHOLE BLOOD MONOCYTES ACTIVATION TEST (WB-MAT) FOR MINOCYCLINE BIOACTIVITY ANALYSIS 70
4.2 IN SITU FORMING HYDROGEL FROM ALDEHYDE-MODIFIED HYALURONIC ACID AND ALDEHYDE-MODIFIED CHONDROITIN SULFATE FOR SYNTHETIC PREIMPLANTATION FACTOR DELIVERY 72
4.2.1 GELATION TIME OF FITC-SPIF-LOADED HAOX-CSOX HYDROGELS: BALANCING PH-DEPENDENT CROSSLINKING FOR CLINICAL TRANSLATION 73
4.2.2 RELEASE STUDY OF FITC-SPIF, T50 %, AND KORSMEYER-PEPPAS PARAMETERS 75
4.2.3 SWELLING PROFILE AND CROSSLINKING DENSITY OF THE DRUG DELIVERY SYSTEM 78
4.2.4 DRUG DELIVERY SYSTEM DEVELOPMENT OF HACOX_37: INFLUENCE OF FITC-SPIF LOADING LEVELS ON CDR, SWELLING BEHAVIOUR, AND KORSMEYER-PEPPAS PARAMETERS 80
4.2.5 DEVELOPMENT OF HACOX_37: INFLUENCE OF CSOX CONCENTRATION ON CDR, SWELLING BEHAVIOUR, AND KORSMEYER-PEPPAS PARAMETERS 83
4.2.6 MOLECULAR WEIGHT BETWEEN CROSSLINKS ($\boldsymbol{Mc}$) AND MESH SIZE (Ξ) AND THEIR ROLES IN RELEASE KINETICS OF FITC-SPIF-LOADED DRUG DELIVERY SYSTEM 86
4.2.7 VISCOELASTIC PROPERTIES AND INJECTABILITY OF THE DRUG DELIVERY SYSTEM 88
4.2.8 FITC-SPIF-INDUCED MACROPHAGE POLARIZATION: AN IN VITRO BIOACTIVITY STUDY 90

5. CONCLUSIONS 94

REFERENCES **97**

LIST OF FIGURES **112**

LIST OF TABLES **117**

LIST OF ABBREVIATIONS **118**

CURRICULUM VITAE **121**

LIST OF PUBLICATION **122**

OVERVIEW OF OTHER ACTIVITIES **122**

1. INTRODUCTION AND CURRENT STATE OF THE ART OF THE ISSUE DEALT WITH

1.1 Introduction

Multiple sclerosis (MS) is an autoimmune-driven neuroinflammation and demyelination of central nervous system (CNS) contribute to escalating motor, sensory, and cognitive deficits. Current treatment strategies primarily involve Disease-Modifying Therapies (DMTs), which have proven effective in slowing disease progression and reducing relapse rates. Recent technology in medicine, such as autoinjectors and oromucosal sprays, have improved the ease of DMT administration by enabling self-administration and reducing the need for frequent clinical visits. However, these innovations come with significant limitations, including high costs and a heavy reliance on patient active involvement. For instance, autoinjectors often require daily replenishment, while oromucosal sprays may necessitate daily dosing. These application scheme creates burdensome regimens that can lead to non-compliance, compromising therapeutic efficacy and underscoring a critical gap in current DMT delivery systems. Addressing these challenges is essential for improving treatment adherence and clinical outcomes, particularly for patients with cognitive or physical impairments.

Recent surveys report a growing preference among patients for implantable drug delivery systems (DDS) that provide sustained DMTs release with minimal patient intervention. Such systems have the potential to enhance compliance, therapeutic effectiveness, and overall quality of life. In response to these unmet needs, this study proposes an injectable DDS based on an aldehyde-modified hyaluronic acid hydrogel (HAOX) integrated with immobilized polyelectrolyte complexes (PEC) composed of aldehyde-modified chondroitin sulfate (CSOX). While hydrogel-based DDS face challenges such as burst release and long-term stability, the incorporation of PEC within the HAOX structure allows for precise tuning of release kinetics, ensuring sustained and controlled delivery of therapeutic agents. Additionally, the HAOX hydrogel provides structural integrity, enabling the DDS to be injected and localized at the target site. This localization enhances drug concentration while minimizing systemic toxicity, addressing a key limitation of conventional delivery methods. The proposed system is designed to deliver two therapeutic agents: Minocycline (MN), an affordable tetracycline antibiotic with neuroprotective properties, and Fluorescein isothiocyanate–modified Synthetic Preimplantation Factor (FITC-SPIF), a

peptide with potent immunomodulatory effects. Together, this approach offers a patient-centric solution that simplifies drug administration, reduces cost, dosing frequency, and eliminates the dependency on active patient involvement.

The research is structured into two distinct phases, each dedicated to developing the DDS for a specific therapeutic agent. This approach enables a detailed investigation of the HAOX-CSOX hydrogel's structural properties and their influence on release performance, offering key insights into the mechanisms controlling MN and FITC-SPIF delivery. Unravelling these mechanisms is critical to enhance the system's therapeutic efficacy and ensuring its clinical applicability.

The implications of this research are substantial. By addressing the inherent limitations of current DMT delivery methods, the proposed DDS holds the promise to optimize MS management. It not only simplifies drug administration and reduces the burden on patients but also offers a modular system with tuneable properties for various biological parameters. Ultimately, this study aspires for a future in which patients benefit from more effective, patient-centred therapeutic strategies, thereby enhancing their quality of life and overall disease management. In an era where innovative and accessible treatment options are critically needed, this dissertation represents a step forward in the field of chronic disease management through advanced DDS.

1.2 Current state of the art

1.2.1 Pathoetiology of multiple sclerosis

MS is as a progressive inflammatory degenerative disease of the CNS influenced by multiple interdependent pathobiological axes rather than a distinctive category (Fig. 1.1). The inflammation simultaneously initiates the dysregulation of cytokines like interleukin-6 (IL-6), transforming growth factor-beta (TGF-β), tumour necrosis factor-alpha (TNF-α), and interferon-gamma (IFN-γ). These cytokines disrupt the blood-brain barrier (BBB) to aid the migration of T and B cells while promoting macrophage polarization into pro-inflammatory phenotype. This interplay promotes reactions that attack the myelin sheath to form lesions (sclera) [1,2].

Currently there is no single therapy that effectively targets the underlying cause of MS due to the overlapping symptoms and disease heterogeneity. Consequently, patients are prescribed complex DMTs as a multimodal treatment to halt the disease progression by reducing the frequency of relapses and the production of pro-inflammatory cytokines. U.S. Food and Drug Administration (FDA) have

approved more than 20 DMTs for MS, with each therapy offering a varying duration of treatment and route of administration (Table 1.1). For example, several DMTs require daily administration, such as oral medications like Teriflunomide. Meanwhile, Glatiramer acetate should be injected daily or three times a week. Cladribine has a longer treatment course lasting 4-5 days over two weeks. On the other hand, infusion therapies vary significantly; Ocrelizumab is administered every six months, while Natalizumab and Mitoxantrone are given more frequently every four weeks [3].

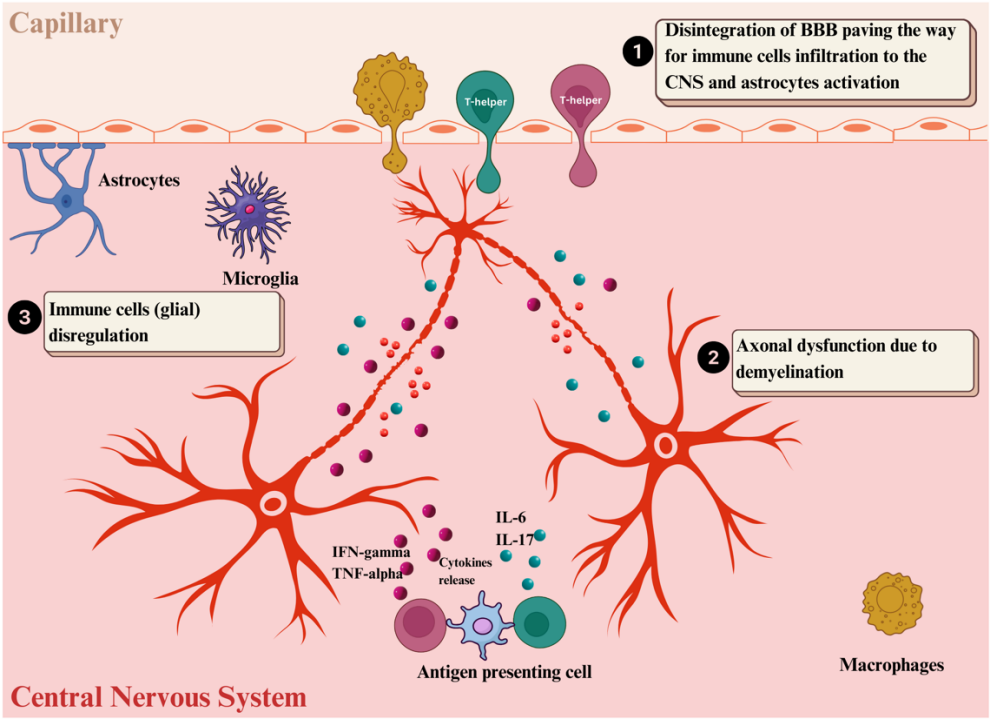

Fig. 1.1: Interdependent pathobiological axes of MS.

While the DMT proven to reduce the relapse frequency by 30-50%, their efficacy is often limited by treatment regimens that demand continues healthcare visits or frequent self-administration [1]. Adherence rates are significantly influenced by patient comfort levels with different routes of administration. For instance, adherence reduced from 69.4% for weekly intramuscular injection to 58.4% for subcutaneous administrations given three times per week [4,5]. The recognized efficacy of injectable DMTs may be compromised by physiological burdens such as needle anxiety, injection site reaction (including pain and redness), and flu-like symptoms such as fever, fatigue, and muscle sores. Although oral therapy offers greater convenience, patients may find it challenging to maintain the frequent dosing schedule required for some DMTs [5]. Patient-prescribed infusion treatments are associated with higher treatment satisfaction due to their efficacy and less frequent administration. However, this treatment

requires hospital visits, which can be inconvenient for some patients. Furthermore, the decrease in compliance is worsened by physiological burdens combined with cognitive and motor impairment, which enhance the challenge for patients to comply with their treatment plans.

Table 1.1 FDA Approved Disease Modifying Therapies [3,6–8].

DMTs	**Route of administration**	**Approved indication**	**Mechanism of action**
Interferon beta 1a	Injection	Clinically Isolated Syndrome (CIS); Relapsing Remitting MS (RRMS)	Immunomodulatory
Interferon beta 1b	Injection	CIS; RRMS	Immunomodulatory
PEGylated Interferon beta 1a	Injection	CIS; RRMS	Immunomodulatory
Glatiramer acetate	Injection / Infusion	RRMS; Active Secondary Progressive MS (SPMS)	Immunomodulatory
Teriflunomide	Oral	RRMS	Suppression of cell differentiation
Fingolimod	Oral	RRMS	Lymphocyte retention and migration arrest
Dimethyl fumarate	Oral	CIS; RRMS; Active SPMS	Immunomodulatory
Diroximel fumarate	Oral	CIS; RRMS; Active SPMS	Immunomodulatory
Monomethyl fumarate	Oral	CIS; RRMS; Active SPMS	Immunomodulatory
Cladribine	Oral	RRMS, SPMS	Immunosuppressive; Impairment of DNA synthesis for T-cell and B-cell
Ozanimod	Oral	RRMS	Immunosuppressive; Bind S1P receptor

Siponimod	Oral	RRMS, SPMS	Immunomodulatory; Bind S1P receptor
Alemtuzumab	Infusion	RRMS	Depletion of CD25+, T-cell, B-cell, monocytes and macrophages
Mitoxantrone	Infusion	RRMS	Cell division and migration arrest
Ofatumab	Infusion	CIS; RRMS; Active SPMS	Immunosuppressive
Ocrelizumab	Infusion	CIS; RRMS; Active SPMS; Primary Progressive MS (PPMS)	Depletion of CD20+ cells
Natalizumab	Infusion	CIS; RRMS; Active SPMS	Inhibit immune cells trafficking to CNS by blocking a-4, ß -1, and ß -7 integrins

The complexity of current modes of administration, each with a different mechanism of action, side effects, and efficacy, can potentially overwhelm patients and lead to frustration. Recent surveys focusing on the relationship between adherence and quality of life reveal that 72% of patients opt for implantable DDS to eliminate dosing burdens, underscoring the urgency for innovations aligning with patient-centric care that considers individual patient needs and preferences [9–11]. Despite well-documented adherence challenges that remains a central issue in MS management, conventional delivery systems impose potential systemic side effects that can compound the problems and ultimately diminish the effectiveness of treatment.

1.2.2 Systemic toxicity of conventional MS treatment: a hidden cost of conventional delivery

MS therapy depends on DMT for disease management with goals to regulate immune responses and decrease exacerbated neuronal damage. However, the absence of harmonized protocols for the administration route, combined with the existing variability in the approved DMTs and multifaceted symptoms, can lead to inconsistent treatment outcomes and make it difficult to compare the efficacy between treatment plans [12]. For example, systemic drug administrations are effective for targeting peripheral therapeutic areas but often associated with a

higher risk of adverse effects [13]. The non-selective nature of systemic route distributes the DMT to both diseased and healthy tissue (Fig. 1.2). Consequently, in the case of MS, the efficacy may be limited when the intended targets are sequestered by the BBB.

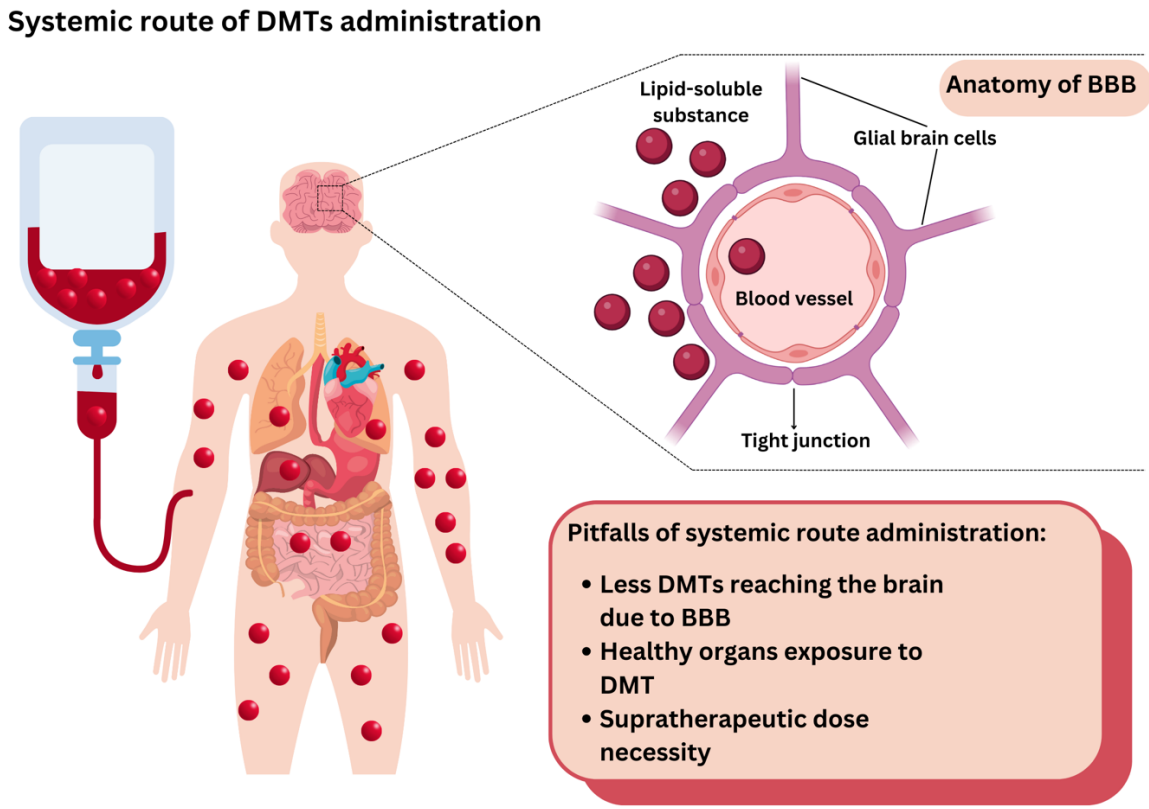

Fig. 1.2: Risk of systemic administration route of the Disease Modifying Therapies.

Although oral and injectable DMTs can be effective in treating MS, their ability to traverse BBB often requires supratherapeutic doses and linked with the propensity to induce systemic toxicity [13]. For example, 60% patients prescribed with weekly or three times per week of intramuscular injection (Avonex®) of Interferon Beta-1 or subcutaneous injections (Rebif®) experienced persistent nausea. This adverse effect comes as systemic cytokines activation with 10 - 15% has reported for hepatotoxicity [14,15]. Such broad immunomodulatory mechanism induces the disruption for both pathological and homeostatic immune cascades, which requires another administration of proinflammatory agent and routine biochemical monitoring.

Similarly, orally taken dimethyl fumarate aggravates the safety concern of inefficiency delivery routes. Although dimethyl fumarate decreases the annual relapse rate by approximately 50%, its bioactive metabolite (monomethyl fumarate) achieves only 1 µg mL^{-1} in the cerebrospinal fluid (CSF). This

concentration deemed far low from the thresholds to induce neuroprotective mechanism. This pharmacokinetic inefficiency is compensated by high oral doses of 240 mg twice daily, which simultaneously induce lymphopenia observed in 15–20% of patients [14,16].

On the other hand, infusion route of ocrelizumab is considered as an alternative to balance between therapeutic efficacy and systemic risk. Efficacy of ocrelizumab entails the slows of disability progression up to 40%, with its mechanism of action rendering the depletion of CD20-positive B cells [14]. However, this cell-suppressive cascade elevates the susceptibility for upper respiratory tract infection which is manageable with the co-administration of antihistamines and corticosteroids [17].

Ultimately, the adverse effects attributed to conventional MS treatments represent a significant yet often overlooked expenditures. These expenditures not only encompass the cost of DMTs but also include the resources required to manage potential complications, such as axillary diagnostics and infusion-related hypersensitivity reactions, which affect approximately 25% of people receiving such treatments [18,19]. Beyond the direct health consequences, these toxicities give rise to a series of socioeconomic burdens, affecting patient access, adherence, and overall quality of life.

1.2.3 Socioeconomic implication of conventional multiple sclerosis treatment and potential treatment strategy

The significant economic strain of MS is substantially driven by the increasing expenditure of DMTs. The annual expense for DMTs increased dramatically between 2011 and 2015, from $26,772 to $43,606. This continued escalation imposes a heavy financial burden on healthcare system and magnifies the challenges for patients in accessing necessary treatments [20]. In addition to these expenditures, which are compounded by the need of regular clinical monitoring, the financial burden of living with MS extends beyond direct medical costs (Fig. 1.3). Many patients must compensate for lost income and expenses related to caregiving. Ultimately, these financial strains contribute to socioeconomic disparities in access to efficacious treatment.

Beyond its financial burden, MS exerts a considerable psychosocial consequence, ranking as the predominant source of acquired disability in young adult populations. With a 3:1 female-to-male prevalence ratio, MS disproportionately affects women during their productive years, resulting in

workforce attrition and a severe decline in living standards [21]. The motor and cognitive impairments associated with MS often lead to early retirement, causing a reduction in earning potential and increased social isolation, which can aggravate mental health issues. Moreover, the chronic and unpredictable characteristics of the disease places considerable emotional and financial pressure on families, underscoring the urgent need for comprehensive support systems and policies to address these complex challenges.

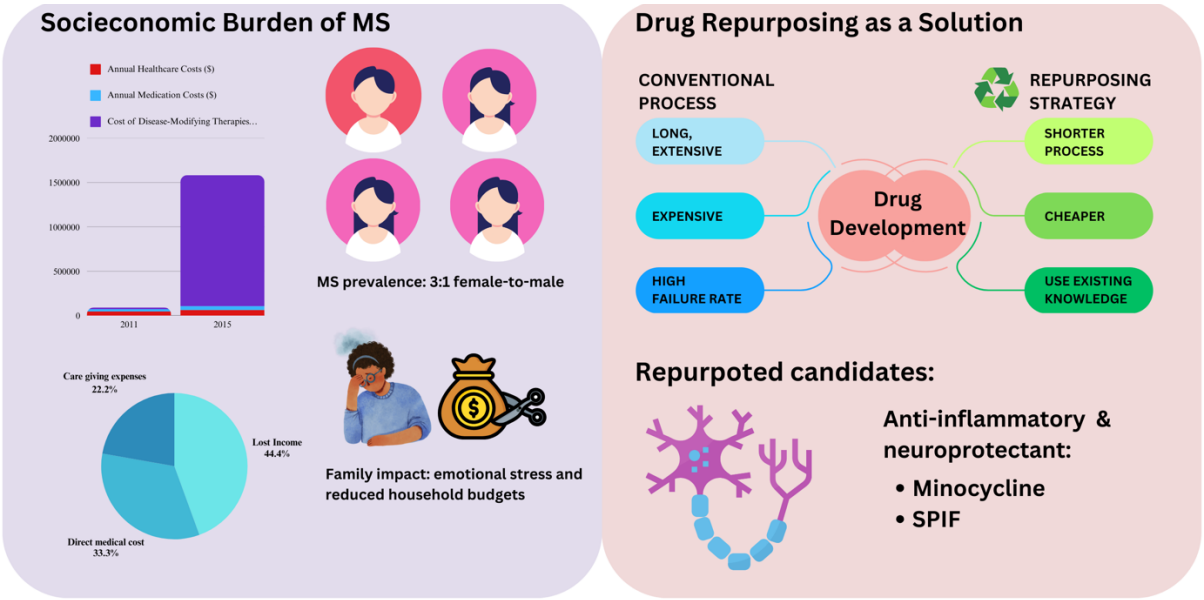

Fig. 1.3: Socioeconomic burden of MS and drug repurposing as one of feasible strategies to overcome the impacts.

One potential strategy to circumvent the socioeconomic burdens of MS is drug repurposing, which involves using existing medication for new therapeutic purposes. Given the urgent need for effective treatments, drug repurposing provides a compelling alternative to traditional drug development, which is often extensive, resource-intensive, and unpredictable, with a high failure rate and substantial financial risks. This approach leverages existing knowledges of approved and investigational drugs, their established physical, chemical, and pharmacological properties, to accelerate the development process. By bypassing early-stage testing, drug repurposing potentially reduces both the time and cost attributed to pharmaceutical research [22].

Drug repurposing strategy has been particularly valuable in conditions like MS, where inflammation is a key pathological feature. As inflammation becomes the hallmark of MS, anti-inflammatory therapies developed for other diseases are also relevant to MS symptoms. Candidates like minocycline (MN) [23] and Synthetic Preimplantation Factor (SPIF) [24] exemplify the potential benefits of this

approach. These examples are capable of targeting both neuroprotection and immunomodulation, underscore the potential of this approach to circumvent the limitations of traditional drug development. Their repurpose as promising candidates underscores the rigorous process by which existing drugs are evaluated for their potential to address the multifaceted challenges of MS.

1.2.4 Minocycline: from antibiotic to neuroprotectant

MN, a second-generation semi-synthetic tetracycline, presents a compelling option for repurposing in MS treatment. This drug potentially accelerates its regulatory pathway for new applications due to its established safety profile and already approved for other indications [23]. The generic availability of MN reduces its cost to $0.50/day, compared to $6,000/month for monoclonal antibodies, making it a cost-effective option for MS treatment [25]. Combined with its wide availability, this positions MN as an attractive candidate for healthcare systems seeking effective and economically viable therapies [25,26]. However, while MN's antimicrobial activity is well-documented, its dual-action potential in MS depends on two mechanisms: microglial depletion and the stabilization of BBB [27,28].

MN demonstrates promise for treating MS due to its ability to suppress neuroinflammation. These immune-modulating effects work by inhibiting microglial activation, leading to reduced pro-inflammatory cytokine production (IL-6, TNF-α) and promoting a Th1-to-Th2 immune shift via decreased IFN-γ production in CD4+ T cells [27,29–31]. MN also contributes to the cellular integrity and permeability BBB repair by maintaining proteins like ZO-1, Occludin, and β-catenin [27,28]. These dual mechanisms align with MS pathophysiology, offering a multitargeted approach distinct from conventional immunotherapies.

A critical gap in MN' repurposing lies in its narrow therapeutic window. Neuroprotection in preclinical models requires high doses (50 mg/kg/day in rodents; 200 mg/day orally in humans) and such concentration are associated with systemic toxicity, including hepatotoxicity [32] and mortality in animal studies [33]. Human trials in MS and stroke show clinical benefits at 100-200 mg/day, yet the concentration found in the CSF remain suboptimal (0.5 µg/mL) compared to neuroprotective thresholds (30–50 µg/mL) [34,35]. The disparity between dosing concentration and CNS bioavailability underscores a translational challenge: achieving efficacious CNS levels without systemic risk.

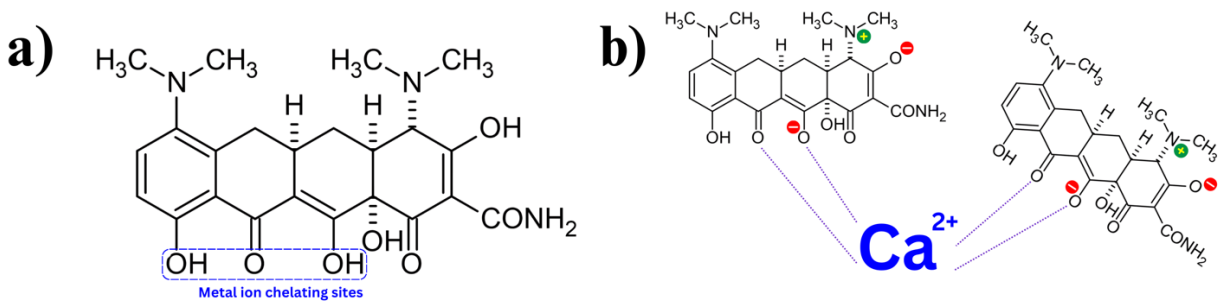

Fig. 1.4: Minocycline structure: a) metal ion chelation sites, b) chelation structure of MN with Calcium [36,37].

MN physicochemical characteristics present a complex challenge for its delivery. Its rigid tetracyclic structure, zwitterionic nature (isoelectric point = 6.4), and pH-dependent solubility hinder BBB penetration and tissue targeting [37]. Evenmore, MN's instability in acidic environments and chelation with dietary cations (Ca^{2+}, Fe^{3+}) decrease oral bioavailability (Fig. 1.4) [38]. While intravenous and intraperitoneal routes improve plasma concentrations [34], they fail to resolve neuroinflammation-specific symptoms. Consequently, enhanced technology of DMT delivery, capable of elevating MN concentrations toward the diseased tissue, is indispensable.

MN's neuroprotective activity is significantly linked to its complex physicochemical profile. While its zwitterionic nature and lipophilicity enable BBB penetration, its rigid tetracyclic structure, pH-dependent solubility, and instability in acidic environments ultimately restrict CNS bioavailability. This inherent challenge combined with systemic toxicity at high dose, highlight the contradictions of MN's pharmacology: its structural features confer both antibacterial efficacy and neuroprotective potential, yet simultaneously undermine its translational viability. Recent study in MN delivery seek to reconcile this duality by exploiting its unique chemistry. The molecule's tetracyclic structure, ionizable groups (pKa 2.8–9.3), and chelation behaviour with metal ions offer opportunities for targeted formulations. For instance, despite the multivalent metal ions compromising MN absorption, the same ions, such as Al^{3+}, Zn^{2+}, Ca^{2+}, and Mg^{2+}, can reduce the epimerization by stabilizing and protecting MN configuration against the assailants [37,39,40]. These strategies aim to bypass systemic limitations, ensuring efficacious concentrations reach inflamed CNS tissue.

MN's repurposing strategy for MS is significantly associated with resolving its dose-dependent toxicity and delivery inefficiency. Previous studies emphasize

its mechanistic potential, yet clinical translation hindered by pharmacokinetic profiles. By prioritizing DDS innovations that leverage MN's chemical properties, future research can bridge the gap between preclinical efficacy and clinical utility, addressing a critical unmet need in MS therapy.

1.2.5 From gestation to neuroprotection: repurposing synthetic preimplantation factor for immunomodulation in multiple sclerosis

In the complex landscape of MS treatment, Synthetic Preimplantation Factor (SPIF) offers a promising approach by targeting both the immune system and neural repair processes. This 15-amino acid peptide (sequence: MVRIKPGSANKPSDD) was initially identified as a key factor in establishing immune tolerance during early pregnancy, where it is secreted by viable embryos and placenta (Fig. 1.5). SPIF'S fast-track clinical approval reduces development risks, making it an attractive candidate for repurposing in MS therapy [41]. Its mechanism of action involves a delicate balancing act, suppressing pro-inflammatory cytokines while simultaneously promoting the secretion of the anti-inflammatory mediators [42]. This dual capacity to modulate immunity and support neural repair makes SPIF a candidate for repurposing in MS, a disease characterized by both inflammation and neurodegeneration.

The immunomodulatory properties of SPIF are recognized by its ability to maintain immune tolerance during pregnancy. SPIF prevents foetal rejection by binding to naive $CD14^{+}$ monocytes to suppress mixed lymphocyte proliferation and inhibits pro-inflammatory cytokine release [42,43]. Notably, SPIF downregulates key drivers of inflammatory cascades (IL-6 and IFN-γ) while promoting TGF-β expression which critical for regulatory T-cell differentiation [24]. Beyond cytokine modulation, SPIF demonstrates neurorestorative potential by directly targeting the neurodegeneration pathway. SPIF capable to promote neuronal migration, reduces microglial activation and apoptosis [24,42]. Furthermore, SPIF ability to cross the intact BBB and modulate the expression of protein kinases (PKA/PKC) further positions it as a dual-action therapeutic, capable of alleviating systemic inflammation while promoting CNS repair [41].

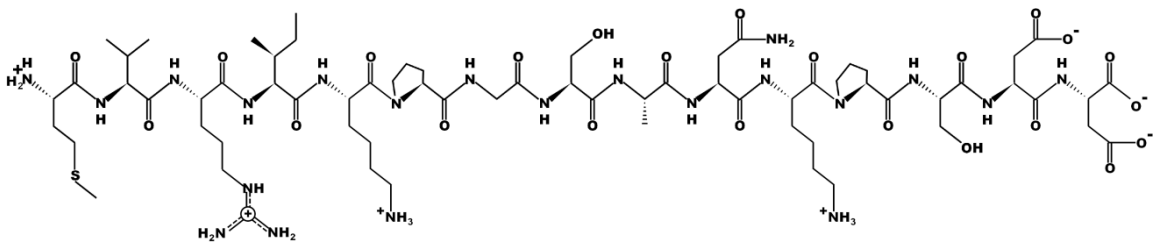

Fig. 1.5: Structure of synthetic preimplantation (SPIF).

The repurposing of SPIF from pregnancy-related immunology to neuroinflammatory diseases is supported by robust preclinical and clinical data. In experimental autoimmune encephalomyelitis (EAE) models, subcutaneous SPIF injection suppressed IL-23 expression, which is critical for sustaining pathogenic T cells. This suppression disrupted relapse frequency, resulting in reduced paralysis and demyelination [41]. Furthermore, clinical administration of low-dose subcutaneous SPIF rapidly reduced relapse severity within 24-48 h without rebound effects, contrasting with slower-acting therapies that require weeks to take effect [42]. This paradigm suggests a distinct therapeutic window for managing acute flares.

Clinical trials underscores SPIF's safety and versatility. A phase I trial in autoimmune hepatitis (NCT02239562) confirmed its tolerability at high subcutaneous doses, paving the way for Phase II studies [44]. Despite its potential, SPIF rapid enzymatic degradation and short half-life in vivo (<2 h) remains a critical challenge to sustaining its efficacy [42]. Preclinical studies have explored multiple delivery routes, including subcutaneous injections and osmotic pumps to overcome the structural instability. However, even though SPIF can cross the BBB, its brain uptake remains limited to approximately 5% of administered doses, underscoring a key challenge for CNS-targeted therapy.

These limitations require delivery strategies which remains a gap yet to be addressed in neuroinflammatory contexts. Additionally, these multifaceted challenges have fuelled debates on optimizing drug delivery to reconcile patient autonomy, clinical efficacy, and safety. This is further complicated by recent findings highlighting patients' desire for implantable DDS, which would reduce the need for frequent and active participation in their own treatment [9–11,45]. However, the primary challenge lies in developing a controlled release system that can be seamlessly integrated into the tissue or implantable devices. The system should be capable to retain a high concentration of DMTs and releases them in a timely manner without substantial structural alterations. These unresolved gaps highlight the need for innovative delivery strategies, with potential solutions provided by advanced materials, though stability and scalability barriers persist.

1.2.6 Hydrogels: promises and pitfalls

Hydrogels offer a promising approach to drug delivery for MS, combining biocompatibility, tuneable mechanics, and localized therapeutic release [46,47]. The three-dimensional polymer networks capable retaining up to 99% water by

weight which replicating the aqueous environment of biological tissues. Furthermore, these high-water structures minimize immune rejection while suitable for entrapping water-soluble DMTs such as MN and SPIF [48]. This architectural mimicry is particularly advantageous for CNS application, where BBB and inflammatory milieu pose significant challenges to systemic drug delivery.

The hydrogel tunability to various environment stems from their crosslinkable architecture, where physical or chemical bonds between polymers create a porous, water-retentive matrix. Additionally, the crosslinking density influences the matrices mechanical and structural adaptability including, mesh size, stiffness, which is adjustable to fit the demands of MS lesions [49]. For instance, softer hydrogel may be better integrated with nervous tissue. On the other hand, denser network offers a critical feature for chronic conditions like MS by providing better diffusion barrier for drug release. Despite these advantageous, significant challenge remains in translating hydrogel-based DDS into clinically viable solutions. Specifically, for repurposed DMTs such as MN and SPIF, where preclinical and clinical studies have primarily relied on systemic route of administration. These challenges underscore the interplay between practicality and functionality in hydrogel design.

Thermosensitive hydrogels, such as poloxamer 407, offer potential for minimally invasive delivery through injectable properties. These systems undergo sol-gel transitions at physiological temperatures, enabling precise localization at target sites via injection to MS-affected CNS regions. Wang et al. (2023) demonstrated this potential in a wound healing model, where Poloxamer-based hydrogels loaded with MN-Ca^{2+} chelates achieved sustained release over 48 h [50]. However, a persistent limitation of such system is burst release, which is marked by a rapid initial discharge of loosely bound drugs from the matrix. While this burst may offer immediate relief for combating bacterial infections, it risks long-term efficacy and necessitating frequent re-administration. Similarly issue affects chitosan-xanthan gum hydrogels, where electrostatic interactions between cationic chitosan and anionic xanthan forms cohesive networks. Despite structurally robust, Ngwabebhoh et al. (2021) reported that 50% of MN was released within 24 h due to insufficient drug-polymer binding [51], mirroring the burst release seen in poloxamer systems. The shared limitation highlights a persistent critical issue as physical crosslinking simplifies preparation and enhances biocompatibility but often fails to retain small, hydrophilic drugs like MN.

On the other hands, different injectable system mitigates the burst by integrating secondary interaction between MN chelate and peptide to enhance structural stability of the carrier. Zhue et al (2022) demonstrated that integrating these nanocomposites into PDLLA-PEG-PDLLA hydrogel reduced the burst by 5–10% and extended sustained delivery to 21 days [52]. Similarly, PLGA nanoparticles encapsulating the MN-Ca^{2+} chelate system achieved prolonged release but introduced scalability barriers due to inflammatory risks from acidic degradation byproducts [53]. This situation underscores a challenge in optimizing retention without compromising manufacturability or biocompatibility.

The delicate balance between functionality and practicality is further illustrated by biopolymer-based hydrogels. Despite as an integral part of extracellular matrix, Hyaluronic acid (HA) and chondroitin sulfate (CS) are preferred for DDS application due to their biodegradability and bioactivity [46,48,54]. HA is capable to support cellular adhesion and modulates inflammatory responses, while CS's sulfated structure enables electrostatic interactions with cytokines and growth factors, offering inherent immunomodulatory benefits. These inherent properties make HA and CS ideal candidates for DDS targeting neuroinflammation in MS. However, their rapid enzymatic degradation in the inflamed CNS environment severely limits their clinical utility [55]. Inflammatory environments, such as in MS, rich in hyaluronidase and chondroitinase degrade HA and CS hydrogels within days, causing premature drug leakage and inconsistent therapeutic delivery. This inherent structural instability requires a system that withstands pathological conditions while maintaining therapeutic efficacy.

The promise of hydrogel in MS therapy thus depends on resolving the interrelated conflicts of drug retention and environmental stability (Fig. 1.6). Despite the foundational studies by Wang et al. (2021), Zhue et al. (2022), and Zhao et al. (2023) uncover pathways forward, they also expose unresolved challenges particularly regarding translability. This situation highlights the need for complementary strategies. Emerging platforms like polyelectrolyte complexes (PEC), which utilize electrostatic interactions to enhance drug-polymer binding, offer tuneable alternatives to address burst release and scalability challenges inherent in hydrogels [47].

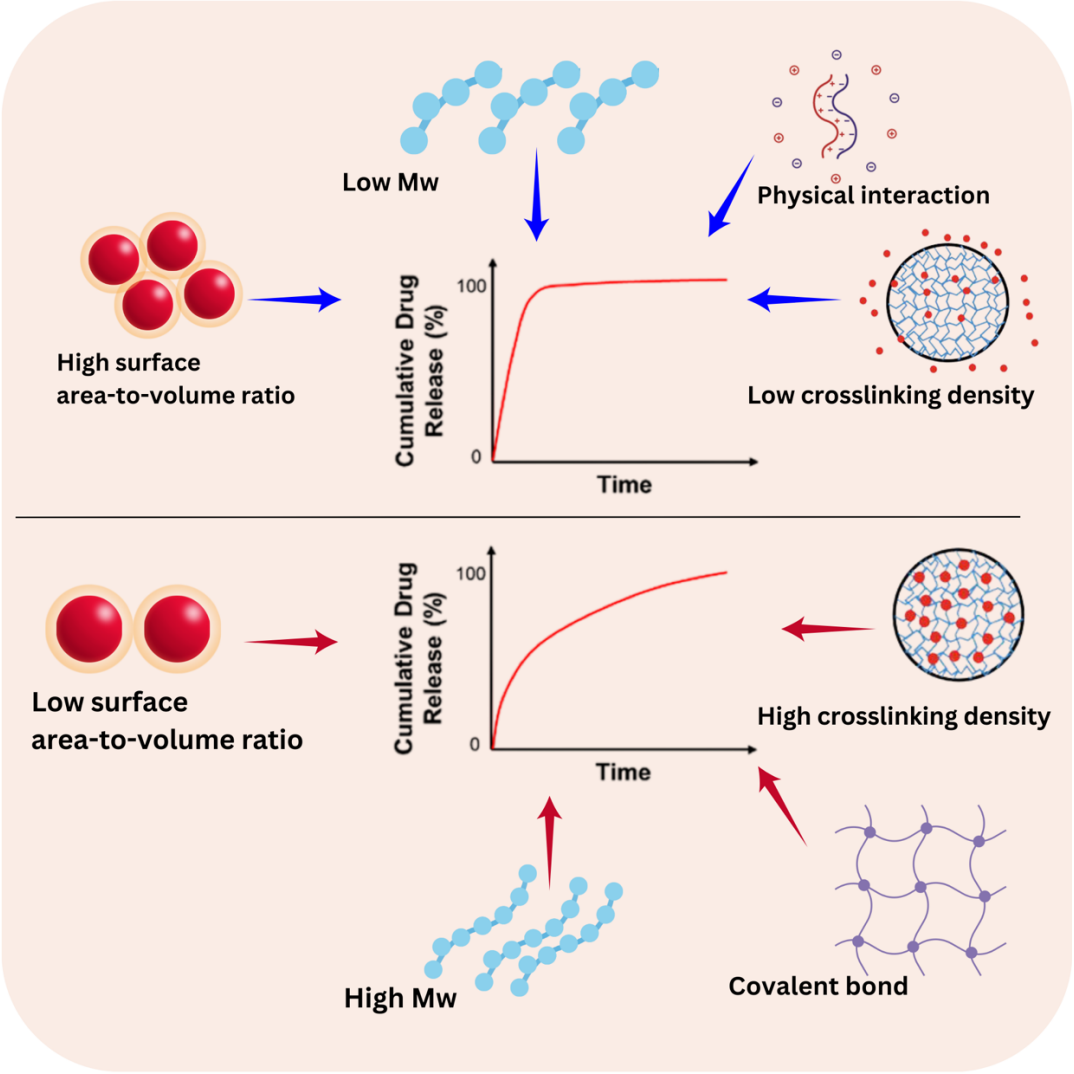

Fig. 1.6: Several factors influencing the kinetics of drug release from hydrogels. Faster drug release arises from smaller particles (higher surface area) and low-MW polymers. Conversely, sustained release is achieved with larger particles (limited surface exposure) and high-MW polymers (dense matrices). Matrices flexibility defined by crosslinking types (covalent, physical) and the density further refines control, enabling customized therapeutic delivery.

1.2.7 Polyelectrolyte complexes (PEC): scalability versus stability

Hydrogels present an alternative yet unfinished solution for MS therapy. Their structural and functional adaptability positions them as ideal candidates for localized delivery, but their clinical translation is hindered by drug-polymer interactions for retention and control release. Based on this situation, polyelectrolyte complexes (PECs) provide a complementary strategy to address the limitations of DDS for MS. PECs offer vast and robust alternatives to chemically crosslinked hydrogels as it uses electrostatic interactions between anionic and cationic polymers to form self-assembled networks (Fig. 1.7). This preparation method simplifies manufacturing process while increasing

biocompatibility by omitting the needs for organic solvents or crosslinkers [56]. This straightforward process position PECs as promising platform for clinical translation.

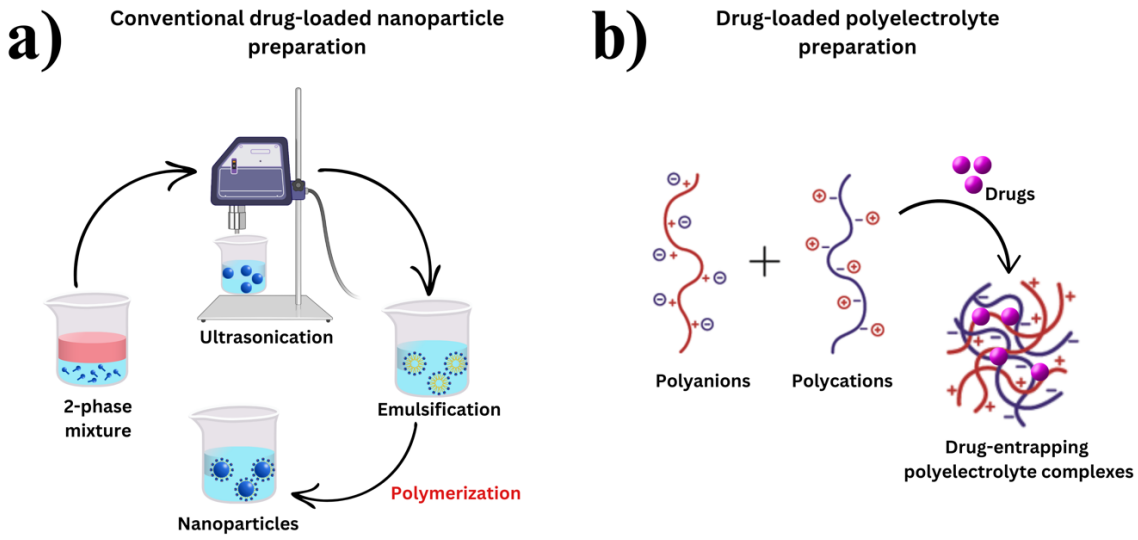

Fig. 1.7: Polyelectrolyte complex offers straightforward drug entrapment process versus conventional nanoparticulate fabrication. Panel a) conventional nanoparticle fabrication involves multiple steps such as solvent selection, mixing, and polymerization. b) In contrast, polyelectrolyte-based self-assembly enables simple, solvent-free drug loading with tuneable nanoparticle properties, offering a scalable alternative to complex multi-step methods.

A central challenge in PEC-based DDS lies in the zwitterionic nature of drugs like MN. At physiological pH, MN's isoelectric point (6.4) oscillates between cationic and anionic states. This dynamic charge profile weakens electrostatic interactions with charged polymers, such as dextran sulfate, leading to inefficient drug entrapment. Zhang et al. (2015) demonstrated that MN-dextran sulfate coacervates achieve ≤ 30% entrapment efficiency due to MN's fluctuating charge, which destabilizes the complex and accelerates drug diffusion [36]. Such inefficiency hinders sustained release, necessitating strategies to stabilize drug-polymer interactions. For instance, incorporating divalent cations like Ca^{2+} can bridge MN and polyanions through chelation, enhancing structural stability. However, this approach introduces new complexities, as excess cations may disrupt physiological ion balance or induce cytotoxicity [37].

The stability of PECs is significantly influenced by physiological conditions. Müller (2014) highlighted that the relative simplicity of PECs preparation, which depends solely on electrostatic interactions comes at the cost of structural

vulnerability under physiological conditions. Fluctuations in pH and ionic strength disrupt these electrostatic conformations [56]. This environmental sensitivity can accelerate drug leakage, particularly for small hydrophilic drugs like MN, which diffuse rapidly through the loosened polymer network. To mitigate this situation, hybrid systems combining PEC with hydrophobic domains or micellar structures have been explored. For example, MN-Ca^{2+} micelles leverage chelation to improve drug retention, extending release profiles beyond 24 h [57]. Yet, these systems introduce cytotoxicity at concentrations > 15 mg mL^{-1}, thereby constraining therapeutic applicability. This issue underscores the critical challenge of optimizing PECs stability without compromising biocompatibility.

This interplay extends to intrinsic polymer characteristics (e.g., chain flexibility, charge density) and extrinsic environmental factors (Fig. 1.7). For instance, low molecular weight polymers tend to form dense-structured complexes that facilitate controlled drug release, whereas high molecular weight polymers create loosely packed networks that enhance diffusion. Physiological ionic strength further screens electrostatic bonds and modulates the instability [58]. Mitigation strategy has been investigated to stabilize the PECs structure leveraging crosslinking approach via photopolymerization or enzyme-mediated crosslinking. Nevertheless, these methods reintroduce the persistent challenges of synthetic complexity and potential toxicity the PEC-based systems were designed to circumvent.

Scalability is another challenge in the development PEC-based control release systems. Natural polyelectrolytes, such as chitosan and CS, offer intrinsic biocompatibility, but introduces batch-to-batch inconsistencies stemming from their natural sourcing. This diversity may complicate large-scale reproducibility [59]. In contrast, synthetic polyelectrolytes, including poly (acrylic acid) and polyethylenimine, generate uniform properties and enable precise control over charge density. However, the synthesis process raises concerns due to residual monomers and cytotoxic degradation products. For example, polyethylenimine-based PECs, despite their efficacy in gene delivery applications, demonstrate dose-dependent cytotoxicity attributed to excessive cationic charge density, which induces membrane destabilization [60]. Devising a hybrid strategy that synergistically combine natural and synthetic polymers may provide compensatory properties for enhanced application. Layer-by-layer (LbL) assembly strategically integrates this approach by merging the biocompatibility of biopolymers with the physicochemical precision of synthetic counterparts to

form PEC with improved stability. Lv et al. (2014) reported that chitosan-alginate LbL coatings on titanium substrates achieved sustained MN release over 14 days [40]. Nevertheless, the translational potential of such systems is limited by the time-intensive, multistep deposition protocols inherent to LbL methodologies.

Despite these challenges, PECs retain significant potential for improving MS therapy. Their modular design enables tailored interactions with charged therapeutics such as MN and SPIF. For instance, SPIF's cationic residues form stable complexes with anionic polymers like heparin, shielding the peptide from enzymatic degradation while enabling controlled release. Similarly, MN's amphiphilic structure facilitates dual interactions with hydrophobic and hydrophilic group, enhancing loading capacity. However, while hybrid systems and advanced formulations offer pathways to improve stability and retention, unresolved issues in scalability and manufacturing reproducibility hinder clinical translation. The incorporation of PEC into injectable hydrogels offers a promising strategy to synergize the strengths of both systems in localized retention and controlled release. This system aligns with the shift toward patient-centric DDS that prioritize minimal intervention and reduced systemic toxicity. Yet, no existing system has successfully reconciled structural stability, high drug loading, and patient-centric design.

1.2.8 Toward a paradigm shift: the HAOX-CSOX hydrogel platform

The identified pitfalls of conventional hydrogels and PECs for MS therapy underscore the need for improved platforms that accommodate structural stability, controlled release, and patient-centric design. The HAOX and CSOX hydrogels present as a solution, leveraging chemical modifications of HA and CS to address these challenges. Regioselective oxidation of HA and CS into their aldehyde-functionalized forms (HAOX and CSOX) enhances the platform's structural integrity and reactivity [61–63].

These modifications introduce α,β-unsaturated aldehydes for enhancing crosslinking efficiency. Unlike saturated aldehydes, these functional groups allow rapid covalent bond formation with aminooxy crosslinkers such as O,O′-1,3-propanediylbishydroxylamine dihydrochloride (PDHA) under physiological conditions [64]. The formed oxime bonds exhibit superior hydrolytic stability due to the electron-withdrawing hydroxyl group adjacent to the C=N bond. This structural feature reduces the susceptibility to hydrolysis, maintaining network integrity across physiological pH ranges. Moreover, the modification of CS into CSOX introduce dual functionality dependent on the degree of functionalization.

Similarly to HAOX, the aldehyde groups in CSOX allow the covalent bond formation with PDHA, while the remaining sulfate groups potentially interact with charged therapeutics like MN and SPIF. By forming a dual crosslinking system (covalent oxime bonds and electrostatic PEC interactions), HAOX-CSOX minimizes burst release while extending therapeutic retention. This dual strategy resolves the historical issues between stability and drug-loading capacity.

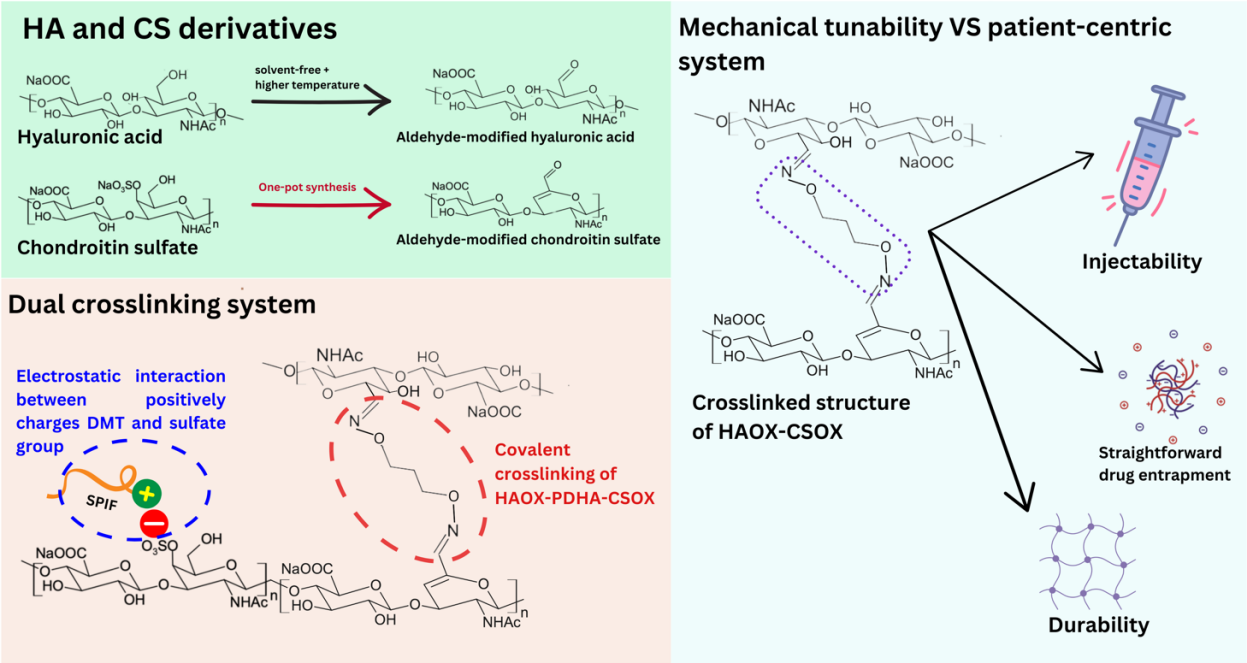

Fig. 1.8: HAOX-CSOX versatility as a drug delivery platform. The system enables a patient-centric platform, offering tuneable mechanical properties (gelation time, elastic modulus), fine-needle injectability, and durable oxime-mediated crosslinking. Electrostatic interactions between CSOX sulfate groups and cationic drugs facilitate efficient physical entrapment.

The HAOX-CSOX hydrogel's mechanical tunability further enhances its clinical relevance. Adjusting the ratio of PDHA to aldehyde groups fine-tunes the hydrogel's viscoelastic properties, enabling injectability through minimally invasive procedures (Fig. 1.8). This aligns with patient preferences for implantable devices that reduce procedural discomfort and recovery time [10,11]. Importantly, crosslinking density directly modulates the hydrogel's mesh size, which defined as the interstitial spaces between polymer chains capable of dictating the diffusion kinetics. Higher crosslinking densities form smaller mesh size thus restricting the mobility of larger molecules (e.g., SPIF), while permitting sustained release of smaller payloads (e.g., MN). Mesh size can be estimated through equilibrium swelling or rubber elasticity theories. Equilibrium swelling

theory is particularly useful for hydrogel with a high polymer concentration, and it calculates the distance by analysing the swelling profile, rendering the relationship between swelling ratio and polymer volume fraction [65–68]. Meanwhile, rubber elasticity theory provides measurement techniques in relation to the mechanical properties of the hydrogel and its structural characteristics [69,70], allowing for prediction based on viscoelasticity measurement. Such control over mesh architecture ensures tailored release profiles, critical for aligning dosing intervals with patient compliance.

System from unmodified HA and CS hydrogels degrade rapidly in inflammatory environments rich in hyaluronidase and chondroitinase, leading to premature drug leakage. In contrast, the crosslinking of HAOX and CSOX resist enzymatic breakdown, maintaining structural stability and predictable drug release. This release can be quantified using the Korsmeyer-Peppas model [67,68], which relates fractional drug release to time via the power-law equation. The diffusional exponent (n) derived from the experimental data typically reflects the transport dynamic. Values between 0.5 and 1 indicate non-Fickian (anomalous) behaviour, where drug diffusion and hydrogel relaxation occur concurrently. On the other hand, rapid degradation often results in $n \geq 1$ (Case-II transport), indicative of significant structural alteration. The enzymatic resistance of HAOX-CSOX ensures time-independent mesh stability, avoiding the collapsing networks seen in traditional systems. Consequently, release parameters (e.g., rate constant k) remain consistent over time, enabling precise pharmacokinetic predictions, which is a cornerstone of patient-centric design.

Safety evaluations underscore the platform's translational potential. Biocompatibility studies confirm that HAOX and CSOX degradation products do not induce cytotoxicity or inflammatory responses at clinically relevant concentrations. For example, PDHA-crosslinked HAOX hydrogels maintain fibroblast viability even under prolonged exposure, while CSOX exhibits no adverse effects on cell cultures [61–64]. These findings position the HAOX-CSOX system as a robust candidate for CNS applications, where localized delivery minimizes systemic toxicity and bypasses the BBB.

The HAOX-CSOX hydrogel platform addresses longstanding limitations of conventional systems by harmonizing covalent crosslinking, enzymatic resistance, and mechanical tunability. This hydrogel supports an injectable system that combines biocompatibility with solutions to MS-specific challenges like frequent dosing and patient compliance. By integrating modular design of hydrogel

and PECs, the HAOX-CSOX platform potentially enables the shift toward patient-centric drug delivery systems, crucial on overcoming preclinical barriers to clinical adoption.

2. AIM OF THE THESES

This study is aimed to develop an injectable HAOX-CSOX hydrogel platform for localized, sustained drug delivery in MS, addressing the adherence burden and pharmacokinetic limitations of current DMTs. We hypothesize that:

1. Covalent immobilization of PECs within the hydrogel network via oxime ligation will minimize burst release and prolong therapeutic delivery by restricting drug diffusion, compared to conventional freely diffusing carriers.
2. Tuning HAOX:CSOX ratios would enable precise control over hydrogel mechanical properties (e.g., gelation time, elastic modulus) and drug release kinetics, balancing injectability with structural stability.

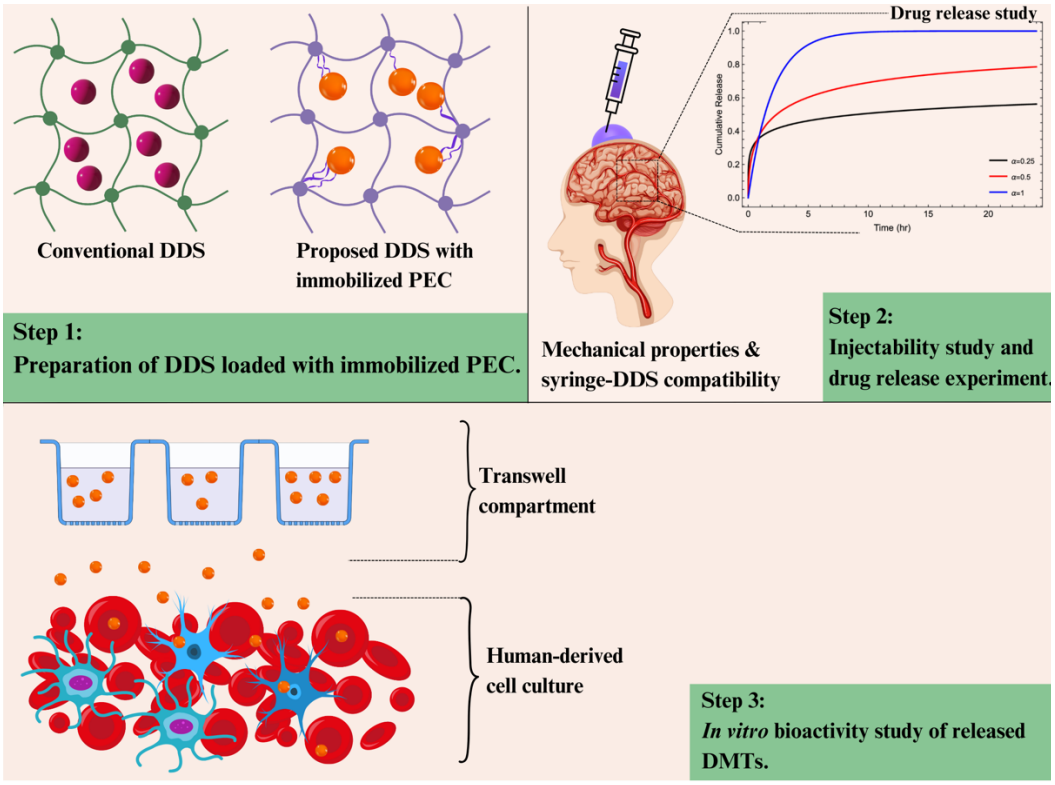

Fig. 2.1: Overview of the thesis objectives. Step 1) Materials selection and entrapment strategy for delivering repurposed DMTs. The purple sphere represents the conventional nanoparticle-based drug entrapment approach, while the orange sphere illustrates the proposed method, where the drug is encapsulated in a PEC immobilized withing the HAOX-CSOX hydrogel structure. Step 2) Characterization of DDS. Step 3) In vitro bioactivity testing to evaluate the compatibility of the DDS with the encapsulated DMTs.

Specifically, this thesis focusses on designing, fabricating, and analysing PEC-loaded HAOX-CSOX DDS for controlled release of anti-inflammatory drugs (Fig. 2.1). Two strategies are used:

1. Designing a MN-loaded system leveraging electrostatic PEC formation (MN/Ca^{2+}/gelatine/CSOX) and covalent HAOX-CSOX crosslinking to protect MN from degradation while ensuring sustained anti-inflammatory release.
2. Engineering a FITC-SPIF delivery platform using HAOX-CSOX double networks to optimize peptide release profiles and validate retained bioactivity post-encapsulation.

By prioritizing patient-centric design through minimally invasive administration, reduced dosing frequency, and localized delivery, this work seeks to advance a translatable alternative to systemic DMTs, bridging material innovation with clinical pragmatism.

3. EXPERIMENTAL SECTIONS

3.1 Materials and methods for in situ formed hyaluronic acid hydrogel loaded with polyelectrolyte complex for minocycline control release

3.1.1 Materials

Materials selected for this study consist of aldehyde-modified hyaluronic acid (HAOX; Molecular weight: 325 kDa; degree of substitution: 7.1%) obtained from Contipro a.s. (Dolni Dobrouč, Czech Rep.). Minocycline hydrochloride (cat. No. M9511; CAS: 13614-98-7) was purchased from Merck (USA). Medical grade syringes and needles were acquired from Servoprax GmbH (Wesel, Germany). A human interleukin-6 (IL-6) enzyme-linked immunosorbent assay (ELISA) kit was supplied by Invitrogen Thermo Fisher Scientific (USA), and the Endotoxin standard (BRP, E0150000) was purchased from Merck (USA). Gelatine derived from pig skin (140 bloom; product number 4275.3) from Carl ROTH GmBH (Karlsruhe, Germany). Sodium chloride (NaCl; Cat No.:16610), and calcium chloride hexahydrate ($CaCl_2.6H_2O$; CAS: 7774-34-7) were supplied by Lach-ner (Czech Rep.). Sodium hypochlorite (NaClO, 11% Cl_2, CAS: 7681-52-9) and di-sodium hydrogen phosphate dodecahydrate ($Na_2HPO_4.12H_2O$, CAS: 10039-32-4) from Penta Chemicals (Czech Rep.). Bovine Chondroitin Sulfate (CS, molecular weight 10–40 KDa; Product code: F0511), composed of chondroitin sulfate A (C4S) and chondroitin sulfate C (C6S) in a 4:6 isomer ratio, was sourced from Bioiberica (Spain). 4-acetamido-2.2.6.6-tetramethyl-piperidine-1-oxyl (4-AcNH-TEMPO; EC no.: 423-840-3) and O.O′-1.3-propanediylbishydroxylamine dihydrochloride (PDHA; source code: BCCG2695; purity 98%) were obtained from Merck (USA). Ethanol (96%) and sodium bromide (NaBr, purity 98%) were purchased from Lach-ner (Czech Rep.). Transwell® insert featuring permeable membrane (25 mm in diameter, 3 μm pore) and 12-wells plate were obtained from Corning, Inc., (Acton, MA, USA). Normal saline (0.9% w/v NaCl), hereafter referred to as "saline", was produced by dissolving 9 grams of non-iodized NaCl in 1 Liter of deionized water.

3.1.2 Chemical modification of chondroitin sulfate via aldehyde functionalization

The synthesis of CSOX was achieved through a one-pot synthesis process, based on a previously reported method by Bobula et al., with modification (Fig. 3.1) [62]. Briefly, CS (1040 mg) was first dissolved in 54 mL of deionized water, accompanied by the addition of $Na_2HPO_4.12H_2O$ (400 mg) and NaBr (103 mg). These reagents provided a buffered environment that facilitates the subsequent oxidation reactions. The oxidation process began upon the addition of 4-AcNH-TEMPO (4 mg, 0.02 mol) as a catalyst. Subsequently, the mixture was then cooled

to 5 °C to control the reaction kinetics and enhance selectivity. Following this, NaClO (560 µL, 11% of active chlorine) was introduced, and the solution was stirred at 5 °C for another 30 minutes. Termination of the oxidation reaction was commenced by the addition of ethanol (5 mL) as the quenching agent. The product was purified by dialysis using a 14 KDa molecular weight cut-off membrane, with deionized water as the dialysis medium, and the process continued with lyophilization. Following dialysis, the purified aldehyde-modified CS was subjected to 48 h lyophilization to obtain a dry fibre.

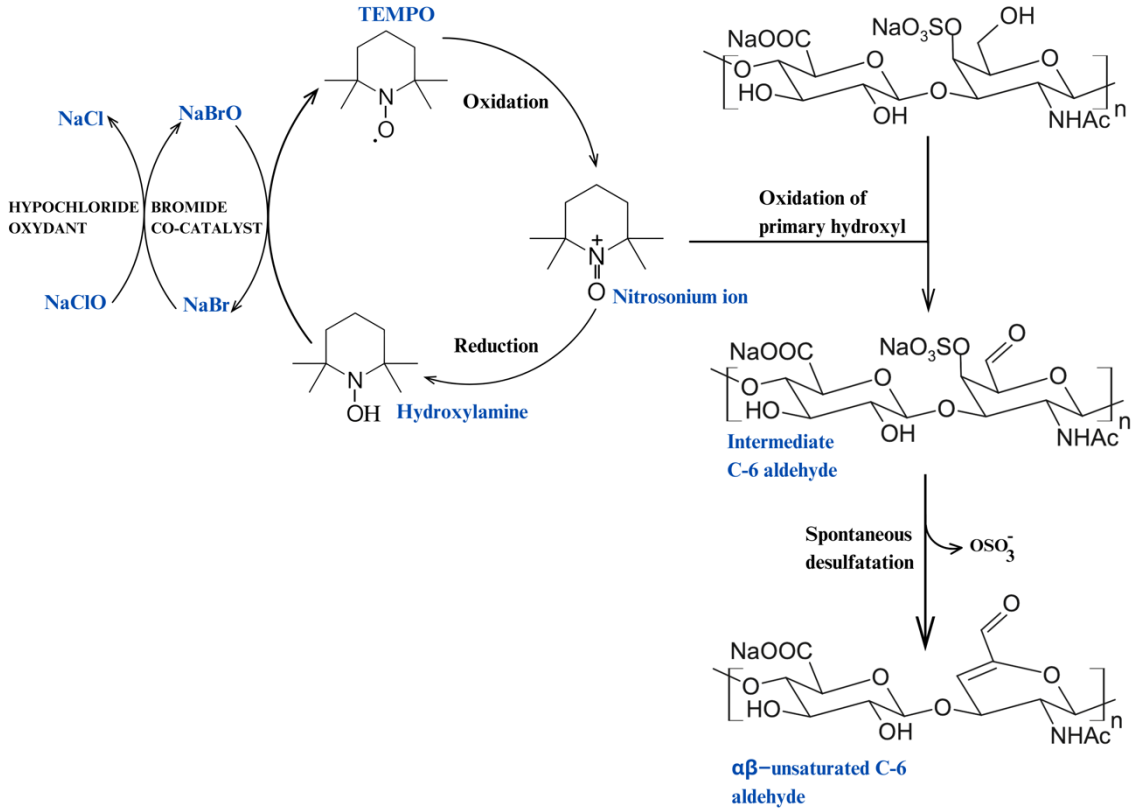

Fig. 3.1: One-pot reaction scheme for the preparation of aldehyde-modified chondroitin sulphate (CSOX).

Quantitative evaluation of the degree of functionalization (DF) for CSOX was conducted using proton nuclear magnetic resonance (^{1}H NMR) spectroscopy, conducted on a Bruker Avance Neo 700 MHz spectrometer. The samples were prepared as 1% (w/v) solutions in deuterated water (D_2O). The obtained spectra were analysed using SpinWorks software.

The DF was estimated from the molar ratio of proton at the H6 position, which resonates at 9.21 ppm, or the protons at the H4 position at around 6.296 ppm, which were compared to the three protons associated with the methyl group of N-acetylgalactosamine (GalNAc) at 2.02 ppm. The calculation was performed using the Equation (3.1).

$$DF = \frac{I_{-CHO}}{I_{-CH_3}} \times 300\% \quad (3.1)$$

I_{-CHO} indicates the integrated signal at either 9.217 ppm or 6.296 ppm, attributed to -CHO of the modified N-acetylgalactosamine unit (GalNAc). Meanwhile, I_{-CH_3} corresponds to the integral of the signal at 2.02 ppm, for -CH_3 of GalNAc. The factor of 300 in the DF calculation accounts for both the proton ration correction and percentage conversion. The methyl group (-CH_3) in GalNAc has three protons, while aldehyde (-CHO) signal represents a single proton. To normalise the integral ratio, the (-CH_3) integral is divided by its three protons, introducing a x3 multiplier to balance the comparison. This adjusted ratio is then converted to a percentage by multiplying by 100, resulting in the combined factor of 300.

The molecular mass of CSOX (M_{CSOX}) was characterized using a dual-method system involving size-exclusion chromatography and multi-angle laser light scattering (SEC-MALLS), following the methodology established by Bobula et al. (2018) [62]. A 100 µL aliquot of a 2% (w/v) CSOX solution, prepared in saline, was introduced into the chromatographic system for analysis. The separation process employed two sequential columns: PL aquagel-OH 40 (7.5 × 300 mm, 8 µm) and PL aquagel-OH 20 (7.5 × 300 mm, 5 µm). These columns were maintained at a stable temperature of 40 °C. The eluent for this analysis consisted of a 0.1 M sodium phosphate buffer, with the pH adjusted to 7.5, then supplemented with 0.05% sodium azide. The column flow rate was set to 0.8 mL min^{-1}, unless otherwise specified. A high-performance liquid chromatography apparatus (Waters, product series: 2489) tandem with UV/Vis detector (Waters model 2489) and a refractive index detector (Waters model 2414) was used for the chromatographic analysis. For molecular mass analysis, a miniDAWN TREOS light scattering instrument (Wyatt Technology) was integrated into the system to capture multi-angle light scattering measurements. All analytical measurement and subsequent M_{CSOX} estimations were performed using ASTRA software (version 5.3.4, Wyatt Technology Corporation).

3.1.3 Hydrogel formulations

A uniform protocol was employed for all the hydrogel preparation, based on covalent crosslinking between PDHA with HAOX or CSOX. Then, a system consisting of syringe pair with luer connection was employed to facilitate the crosslinking process (Fig. 3.2). The detailed nomenclature and formulation of the DDS consists of specific concentrations of HAOX or CSOX combined with PDHA and MN in saline, presented in Table 3.1.

Nomenclature

- HAOX_**MN**: DDS prepared using HAOX as the primary structural element entrapping **MN**.
- CSOX_**MN**: DDS prepared using CSOX as the primary structural element entrapping **MN**.
- HAOX_**CHELATE**: DDS prepared using HAOX as the primary structural element. "**CHELATE**" indicates the complex formed between **MN and CA**.
- HAOX_**PECS**: DDS prepared using HAOX as the primary structural element. "**PECS**" refers to the PEC formed from **MN, CA, GA, and CS**.
- HAOX_**PECOX**: DDS prepared using HAOX as the primary structural element. "**PECOX**" refers to the PEC formed from **MN, CA, GA, and CSOX**.

Table 3.1 Series of studied formulations for MN-DDS.

Formulations	HAOX (mg mL^{-1})	CSOX (mg mL^{-1})	CS (mg mL^{-1})	CA (□M)	GA (mg mL^{-1})	PDHA (mg mL^{-1})	MN (□g mL^{-1})
HAOX	20	-	-	-	-	0.32	-
CSOX-MN	-	100	-	-	-	1.865	200
HAOX-MN	20	-	-	-	-	0.32	200
HAOX-CHELATE	20	-	-	7.2	-	0.32	200
HAOX_PECS (unbound PEC)	20	-	5	7.2	1	0.32	200
HAOX_PECOX (immobilized PEC)	20	5	-	7.2	1	0.462	200
HAOX	20	-	-	-	-	0.32	-

3.1.4 Preparation of HAOX-based hydrogel and CSOX-based hydrogel

The hydrogels based on HAOX or CSOX were prepared by first dissolving each polymer in saline at 60 °C for 3 h, then continuing with stirring at 25 °C overnight to ensure complete solubilization. Concurrently, a PDHA solution was prepared by dissolving 150 mg of PDHA in 10 mL of saline at 25 °C. The pH of the PDHA solution was set to 7.0 using NaOH.

The crosslinking process employed a pair of syringe system, connected via a luer lock adapter (see Fig. 3.2). For HAOX_MN or CSOX_MN hydrogels, one syringe was filled with HAOX or CSOX solution, while the other held the mixture of MN and PDHA solution. In the case of HAOX_CHELATE, one syringe contained the solution of HAOX and CA, with the other syringe held MN and PDHA. The solutions were mixed in an adjustable 80:20 ratio to optimize injection ease and hydrogel properties. After mixing, the formulation was transferred into a Teflon mold.

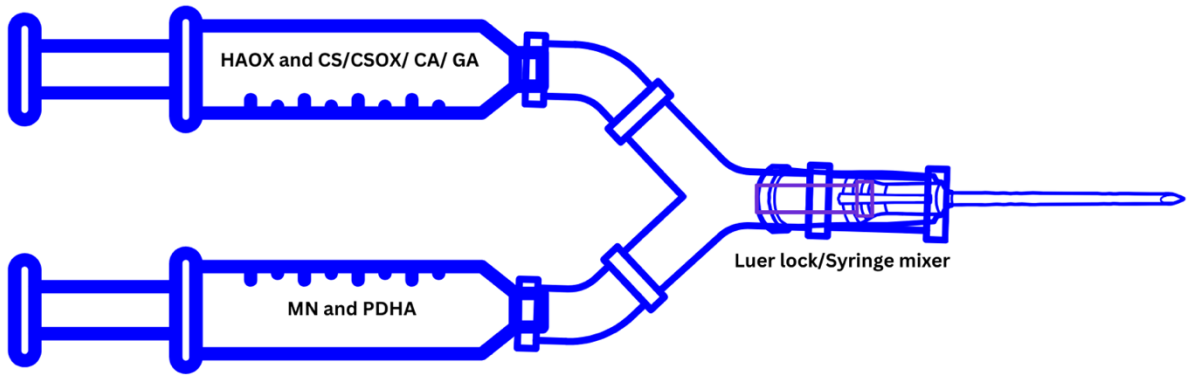

Fig. 3.2: Schematic of a pair-syringe system connected by a luer lock adapter or mixing port used in the crosslinking process of HAOX and HAOX-CSOX hydrogel.

3.1.5 Preparation of HAOX hydrogel incorporating unbound PEC (HAOX_PECS)

The HAOX_PECS formulation was developed in accordance with the method described in section 3.1.4, through the solubilization of HAOX, Calcium (CA), Gelatine (GA), and CS in saline. The two prepared solutions were mixed at an 80:20 ratio utilizing a dual-syringe setup and dispensed into a Teflon mold, resulting in hydrogels containing MN at concentration of 200 $\mu g\,mL^{-1}$. The HAOX concentration was fixed at 20 $mg\,mL^{-1}$ to facilitate tuning of the hydrogel's physicochemical properties. The PDHA concentration for formulations used in section 3.1.4 and 3.1.5 was calculated by applying a 1:1 stoichiometric ration between the aldehyde groups in HAOX and the

hydroxylamine groups in PDHA (Fig. 3.3). The mass concentration of PDHA (C_w^{PDHA}) was computed using the following formula:

$$C_w^{PDHA} = \frac{C_w^{HAOX} . V_{HAOX} . M_{PDHA} . DS_{HAOX}}{V_{PDHA} . P . P_p . M_{HAOX}} \quad (3.2)$$

In this context, C_w^{HAOX} represents the HAOX mass concentration (w/v) in the first syringe, DS_{HAOX} denotes the degree of substitution of HAOX, P refers to the ratio of aldehyde to hydroxylamine groups, which is set to 1. P_p indicates the number of hydroxylamine groups in PDHA (2), V_{HAOX} is the volume of HAOX solution in the first syringe, V_{PDHA} is the total volume of MN mixed with PDHA solution, M_{PDHA} is the molar mass of PDHA (179 g mol^{-1}), and M_{HAOX} is the molar mass of the HA disaccharide unit (400 g mol^{-1}).

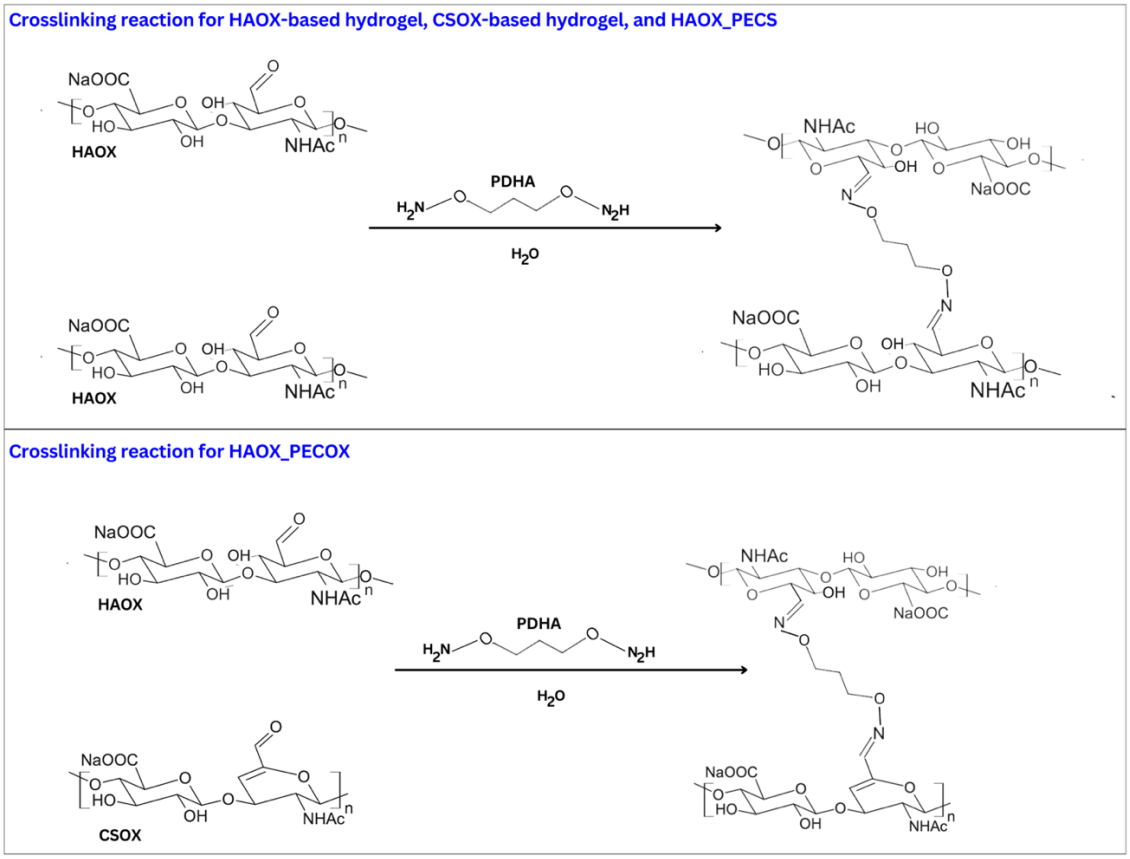

Fig. 3.3: Chemical reaction for DDS formation with 1:1 ratio of the cross-linkable groups of aldehydes from HAOX and hydroxylamine from PDHA.

3.1.6 Preparation of HAOX containing immobilized PEC (HAOX_PECOX)

The HAOX_PECOX was prepared by dissolving HAOX, CA, GA, and CSOX in saline for 3 h at 60 °C, with overnight stirring at 25 °C. The crosslinking procedure was consistent with the other formulations, except for a different

concentration of the crosslinker. The following equation (3.3) was used to calculate the PDHA concentration in HAOX_PECOX, taking into account aldehyde groups from both HAOX and CSOX to ensure a 1:1 molar ratio with hydroxylamine groups.

$$C_w^{PDHA} = \left(\frac{C_w^{HAOX} . V_{HAOX} . M_{PDHA} . DS_{HAOX}}{V_{PDHA} . P . P_p . M_{HAOX}}\right) + \left(\frac{C_w^{CSOX} . V_{CSOX} . M_{PDHA} . DS_{CSOX}}{V_{PDHA} . P . P_p . M_{CSOX}}\right) \quad (3.3)$$

The values in the second set of parentheses correspond to the CSOX analogues of those in the first set, where M_{CSOX} represents the molar mass of CSOX disaccharide unit (600 g mol^{-1}).

3.1.7 Gelation time

The gelation time of DDS was evaluated using a Discovery Hybrid Rheometer–3 (TA Instruments) with 40 mm diameter plate-plate configuration and a 400 µm gap. Following the introduction of the crosslinker, both the elastic (G′) and viscous (G″) moduli were continuously assessed. An oscillatory time sweep was performed for 180 s at 25 °C, with data collected every 6 s. The system maintained a constant strain of 5% and an angular frequency of 6.283 rad s^{-1} (1.0 Hz). The polymer solution (0.8 mL) was placed on the Peltier plate. Then, 200 µL of PDHA-MN solution was introduced. Pre-shear was applied at 2000 s^{-1} for 3 s to ensure solution homogeneity before gelation began. Gelation time was determined by identifying the crossing points between G′ and G″, indicating the transition from viscous to elastic behaviour. The process was conducted three times, and average values along with standard deviations were computed.

3.1.8 Swelling ratio

The swelling ratio (Q) for the DDS was computed based on the equation provided below:

$$Q = \frac{(m_t - m_r)}{m_r} \times 100\% \quad (3.4)$$

The hydrogel swelling ratio was measured through a mass change evaluation, comparing the hydrogel mass in its relaxed state before swelling (m_r) with the mass after swelling (m_t). The DDS were transferred into Transwell® inserts (Fig. 3.4), and 2 mL of saline was used as the swelling medium. The variation in the gravimetric change was measured following: 1, 3, 7, 10, and 14 days, with all experiments conducted at 37 °C.

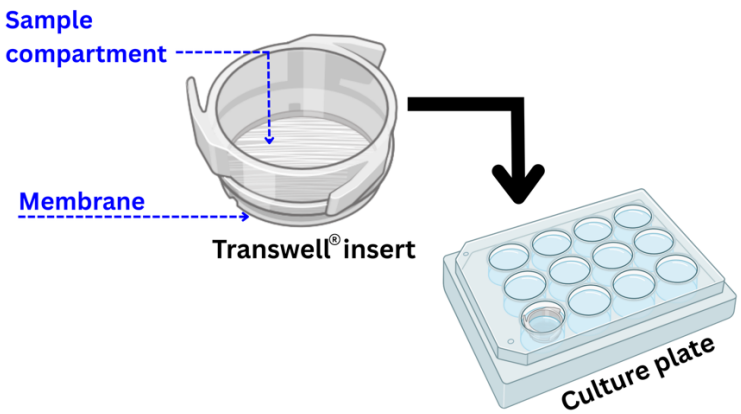

Fig. 3.4: Illustration of Transwell® system. A porous membrane separates two chambers, with DMTs-loaded DDS introduced in the upper compartment and drug release is quantified in the lower compartment.

3.1.9 Drug release experiment

The release of MN from the DDS was evaluated *in vitro* using a Transwell® set up. The formulation (1 mL) was crosslinked and transferred to the donor compartment of a Transwell® insert, while the base was filled with saline (2 mL) as the release medium (Fig. 3.4). The system was maintained at 37 °C and 96% relative humidity (Witeg Wisd Incubator, WITEG Labortechnik) to simulate physiological environments.

The release medium in the lower compartment was fully aspirated at designated interval and promptly replenished with fresh saline (2 mL). The concentration of MN in the release medium was quantified using HPLC with an Acquity UPLC Waters system equipped with a PDA-QDA detector.

The quantity of MN released over time was expressed as the cumulative drug release (CDR), as shown in equation (3.5).

$$\text{CDR} = \frac{m_t}{m_\infty} \text{ x } 100\% \tag{3.5}$$

Here m_t refers to the mass of drug released at a particular time, whereas m_∞ correspond to the total mass of loaded drug. The Korsmeyer–Peppas model [68], described by Equation (3.6), was applied to elucidate the release mechanism of MN.

$$kt^n = \frac{m_t}{m_\infty} \tag{3.6}$$

The equation allowed for the estimation of both the diffusion factor (n) and the kinetics constant (k), which are influenced by the design and spatial configuration of the delivery matrix. An $n \leq 0.5$ signifies Fickian diffusion, while $0.5 \leq n \leq 1$ is

indicative of anomalous (non-Fickian) transport, the n = 1 corresponds to case-II transport, and $n \geq 1$ is associated with super case-II.

3.1.10 Mesh size, M_c, and crosslinking density

The influence of PEC on the structural assembly of the hydrogel matrix was analysed by defining the molecular mass between two consecutive junctions (M_c) using two theoretical frameworks outlined by Matthew Rehman [65]. The first framework was calculated using rubber elasticity theory by Paul Flory [71], and the second was derived from equilibrium swelling principles by Nikolaos Peppas [66,67]. The theory of rubber elasticity assumes the capacity of the hydrogel network to reverts to its original conformation when subjected to a deformation. The theory was initially proposed by Treloar [71] and Flory [69] for vulcanized rubber and later adapted for polymers by Flory himself [67]. Nonetheless, the initial theoretical framework fails to account for hydrogel prepared in solvent-based condition. Consequently, modifications to the theory for such hydrogels were proposed by Silliman and subsequently refined by Peppas and Merrill [67]. The M_c value based on rubber elasticity theory can be estimated by equation (3.7).

In the rubber elasticity theory, M_c was calculated from the swelling data in equilibrium state using equation (3.7).

$$\tau = \frac{\rho_p RT}{M_c}\left(1 - \frac{2M_c}{M_n}\right)\left(\alpha - \frac{1}{\alpha^2}\right)\left(\frac{v_{2,s}}{v_{2,r}}\right)^{\frac{1}{3}} \quad (3.7)$$

Here τ denotes the stress applied to the hydrogel, ρ_p represents the density of dry polymer, R stands for the universal gas constant, T refers to the experimental temperature, α indicates the elongational ratio, and M_n corresponds to the average molecular weight of the monomers is 300,000 g mol^{-1} for HAOX. The M_n of HAOX-CSOX was calculated using the dispersity (Đ = 1.39) and weight-average molar mass (Mw = 291,000 g mol^{-1}) obtained from SEC-MALLS analysis. Prior to analysis, a 20 mg mL^{-1} HAOX:CSOX (1:1) solution in saline was prepared and stirred overnight. Applying following equation:

$$Đ = \frac{M_w}{M_n} \quad (3.8)$$

The calculation yielded M_n for 209,352 g mol^{-1}. Meanwhile, $v_{2,s}$ represents the polymer volume fraction at equilibrium swelling, $v_{2,r}$ indicates the polymer volume fraction in the reference state (relaxed), which can be determined from equation (3.9) and (3.10), respectively,

$$v_{2,s} = \left(1 + \frac{\rho_p}{\rho_s}.\ \left(Q_{M,s} - 1\right)\right)^{-1} \tag{3.9}$$

$$v_{2,r} = \left(1 + \frac{\rho_p}{\rho_s}.\ \left(Q_{M,r} - 1\right)\right)^{-1} \tag{3.10}$$

where ρ_p denotes the dry polymer density, with values of 1,299,000 g m^{-3} for HAOX [72] and 120,000 g m^{-3} for CSOX [73], $Q_{M,s}$ is equilibrium mass swelling ratio, $Q_{M,r}$ is equilibrium mass in relaxed state,

$$Q_{M,s} = \frac{m_s}{m_d} \tag{3.11}$$

$$Q_{M,s} = \frac{m_r}{m_d} \tag{3.12}$$

where m_s is hydrogel mass in the equilibrium swollen state, m_r represents the mass of the hydrogel in its relaxed state, and m_d is mass of xerogel.

Effective crosslinking density (v_e) can be defined using equation (3.13).

$$v_e = \frac{\rho_p}{M_c} \tag{3.13}$$

On the other hand, the relationship between τ and G is elaborated by [74]:

$$\tau = G\ \left(\alpha - \frac{1}{\alpha^2}\right) \tag{3.14}$$

Substitution of (3.14) to (3.7), resulting in equation (3.15),

$$M_c = \frac{\rho_p\, RT \left(\frac{v_{2,s}}{v_{2,r}}\right)^{\frac{1}{3}}}{G + \frac{2\rho_p RT}{M_n} \left(\frac{v_{2,s}}{v_{2,r}}\right)^{\frac{1}{3}}} \tag{3.15}$$

where G is shear modulus of the hydrogel in equilibrium swollen state, which can be calculated using equation (3.16).

$$\frac{G_S}{G_r} = \frac{v_e RT \left(v_{2,s}\right)^{\frac{1}{3}}}{v_e RT \left(v_{2,r}\right)^{\frac{1}{3}}} = \frac{\left(v_{2,s}\right)^{\frac{1}{3}}}{\left(v_{2,r}\right)^{\frac{1}{3}}} \tag{3.16}$$

Here G_S is the shear modulus in equilibrium swollen state, G_r is the shear modulus in relaxed state.

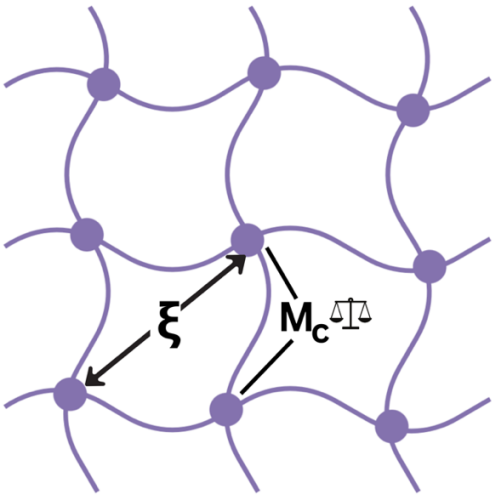

Fig. 3.5: Illustration of mesh size and molecular mass between crosslinks.

On the other hand, the equilibrium swelling theory is derived from the original Flory-Rehner theory, which posits that two opposing forces act on a polymeric gel when it is immersed in a solvent. The primary driving force behind the swelling process is largely enthalpic in nature. As the network volume increases, the polymer chains become stretch, leading to a reduction entropy. The compatibility of a polymer with a solvent is typically quantified using an interaction parameter (χ). At equilibrium, these two opposing forces reach a state of balance. This concept is also relevant to the chemical potential of the solvent, both within the gel and in the surrounding environment. Peppas and Merrill adapted the original Flory-Rehner theory specifically for hydrogels crosslinked in aqueous environment. The calculation of M_c based on equilibrium swelling theory following Equation (3.17).

$$\frac{1}{M_c} = \frac{2}{M_n} - \frac{v\left(ln(1 - v_{2,s}) + v_{2,s} + \chi . v_{2,s}^2\right)}{V_1 v_{2,r}\left(\left(\frac{v_{2,s}}{v_{2,r}}\right)^{\frac{1}{3}} - \left(\frac{v_{2,s}}{2. v_{2,r}}\right)\right)} \quad (3.17)$$

Here, v corresponds to the specific volume of the polymer, equal to 0.764 g mol^{-1} [75], and χ is the Flory-Huggins interaction index for HA in aqueous solutions (0.439) [75], V_1 is the molar volume of the solvent (18 cm^3 mol^{-1}) [75].

The mesh size of hydrogels is typically measured on a nanometre scale. Determining this size precisely is crucial for assessing whether the drug, which is similar in size, will remain trapped within the matrix or diffused out (Fig. 3.5). Hydrogel mesh sizes generally fall between 5 and 500 nm, a range that often

challenges detection by imaging methods. However, this parameter can be calculated using the following the equation (3.18).

$$\xi = l v_{2,s}^{-\frac{1}{3}} \left(\frac{2C_n M_c}{M_r}\right)^{\frac{1}{2}} \quad (3.18)$$

Here, l corresponds to the virtual bond length, which is defined as the distance between consecutive glycosidic oxygens spanning a monosaccharide unit (0.52 nm for HAOX [75], 0.48 nm for CSOX [76]); C_n refers to the Flory characteristic ratio (27 for HAOX [75], 15.705 for CSOX [76], while M_r denotes the molar mass of the repeat disaccharide unit (400 gmol^{-1} for HA, 600 gmol^{-1} for CSOX). For the M_c and ξ for immobilized PEC formulation, the influence of CSOX structure on these two parameters was determined according to the monomer's volumetric fraction in the crosslinked structure.

3.1.11 Injectability

The ease of injection, commonly known as Injectability was measured using 18, 19, and 20 Gauge (G) needles with a length of 40 mm. The gauge (G) defines the width of the hollow centre (lumen) through which fluids pass. Needle dimensions were selectively chosen based on standard practices among healthcare professionals to reflect common usage. The hydrogels were prepared using a dual-syringe configuration interconnected through a luer lock adapter. The precursor solutions were separately loaded into a pair of syringes, with one containing polymer-based component and the other contained solution of MN and PDHA. The two components were combined at an 80:20 volume ration over 10 s before testing. Subsequent injectability assessments were conducted at ambient condition using the Instron 3342 Single Column Materials Testing System, equipped with a 100 N compression plate at a speed of 50 mm/min. Parameters such as injection pressure, plunger displacement, dynamic glide force (*DGF*), and maximum force ($F_{\max}$) were quantified using Bluehill software. Measurement was taken in triplicate, and outcomes were expressed as mean with corresponding standard deviation.

3.1.12 Viscoelastic properties of the drug delivery system

The rheological behaviour of the hydrogels was assesses using a Discovery Hybrid Rheometer–3 (TA Instruments). A 20 mm diameter crosshatched stainless-steel plate setup was employed throughout to minimize slippage during measurements. All tests were performed under isothermal conditions at 25 °C. To investigate the viscoelastic profile, oscillatory strain sweep experiment were carried out. These were designed to identify the upper boundary (γL) of the linear viscoelastic region (LVE) and to quantify the storage (G') and viscous (G'') moduli within this linear range. Each sample was subjected to sinusoidal

oscillation at a constant angular frequency of 6.28 rad s^{-1} (1 Hz,), with strain the amplitude gradually increased from 0.001 to 2.0 rad. The threshold γ_L was determined as the strain level at which the G' exhibited dependence on strain, with permissible deviations for G' around the plateau value not exceeding ± 5%. The final G' and G'' values were computed by averaging the responses within the LVE domain.

3.1.13 Whole blood monocytes activation test (WB-MAT)

The Whole Blood Monocytes Activation Test (WB-MAT) was conducted to investigate the bioactivity of MN released from the DDS, using a modified protocol adapted from previously established methods [77,78]. Prior to blood collection, informed consent was obtained from three healthy adult donors. Whole blood was drawn aseptically into sterile, heparinized tubes and designated as samples A, B, and C. To stimulate interleukin-6 (IL-6) production, a lipopolysaccharide (LPS) stock solution was prepared and serially diluted in saline to obtain final working concentrations of 5, 1, and 0.25 IU mL^{-1}. Subsequently, each LPS concentration (100 µL) was transferred into sterile microtubes and mixed with 1000 µL of saline.

To evaluate the bioactivity of MN, the release medium collected from the DDS was first analysed by HPLC to quantify the concentration of MN. Then, dilution of this solution to 5 µg mL^{-1} was performed using saline. Following dilution, a 1000 µL aliquot of the diluted MN was transferred into sterile microtube, followed by the addition of either 10 µL of LPS at 2.5 IU mL^{-1} or 10 IU mL^{-1} to initiate immune stimulation. A100 µL aliquot of freshly drawn heparinized blood from each donor was added to the respective microtubes containing both the MN sample and LPS. The mixtures were gently vortexed and subjected to overnight incubation at 37 °C.

Following incubation, the tubes were inverted gently and centrifuged at 13.000 rpm for 10 minutes. The resulting supernatants were carefully transferred into fresh tubes for IL-6 quantification using a commercial ELISA kit, following the manufacturer's guidelines. Absorbance readings were recorded using an Ensight Multimode Reader, and data were analysed with Kaleido software (PerkinElmer, Waltham, USA).

3.2 Materials and method for in situ forming hydrogel from aldehyde-modified hyaluronic acid and aldehyde-modified chondroitin sulfate for synthetic preimplantation factor delivery

3.2.1 Materials

This study utilized aldehyde-modified hyaluronic acid (HAOX; Mw 325 kDa, with degree of substitution of 7.1%) supplied by Contipro a.s. (Dolni Dobrouč, Czech Rep.). Fluorescein isothiocyanate-6-Aminohexanoic acid-Synthetic Preimplantation Factor (FITC-Ahx-MVRIKPGSANKPSDD or FITC-SPIF, product code: PEP0235) was purchased from Iris Biotech (Germany). Medical grade syringes and needles were obtained from Servoprax GmbH (Wesel, Germany). Bovine Chondroitin Sulfate (CS, molecular weight 10–40 KDa; Product code: F0511), composed of chondroitin sulfate A (C4S) and chondroitin sulfate C (C6S) in a 4:6 isomer ratio was procured from Bioiberica (Spain).

Chemical reagents for polymer modification and crosslinking included 4-acetamido-2,2,6,6-tetramethyl-piperidine-1-oxyl (4-AcNH-TEMPO; EC no.: 423-840-3) and O.O′-1.3-propanediylbishydroxylamine dihydrochloride (PDHA; source code: BCCG2695; purity 98%), both obtained from Merck (USA). Ethanol (98% purity), Sodium chloride (NaCl, Cat No.:16610), and sodium bromide (NaBr, 99.8%) were provided by Lach-ner (Czech Rep.). Additionally, sodium hypochlorite (NaClO, 11% Cl_2; CAS: 7681-52-9) and disodium hydrogen phosphate dodecahydrate ($Na_2HPO_4.12H_2O$; CAS: 10039-32-4) were supplied by Penta Chemicals (Czech Rep.). Deionized water and 9 g non-iodized sodium chloride were combined to prepare 1 Liter of normal saline (0.9% w/v NaCl, referred to as “saline”).

In vitro gene expression studies used the THP-1 cell line (ATCC). RPMI-1640 cells culture medium in medium enriched with foetal bovine serum (FBS-12A), D-glucose, penicillin/streptomycin, sodium pyruvate, with components sourced from Biosera (France), Capricorn Scientific (Germany), and Merck (USA). Phorbol 12-myristate-13-acetate (PMA; CAS: 16561-29-8) was obtained from Merck (USA). RNeasy Mini Kit (QIAGEN, Germany), High-Capacity Reverse Transcription Kit obtained from ThermoFisher (USA). qPCR analysis was performed using commercial probes targeting GAPDH, TGF-β1, IL-10, CXCL8, PTGS2, IL1b, and TNF alpha, sourced from Merck (USA).

The preparation of CSOX employed the same method as in 3.1.2

3.2.2 Hydrogel formulations

The formulation of DDS for controlled delivery of FITC-SPIF was achieved by covalent crosslinking of either HAOX or CSOX with PDHA. Detailed formulations for these hydrogels are provided in Table 3.2, with the subsequent formulations (Table 3.3 – 3.4) established for optimization.

Nomenclature

- **HAOX_1X**: DDS with **Formulation 1**, containing only 2% (w/v) HAOX, prepared at pH **X** (where pH values are 5 or 6.8 rounded to 7).
- **HACOX_2X**: DDS with **Formulation 2**, containing 1% HAOX and 0.5% CSOX, prepared at pH **X**.
- **HACOX_3X**: DDS with **Formulation 3**, containing 1% HAOX and 1% CSOX, prepared at pH **X**.
- **HACOX_37_YYY**: DDS with **Formulation 3**, containing 1% HAOX and 1% CSOX, prepared at pH **6.8**, with **YYY µg** of FITC_SPIF.
- **HACOX_Z7_250**: DDS prepared with 1% HAOX. "**Z**" represents the concentration of CSOX, formulated at pH **6.8**, and containing **250 µg** of FITC_SPIF.

All the concentrations are in w/v percentage.

Table 3.2 Formulations for designing a suitable delivery system for SPIF.

Formulations	**HAOX (mg mL^{-1})**	**CSOX (mg mL^{-1})**	**FITC-SPIF (□g mL^{-1})**	**PDHA (mg mL^{-1})**	**pH**
HAOX_15	20	0	100	0.32	5
HACOX_25	15	5	100	0.39	5
HACOX_35	10	10	100	0.465	5
HAOX_17	20	0	100	0.32	6.8
HACOX_27	15	5	100	0.39	6.8
HACOX_37	10	10	100	0.465	6.8

Table 3.3 Development of HACOX_37: Influence of FITC-SPIF loading levels on CDR, swelling behaviour, and Korsmeyer-Peppas modelling.

Formulations	HAOX (mg mL^{-1})	CSOX (mg mL^{-1})	FITC-SPIF (□g mL^{-1})	PDHA (mg mL^{-1})	pH
HACOX_37	10	10	100	0.465	6.8
HACOX_37_250	10	10	250	0.465	6.8
HACOX_37_500	10	10	500	0.465	6.8

Table 3.4 Development of HACOX_37: Influence of CSOX concentration on CDR, swelling behaviour, and Korsmeyer-Peppas modelling.

Formulations	HAOX (mg mL^{-1})	CSOX (mg mL^{-1})	FITC-SPIF (□g mL^{-1})	PDHA (mg mL^{-1})	pH
HACOX_37_250	10	10	250	0.465	6.8
HACOX_47_250	10	20	250	1.49	6.8
HACOX_57_250	10	30	250	2.11	6.8

3.2.3 Preparation of HAOX-based hydrogel (HAOX_15, HAOX_17)

The experimental procedure started by dissolving HAOX in saline containing FITC-SPIF at 60 °C for a duration of 3 h. This solution was then stirred overnight at 25 °C to ensure complete dissolution. In parallel, PDHA (150 mg) was dissolved in 10 mL saline at 25 °C, and the pH was adjusted to either 5 or 6.8 using hydrochloric acid (HCl). Crosslinking process was facilitated by a two-component syringe assembly connected by a luer lock adapter (Fig. 3.6). One syringe was filled with the polymer solution, while the second syringe contained the PDHA solution. Subsequently, equal volumes from both syringes (1:1 ratio) were thoroughly mixed and transferred into a Teflon mold.

The PDHA concentration for section 3.2.2 was determined based on equation (3.2), ensuring a stoichiometric 1:1 ratio between the aldehyde groups on HAOX and hydroxylamine groups on PDHA (Fig. 3.3), thus enabling optimized covalent crosslinking.

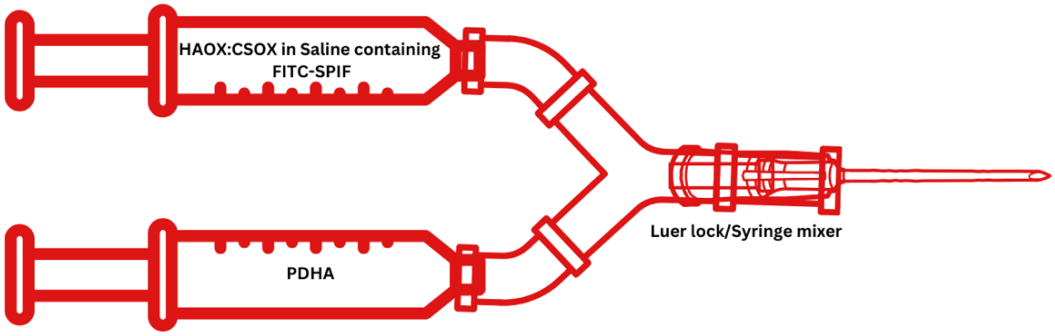

Fig. 3.6: Schematic representation of a dual-syringe configuration connected by luer lock or mixing port for crosslinking process of HAOX-CSOX hydrogel.

3.2.4 Hydrogel preparation for HAOX containing immobilized CSOX

The formulation of DDS featuring a double network composed of HAOX and CSOX began with dissolving both polymers in a saline containing FITC-SPIF at 60 °C for 3 h. The solution was continuously stirred at 25 °C overnight to ensure complete solubilization of the system. The crosslinking process used the same methods as the other formulations, but with a different concentration of crosslinking. The calculation of PDHA concentration accounted for the aldehyde groups present in both HAOX and CSOX, with a consistent 1:1 ratio for crosslinkable groups of both aldehydes and hydroxylamine. The PDHA concentration in Section 3.2.4 was calculated using Equation (3.3).

3.2.5 Gelation time

The gelation time characterization for FITC-SPIF DDS resembles method 3.1.7, differing only in the ratio of the derivatives to the PDHA. A total of 500 µL of the HAOX-CSOX solution was transferred onto the Peltier plate to form four equal droplets; subsequently, 500 µL of PDHA solution was introduced.

3.2.6 Swelling ratio

The swelling ratio (Q) of the FITC-SPIF DDS was measured using the method outlined in section 3.1.8, with 2 mL PBS was selected as the release medium.

3.2.7 Drug release experiment

The drug release quantification for FITC-SPIF followed a methodology analogous to section 3.1.9, with notable differences of UV-vis spectroscopy was used instead of HPLC, and PBS was employed as the release medium. The CDR was calculated using both standard curve and the Limit of detection (LoD) and limit of quantification (LoQ). Both LoD and LoQ are crucial to assess the sensitivity and reliability of the method by defining its operational range. The

calculation of LoD and LoQ follow equation (3.19) and (3.20) based on the methods established by [79–81].

$$LoD = 3\ \frac{S_a}{b} \tag{3.19}$$

$$LoQ = 10\ \frac{S_a}{b} \tag{3.20}$$

In this context, S_a refers to the standard error of the instrument response, whereas b denotes the regression coefficient (slope) of the linier calibration curve.

3.2.8 Mesh size, M_c, and cross-linking density

The calculation of M_c and ξ for FITC-SPIF DDS followed a methodology analogous to section 3.1.10.

3.2.9 Injectability

The measurement of injectability employed a methodology similar to that outlined in section 3.1.11, differing only in the ratio of the derivatives to the PDHA. A solution with equal parts gel-forming solution and PDHA was rested for 10 mins prior to testing with the syringe system.

3.2.10 Viscoelastic properties of the drug delivery system

The rheological analysis of SPIF DDS followed a similar method as described in section 3.1.12.

3.2.11 FITC-SPIF-induced macrophage polarization: an in vitro bioactivity study

The bioactivity of FITC-SPIF released from DDS was evaluated using a macrophage-based inflammation model, with adjustment made as outlined in reference [82]. THP-1 cells were cultured in RPMI medium supplemented with 10% foetal bovine serum, D-Glucose, L-Glutamine, Penicillin/streptomycin, and Sodium Pyruvate, and incubated at 37°C and 5% CO_2. Macrophage differentiation was initiated by 72-h exposure to 100 nM PMA, followed by a 24-hour resting period in complete media with the absence of PMA. After differentiation, the cells were pretreated for 48 h with either fresh solution of FITC-SPIF or FITC-SPIF released from the DDS. The macrophages were then stimulated with TNF-alpha at a concentration of 100 ng mL^{-1}. Triplicate samples were collected for quantitative reverse transcription polymerase chain reaction (qRT-PCR) analysis at two time points: (1) baseline (0 h), immediately following the 48-h FITC-SPIF incubation period but prior to TNF-α exposure), and (2) 6 h post-TNF-α stimulation (54-h total experimental timeline).

The gene expression analysis focused on IFN-γ activation as well as pro-inflammatory genes (CXCL8, PTGS2, TNF, IL-6, and IL-1β) and anti-

inflammatory regulators (IL-10 and TGF-β). Threshold cycle (CT) values were normalized to the endogenous control of housekeeping gene (GAPDH).

3.3 Data processing and statistical approaches

Data were analysed by one-way analysis of variance (ANOVA), considering p-value < 0.05 as statistically significant. Asterisks denote significance levels as follow: * for $p \leq 0.05$, ** for $p \leq 0.01$, *** for $p \leq 0.001$, **** $p \leq 0.00001$, ns for non-significant. Sample size is represented as “n”.

4. RESULT AND DISCUSSION

4.1 In situ injectable hyaluronic acid hydrogel loaded with polyelectrolyte complex for minocycline control release

The clinical application of MN in MS is restricted by its pharmacokinetic drawbacks and burdensome administration, making advanced delivery technologies essential to improve therapeutic outcomes. To mitigate these concerns, this study introduces an injectable hydrogel system incorporating PEC to localize and modulate MN's release. PEC offer a versatile method to construct particulate systems without harsh fabrication techniques. However, the delivery of small molecules via PEC was constrained by rapid release, as their small size facilitates diffusion. To address this challenge, strategies were developed to enhance the retention of small molecules within the PEC matrix, thereby reducing their rapid diffusion and release. As a tetracycline derivative, MN can chelate Ca^{2+} ions while retaining its biological activity. Meanwhile, HAOX, CS, or CSOX are biocompatible polysaccharides native to the ECM tissue. HAOX serves as a base component for the whole DDS to be injectable and stationary, and CS or CSOX provides a high binding affinity for Ca^{2+}. Particularly for CSOX, it also serves as a crosslinkable structure to form immobilized PEC. Then, PDHA acts as the crosslinker for HAOX and CSOX, and Ca^{2+} is leveraged as the bridge to link MN to CS or CSOX. Moreover, GA, as a positively charged biopolymer, can stabilize PEC formation by reacting with CS or CSOX.

This DDS leverages a combination of crosslinkable biopolymers to reduce the burst release commonly associated with conventional formulations, thereby prolonging the therapeutic window and improving patient compliance. Furthermore, the proposed DDS not only enhances the stability of MN but also allows for a more biocompatible system to not elicit harmful immune responses or toxic effects in the body. The design of this DDS plays crucial role in ensuring sustained drug levels for managing disease progression and alleviating symptoms in MS. The simultaneous formation of PECs and the hydrogel matrix may provide a safe and cost-efficient preparation. Additionally, the DDS provides tuneable properties by varying the concentrations of the materials, offering a more effective and patient-friendly treatment option.

Several formulations will be characterized to identify the optimum composition for the MN releasing system (Fig. 4.1). This approach evaluates the influence of several key parameters, including polymer concentration, crosslinking density, and injectability, on the DDS performance. Each formulation is analysed to identify its gelation time, swelling behaviour, drug release kinetics, drug release profile, and biocompatibility. These characterizations help to identify the formulation that not only provides the desired therapeutic efficacy but also ensures stability and safety for prospective clinical applications. This iterative

process will ultimately lead to the development of an optimum and reliable formulation tailored to specific therapeutic needs.

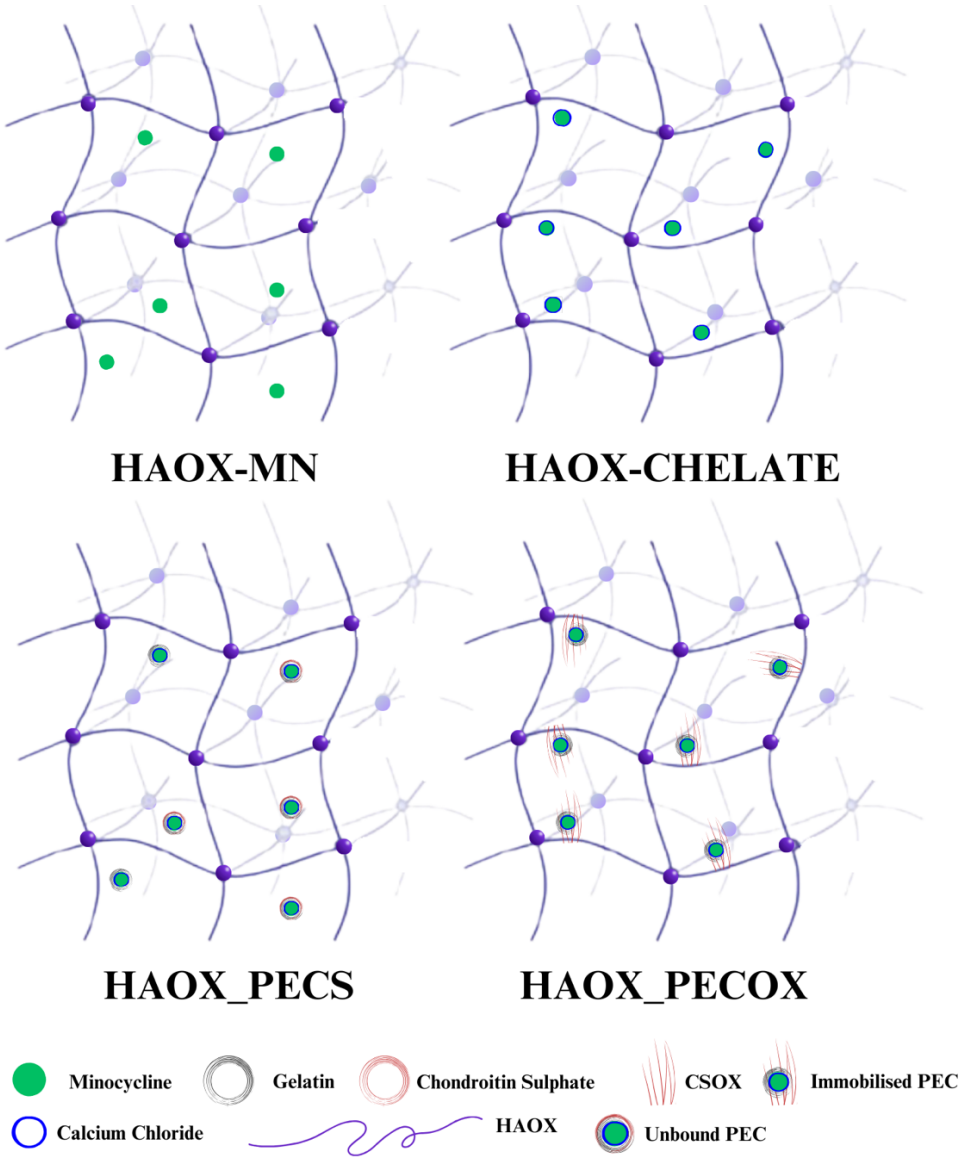

Fig. 4.1: Formulation tested as the drug delivery system for MN control release.

4.1.1 Synthesis of aldehyde-modified chondroitin sulfate (CSOX)

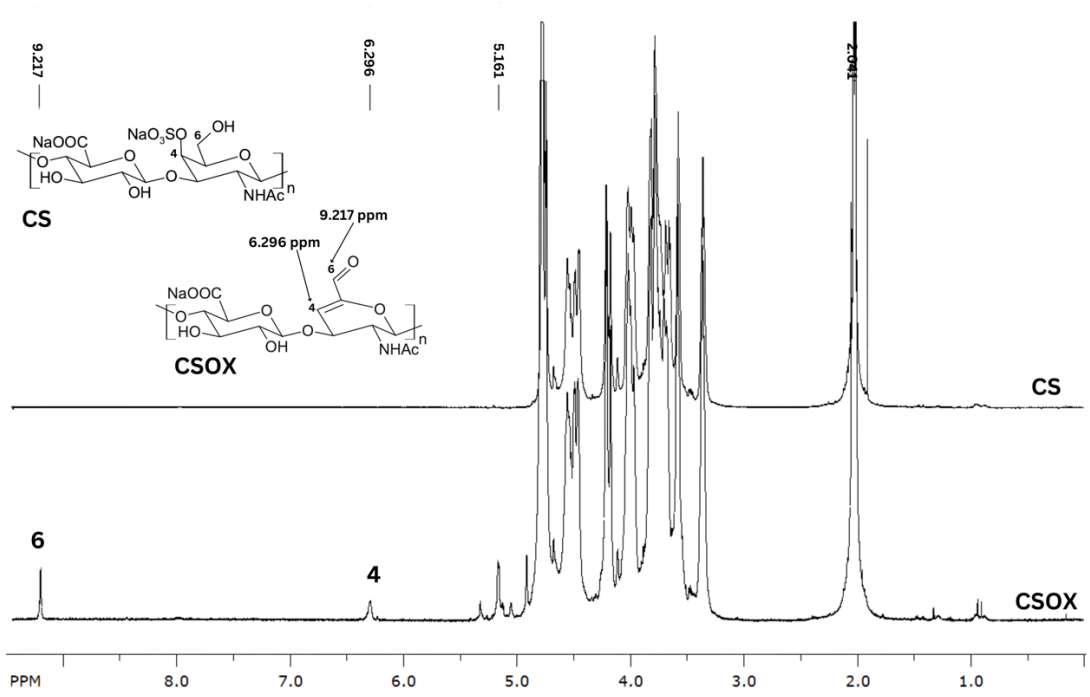

Fig. 4.2: ^{1}H NMR of aldehyde modified chondroitin sulfate.

One-pot synthesis provides a versatile method for polysaccharide modification by allowing simultaneous chemical reactions in a single vessel. The simplified synthesis approach has been proven to reduce extensive purification processes while minimizing the time and resources [62]. This method enables the production of polysaccharides with defined structures to address the issue posed by its inherent heterogeneity. Furthermore, the natural structure underwent regio- and chemo selective modifications to introduce diverse functional groups or structural transformations to enhance their properties for specific applications.

This study used one-pot synthesis to transform CS into CSOX to form immobilized PEC. The selective oxidation process uses TEMPO, NaBr, and NaClO, and the reaction proceeds under mild alkaline conditions that are optimal for the selective oxidation of primary alcohols while leaving secondary alcohols unaffected. TEMPO serves as a source of stable nitroxyl radical that acts as a catalyst in oxidation. Meanwhile, NaBr acts as a co-catalyst that supports oxidation by regenerating nitrosonium ions from TEMPO during the reaction cycle. The nitrosonium ion exhibited regioselective reactivity toward the hydroxyl group located at the C-6 position of the D-galactosamine (GalNAc) residue, facilitating its oxidative elimination to yield a structurally unsaturated product. On the other hand, NaClO maintains the oxidative potential needed to drive the reaction forward by regenerating the nitrosonium ion and bromine species. The

generated CSOX structure (Fig. 3.1) can be crosslinked with the PDHA simultaneously with the HAOX crosslinking process.

^{1}H NMR confirmed the characterization of the CSOX structure by focusing on the proton signals corresponding to the C-4 and C-6 positions, as well as the saturated carboxyl group, which exhibited chemical shifts at 6.296 ppm and 9.217 ppm, respectively (see Fig. 4.2). The spectra showed that the oxidation process with 0.5 molar equivalents of NaClO produced CSOX with a DF of approximately 20%. Furthermore, SEC-MALLS determined the CSOX's molecular mass to be around 12 kDa.

The one-pot synthesis method offers an efficient strategy for modifying CS without requiring the isolation of intermediates and circumvents multiple protection and deprotection reactions. The approach is not only promoting green technology by minimizing chemical waste [83,84] but is also capable of preserving CS's natural pyranose ring. Disruption in the ring may reduce the biocompatibility associated with cellular recognition, mechanical integrity, and solubility [85]. With yields more significant than 99% [86], this facile chemical reaction has proven to reduce the heterogeneity of polysaccharides, which increases complete structure-activity relationship studies. Thus, detailing its mechanism of action and optimizing further applications. The results underscore the precision and effectiveness of this method in successfully modifying CS, highlighting its potential for further biomedical and material sciences applications.

4.1.2 Interdependent physicomechanical properties: gelation duration and structural resilience for injectable HAOX-based DDS

The design of an *in situ* injectable hydrogel for drug delivery requires integrated approaches to fine-tune gelation duration, structural stability, and clinical practicality. This study systematically evaluated HAOX-based formulations, emphasizing the influence of polymer composition and crosslinking dynamics for functional performance.

Gelation time, pivotal for ensuring injectability and structural integrity, varied significantly across formulations. HAOX and its engineered variants (HAOX-MN, HAOX_PECS, and HAOX_PECOX) achieved rapid gelation within 33 – 50 s (Fig. 4.3). This rapid gelation is consistent with previous studies on HAOX-based systems [87,88], where the high concentration of reactive aldehyde groups in HAOX facilitates efficient crosslinking with PDHA, leading to quick network formation. The comparable gelation times across these formulations ($p > 0.05$) suggest that the inclusion of MN and PEC does not significantly hinder the crosslinking kinetics. This finding aligns with the literature, which highlights the robustness of oxime click chemistry in achieving rapid and efficient gelation for injectable hydrogels [89,90]. In contrast, HAOX-CHELATE, incorporating

calcium-chelated MN, exhibited delayed gelation (≈ 95 s) due to competitive binding of Ca^{2+} ions at HAOX reactive sites, a phenomenon consistent with reports on cation-mediated crosslinking interference [91,92]. The slowest gelation occurred in CSOX-MN (≈ 160 s), where shorter CSOX chains require more time to establish effective intermolecular interactions [71,93]. This experimental evidence corroborates Flory-Huggins's theory, which posits that lower molecular weight polymers exhibit higher diffusivity and reduced entanglement [71], leading to slower network formation and potentially compromising the hydrogel's mechanical properties. The prolonged gelation of CSOX-MN may also contribute to inhomogeneous drug distribution within the matrix, increasing the risk of burst release and suboptimal dosing. Similar outcomes were reported in comparable systems where prolonged gelation compromised homogeneity [94].

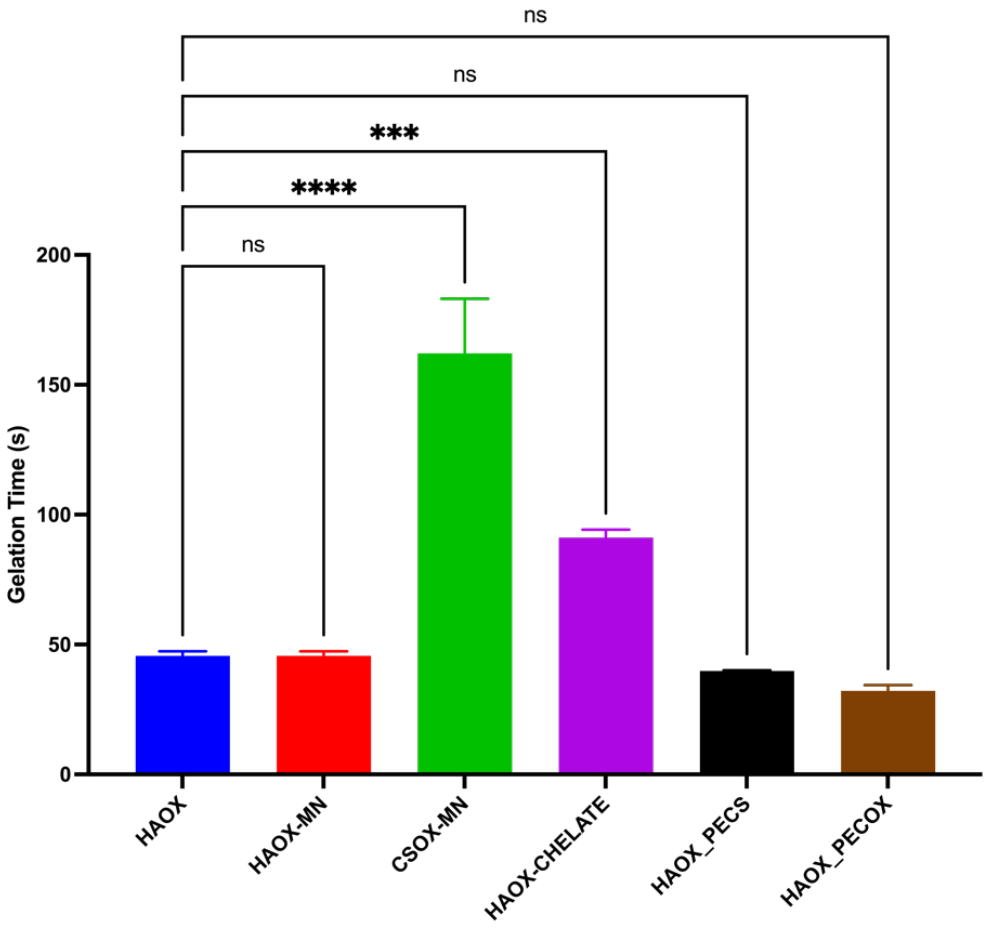

*Fig. 4.3: Comparative assessment of gelation profile for hydrogels based on CSOX, HAOX, and PEC (unbound and immobilized). Result from triplicate trials (n =3) show **** $p < 0.0001$ for CSOX-MN versus PURE HAOX).*

Conversely, while rapid gelation remains clinically desirable, excessively fast crosslinking potentially generates rigid networks with poor conformance to tissue or device geometries [95]. The 30-50 s gelation window observed for HAOX,

HAOX-MN, HAOX_PECS, and HAOX_PECOX corresponds to established clinical benchmarks [96], supporting their suitability for injectable DDS.

Post gelation, the mechanical durability of hydrogel-based DDS is crucial to their clinical utility, as physiological stresses, ranging from shear forces during injection to dynamic tissue interactions, threaten structural integrity and therapeutic performance. Amplitude sweep tests confirmed gel-like behaviour across formulations, with *G'* demonstrating solid like characteristics (Fig. 4.4). The LVE region (30 – 45% strain) revealed a shear-independent *G'* plateau, indicating robust network elasticity. Notably, secondary interactions (e.g., sulfate-mediated electrostatic bonds) did not destabilize the network ($p > 0.05$), contrasting significantly with prior HA systems where additive induced *G'* fluctuations [87,88]. This divergence underscores the advantage of HAOX_PECOX's covalent crosslinking strategy, which integrates CSOX-derived electrostatic interactions without compromising matrix cohesion, a technology unachieved in earlier HA-based DDS.

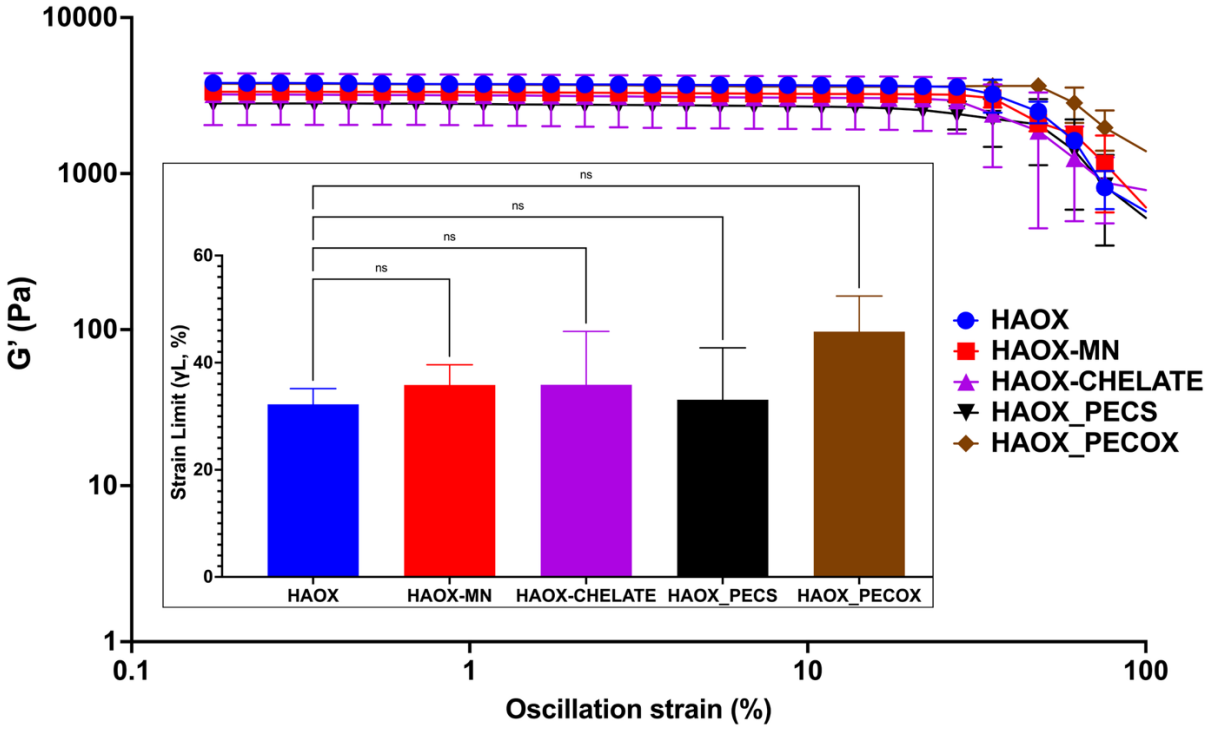

*Fig. 4.4: Comparative analysis of hydrogel viscoelasticity (n=3) across HAOX-based formulations. Main plot: G' averaged across the LVE region (mean ± SD). Inset: strain limit (γL), defined as the strain amplitude where G'deviates >5% from the plateau value. Values represent mean γL (%) per formulation. Significant differences between HAOX_PECS and PURE HAOX indicated (**P ≤ 0.01).*

In this study, HAOX_PECOX demonstrated structural disintegration onset at 45% strain (Fig. 4.4), evidenced by a declining G' characteristic of shear-thinning behaviour. While injectable HA hydrogels generally exhibit similar strain-

dependent disintegration patterns [87,88,97–99], yet the HAOX_PECOX formulation displayed gradual modulus reduction. This behaviour is distinct from the abrupt collapse typical of physically crosslinked system [51,100–102]. This controlled mechanical failure indicates potential tolerance to transient physiological stresses such as tissue compression without catastrophic failure, suggesting critical advantages for long-term implantation durability. The 1 Hz oscillatory testing protocol used for this study, however, may not fully capture frequency-dependent viscoelastic responses relevant to dynamic in vivo environments like pulsatile blood-flow or muscle contraction [99].

LVE data enable predictive modelling of shear behaviour during injection, guiding formulation adjustments to balance injectability with post-injection stability. Injectability integrates hydrogel viscosity, needle geometry, and gelation time to mitigate clogging while optimizing patient comfort. Critical parameters include F_{max} (maximum force to initiate extrusion), P_{max} (maximum fluid stress experienced by the hydrogel inside the syringe/needle), and DGF (steady force for sustained expulsion) [96], which reflect the interplay between rheology and device design.

Table 4.1 Injectability assessment of HAOX_PECOX formulation using dynamic glide force (DGF) and maximum force (F_{max}) metrics (n=3).

Formulation	**Needle size (G)**	**⌀ (mm)**	$\boldsymbol{P_{max}}$ **[kPa]**	$\boldsymbol{F_{max}}$ **[N]**
HAOX_PECOX	18	1.27	358 ± 33	5.8 ± 0.3
	19	1.07	494 ± 67	7.8 ± 1.1
	20	0.9	577 ± 13	9.0 ± 0.2

Symbol definition:
⌀ = Inner diameter of the needle.

Injectability analysis of HAOX_PECOX demonstrated a robust linear correlation ($R^2 > 0.95$, Fig. 4.5) between decreasing needle diameter and increasing DGF, adhering to Hagen-Poiseuille principles (Table 4.1). The Hagen-Poiseuille's theory provides a foundational understanding in injectability, revealing how pressure, viscosity, and needle geometry govern flow rate and support safe, effective formulation design [103]. For 20 G needle, measured values of F_{max}= (9.0 ± 0.2) N and DGF = (8.0 ± 1.0) N remained below the established 40 N patient comfort threshold [96]. The formulation's gradual viscosity elevation prevented abrupt pressure spikes during injection, effectively mitigating the tissue trauma/extrusion force trade-off inherent to larger needles. Mechanistically, the covalent HAOX-CSOX network maintained structural integrity under shear (evidenced by stable G' plateau), contrasting sharply with conventional HA hydrogel where physical crosslinks enable rapid shear-thinning

and structural recovery [104]. This covalent architecture combined with immobilized PECs represents a significant improvement over physically crosslinked systems, simultaneously resolving the rigidity-injectability paradox while enabling sustained MN release. Unlike thermosensitive PLGA-PEG-PLGA hydrogels requiring specialized devices [50,100,105]), HAOX_PECOX demonstrated compatibility with standard syringes which is a critical advantage for resource-limited settings.

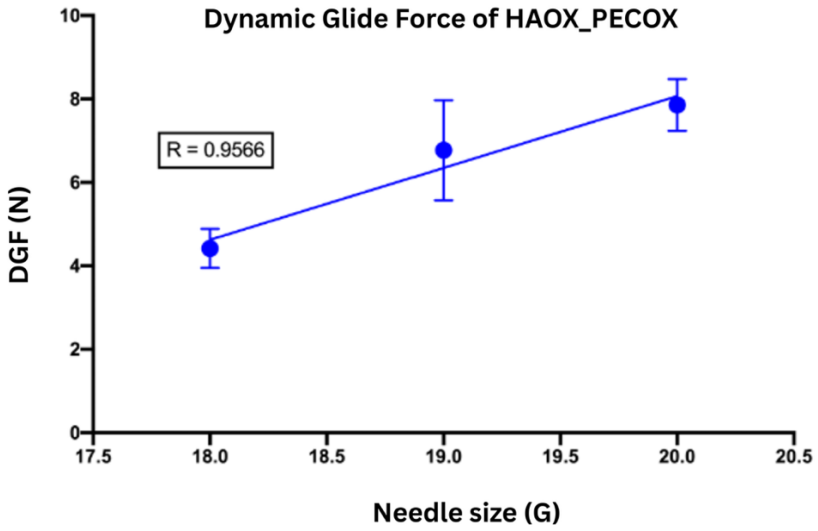

Fig. 4.5: Correlation between DGF and syringe-needle geometry (40 mm needle length). The x-axis denotes needle gauge (G), with corresponding inner diameters provided in Table 4.1.

4.1.3 Minocycline release profiles and the mechanism in injectable HAOX-based drug delivery system

Systemic administration of MN for MS therapy fails to achieve sustained therapeutic concentrations in the CNS due to rapid clearance and limited BBB penetration [32,38]. This limitation underscores the necessity for injectable DDS that potentially balance rapid drug clearance via system localization and symptom management through control release. This study evaluates five distinct formulations (HAOX-MN, CSOX-MN, HAOX-CHELATE, HAOX_PECS, and HAOX_PECOX) for cumulative drug release (CDR), burst release (drug release within first 24 h of DDS exposure to the medium), T50% (time to 50% of release), and Korsmeyer-Peppa modelling, demonstrating how polymer-drug interactions dictate release rate, offering mechanistic insights to optimize DDS design for CNS-targeted therapy.

The HAOX-MN formulation exhibited rapid burst release (50% MN within 24 h; Fig. 4.6 b), attributable to HAOX hydrophilicity and weak drug-polymer interactions. Hydration-induced mesh enlargement facilitated unimpeded diffusion of this small, soluble molecule, yielding 85% cumulative release over 288 h (Fig. 4.6a). This diffusion mechanism parallels observations in comparable

hydrophilic systems [106,107], though HAOX-MN's specific release rate represents a distinct behaviour profile. While the short T50% (≈ 32 h; Fig. 4.7) demonstrates acute-phase utility for conditions like optic neuritis, the limited sustained release constrains chronic management applications. Although the formulation's simplicity raises questions about long-term efficacy, its optimized burst kinetics remain clinically valuable for acute symptom intervention.

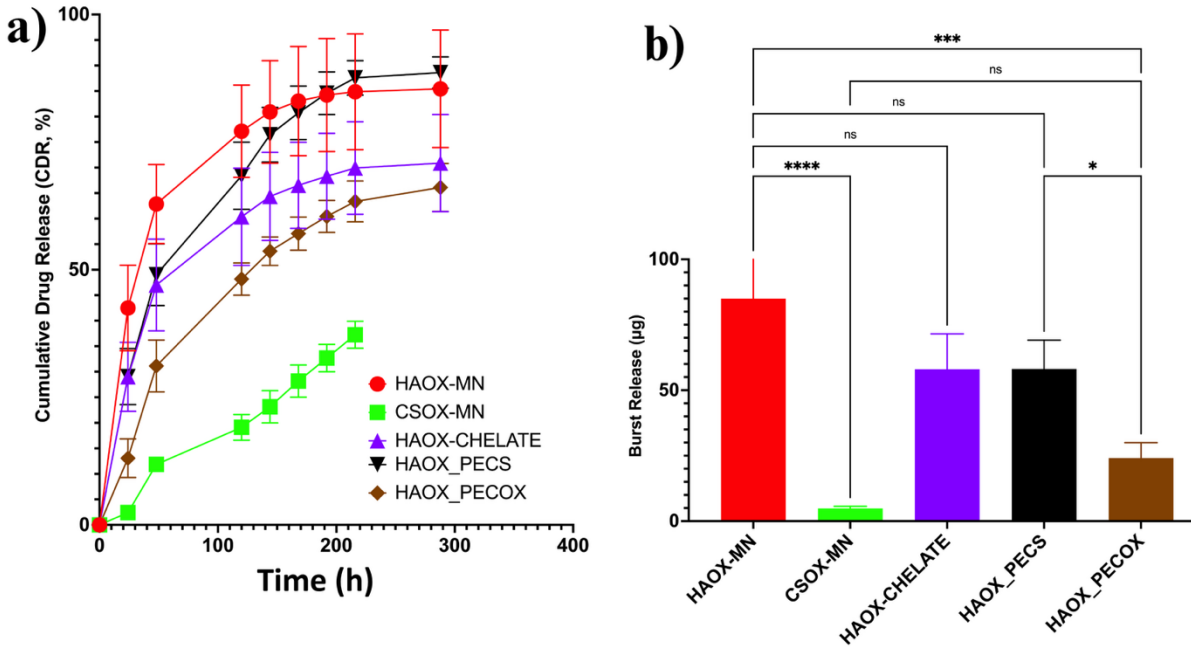

*Fig. 4.6: Sustained and burst-release patterns of minocycline from DDS: Subfigure (a) illustrates time-dependent CDR for HAOX-CSOX hydrogels; Subfigure (b) quantifies burst-release. Statistical analysis (n=3): ** $p < 0.01$, *** $p < 0.001$, ns is non-significant.*

CSOX-MN formulation minimized burst release (2.5% in 24 h; Fig. 4.6 b) through electrostatic interactions between MN's amine groups and CSOX's sulfate moieties. However, sulfate-induced water uptake caused structural instability leading to hydrogel collapse [108,109], limiting cumulative release to 36% over 216 h (Fig. 4.6a). This water sequestration effect, known to retard drug diffusion in hydrogel matrices [110], creates a critical design paradox: sulphated polymers enhance MN retention but risk mechanical integrity under physiological conditions. Although increased polymer molecular weight has been proposed to improve stability [111,112], the observed reduction in drug-loading capacity necessitates careful balance between retention and durability.

Hybrid formulations were developed to reconcile HAOX-MN's burst release with CSOX-MN's sustained profile. HAOX-CHELATE incorporated calcium for MN chelation yet displayed burst and cumulative release (70.6% over 288 h; Fig. 4.6) mirroring HAOX-MN. This behaviour stems from stoichiometric imbalance preventing complete PEC formation. Despite partial release delay (T50% ≈ 46 h;

Fig. 4.7), the formulation's limitations align with fundamental challenges in chelation-based DDS [36,37,53,113,114], particularly regarding precise stoichiometric control identified in prior studies.

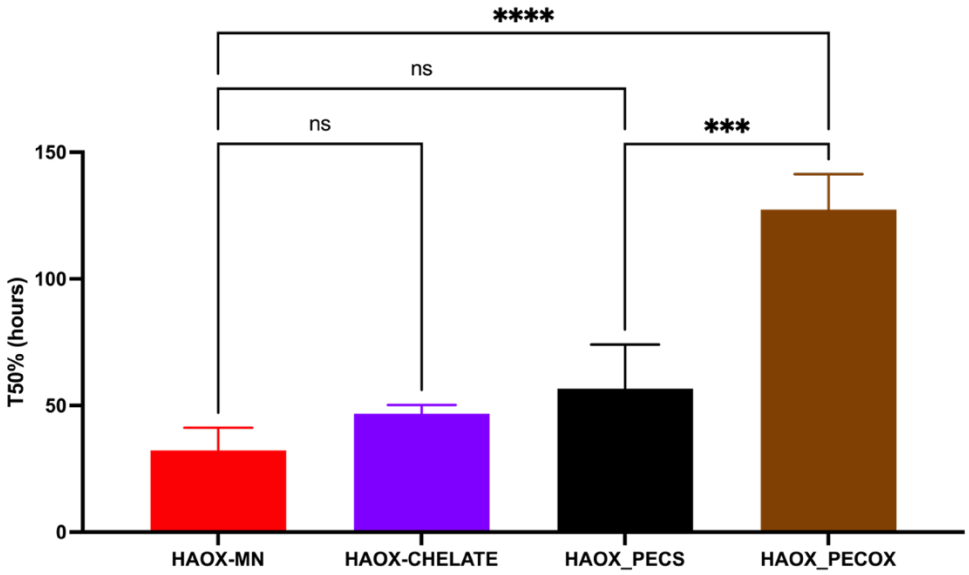

*Fig. 4.7: Comparative assessment of the time to 50% drug release (T50%) across DDS formulation (n =3, ** $p < 0.01$, *** $p < 0.001$, ns is non-significant).*

HAOX_PECS introduced unbound PECs via CS and gelatine (GA), intending to stabilize MN-CA chelates. However, the burst and cumulative release remained high (88.63% over 288 h; Fig. 4.6), suggesting that the ionic interactions between CS and the MN-CA complex were not strong enough to significantly hinder MN solubility. Instead, these interactions may have created a dynamic equilibrium, allowing the PEC to remain soluble in water and facilitating rapid MN release. This finding contrasts with previous studies, which have reported that PEC can effectively reduce burst release by enhancing drug-polymer interactions [36,37]. The discrepancy may be attributed to differences in the composition and concentration of the PEC used in this study, highlighting the need for further optimization of PEC formulations.

The HAOX_PECOX formulation addressed these limitations by immobilizing PECs withing HAOX matrix by substituting CS with CSOX. This approach reduced burst release to 23.6% ($p < 0.001$ vs HAOX-MN; Fig. 4.6 b) and extended T50% to ≈127 h (Fig. 4.7), achieving 65% cumulative release over 288 h (Fig. 4.6 a). Structural stabilization via CSOX substitution enhanced hydrogel integrity, while immobilized PECs created a dense network that hindered MN diffusion by reduced PEC solubility. This prolonged release profile aligns with the demands of chronic MS management, validating its translational potential.

Table 4.2 Korsmeyer-Peppas release fitting across formulations.

Formulations	k	n	R^2
HAOX-MN	0.188 ± 0.07	0.299 ± 0.08	0.994
CSOX-MN	n.a	n.a	n.a
HAOX-CHELATE	0.135 ± 0.04	0.311 ± 0.04	0.991
HAOX_PECS	0.087 ± 0.01	0.461 ± 0.01	0.992
HAOX_PECOX	0.054 ± 0.02	0.520 ± 0.07	0.991

Mechanistic analysis employed the Korsmeyer-Peppas model to quantify release dynamic through the rate constant (k) and diffusion exponent (n) [68,87,88]. This model, restricted to ≤60% cumulative release due to inherent stability assumptions [68,115], excluded CSOX-MN from characterization. Analysis of eligible formulations (Table 4.2) revealed Fickian diffusion ($n < 0.5$) in HAOX-MN (k = 0.188) and HAOX-CHELATE (k = 0.135), indicating MN transport dominated by concentration gradient rather than other mechanisms, such as matrix erosion. Analogous Fickian release kinetics associated with weak drug-polymer interactions have been documented in similar systems [36,116].

Meanwhile, HAOX_PECS exhibited transitional kinetics (n = 0.461), suggesting partial influence of polymer relaxation, while HAOX_PECOX demonstrated anomalous transport (n = 0.520) through combined diffusion and several other intrinsic process, including polymer relaxation and PEC decomplexation [60,117]. This mechanistic heterogeneity underscores the role of DDS architecture in modulating release. For instance, a simpler entrapment strategy produced a higher n. While the model's applicability is restricted to ≤ 60% release data, yet the high R^2 values (0.991 – 0.994) validate its strong correlation between the observed and predicted release rates.

While HAOX_PECOX demonstrated promising prolonged release *in vitro*, its clinical translation requires addressing potential destabilization under physiological conditions. Environmental factors such as ionic strength can destabilize PECs [40,53,114,118], a particular concern for HAOX_PECOX's stability. This risk is evidenced by *in vitro* studies demonstrate that monovalent ions (e.g., Na^+, Li^+) accelerate drug release through weakened electrostatic interactions [119–121], while divalent ions (e.g., Ca^{2+}, Mg^{2+}) enhance PEC stability [36,122]. To directly improve HAOX_PECOX's translational viability, future iterations should integrate counterion modulation strategies. Furthermore, while our current formulation shows favourable release kinetics, *in vivo* validations remain essential to confirm whether these laboratory-observed pharmacokinetics profiles translate to therapeutic efficacy.

4.1.4 Interplay between crosslinking density, swelling behaviour, and sustained MN release in hydrogel-based delivery system

The structural and functional efficacy of hydrogel-based DDS is generated from the intricate balance between crosslinking density, swelling dynamics, and controlled release kinetics. This study demonstrates that while crosslinking density and mesh size traditionally dictate hydrogel behaviour, electrostatic interactions and polymer relaxation mechanism play equally critical roles in modulating drug release profiles. The systematic evaluation of HAOX-CSOX DDS reveals that covalent immobilization of PECs potentially reconciles the competing demands of structural stability and sustained release.

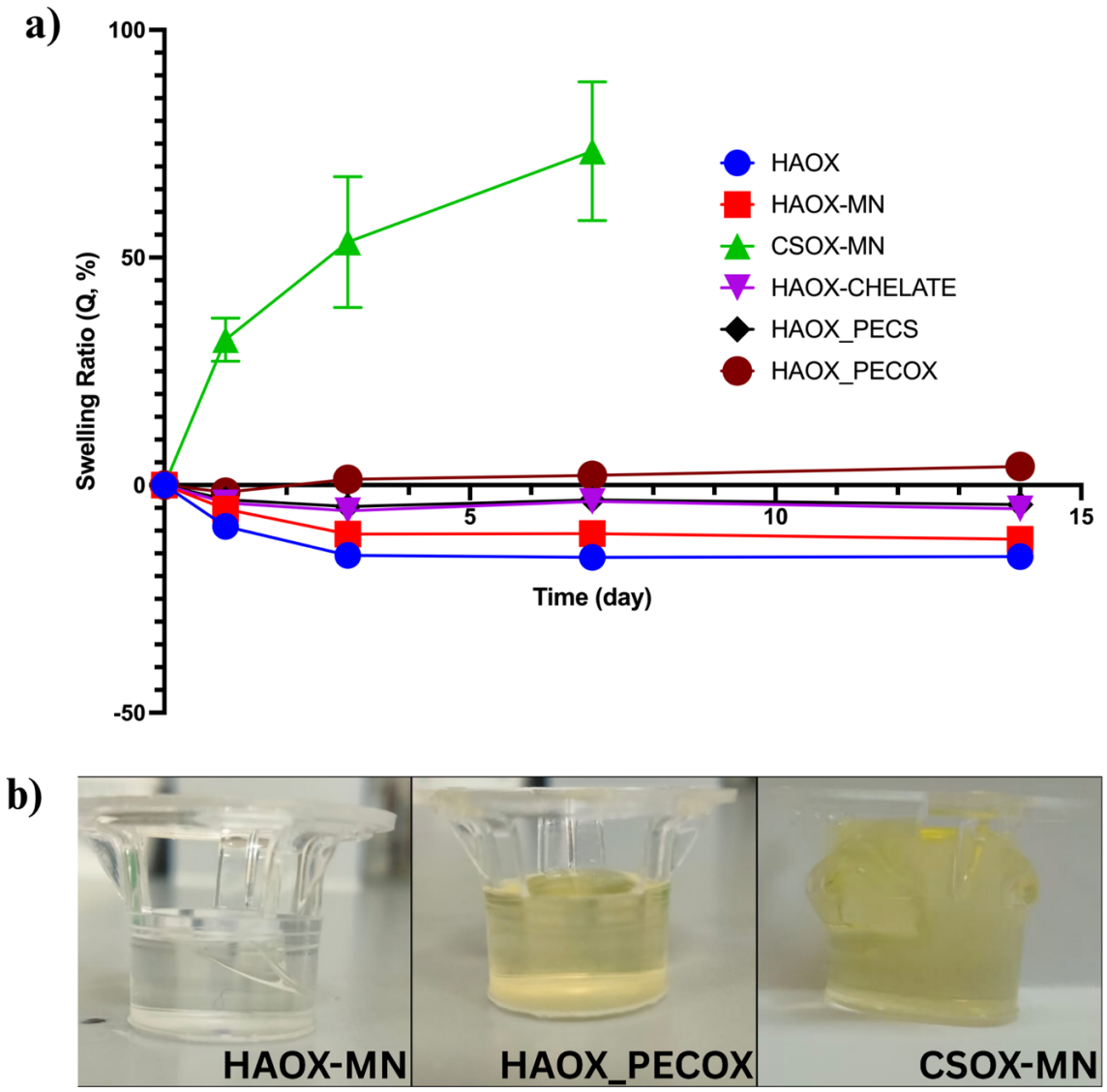

Fig. 4.8:Hydrogel swelling assessment. a) Quantitative swelling profile of DDS formulations (swelling ratio vs. time; n=3). b) Qualitative structural evaluation: HAOX-MN, HAOX_PECOX, and CSOX-MN structural morphology following 7 days in contact with the release medium.

Swelling analysis revealed distinct hydration mechanisms across formulations (Fig. 4.8a,b). HAOX-based hydrogels universally displayed low to non-swelling characteristics, analogous to phenomena reported in crosslinked HA systems [61,87,88,123]. During the initial contact with the release medium (24 h), all formulations except CSOX-MN experienced weight reduction attributed to the leaching of uncrosslinked components. Interestingly, HAOX_PECOX exhibited a slightly higher rate of water uptake despite higher crosslinking density (13.492 ± 0.013 mol m^{-3} versus ≈ 9.5 mol m^{-3} for others; $p < 0.001$, Table 4.3). This distinct behaviour arises from the hydrophilic sulfate groups introduced by covalently anchored CSOX, which enhance hydration without compromising structural coherence. This mechanism aligns with the established principles of sulphated polymer hydration [108].

Experimental confinement within Transwell® inserts were employed to replicate the conditions of an implanted drug reservoir by minimizing multidirectional fluid contact and enforcing unidirectional diffusion across a single interface [124]. Combining this confinement and the retractive forces from crosslinking junctions helps maintain the structural integrity of the hydrogels by reducing water absorption and contributing to asymmetric swelling behaviour [124–127].

Table 4.3 Crosslinking density across different formulations (n=3).

Formulations	**Crosslinking density (mol m^{-3})**
HAOX	9.516 ± 0.026
HAOX-MN	9.438 ± 0.081
HAOX-CHELATE	9.373 ± 0.053
HAOX_PECS	9.248 ± 0.058
HAOX_PECOX	13.492 ± 0.013

In contrast, the crosslinked structure of CSOX-MN (10% w/v) exhibited enhanced sulfate-driven swelling (>50% weight gain; Fig. 4.8b), leading to hydrogel network destabilization after 7-days in contact with the release medium. This enhanced swelling behaviour, while visually manifested as volumetric expansion, compromised structural integrity through two mechanisms: (1) inadequate molecular preventing effective chain entanglement to resist swelling stress, and (2) water retention creating internal osmotic pressure that exceeded the network's yield strength. The resulting structural deterioration (also detailed in Section 4.1.3) hindered sustained MN release by impeding fluid exchange while accelerating stress-induced degradation. This demonstrates the critical need to balance hydrophilicity with crosslinking efficiency to maintain functionality over intended application period.

The analysis of M_c *and* ξ (Table 4.4) using rubber elasticity and equilibrium swelling theories revealed marginal variation in ξ across formulation (275 – 342 nm), insufficient to explain the 3.5-fold difference in MN release rate. HAOX_PECOX, despite its denser network (M_c 93,314 g mol^{-1}, ξ = 279 nm*)*, achieved sustained release over 288 h (k = 0.027; Table 4.2), while HAOX-MN (M_c= 130,222 g mol^{-1}, ξ = 275 nm) exhibited rapid Fickian diffusion (k = 0.168; Table 4.2). This divergence highlights that in low-swelling systems, secondary interactions of PECs override mesh size as the primary release modulator. The immobilized PECs in HAOX_PECOX create electrostatic barriers between sulfate anions and protonated MN at physiological pH, effectively decelerating MN diffusion. Conversely, HAOX-MN's lack of ionic modifiers results in unhindered MN mobility, despite comparable ξ values. These findings challenge conventional view that prioritizes mesh size as the key diffusion determinant [65,128–131] and underscores the proposed contribution of this work: the development of HAOX_PECOX, a formulation that leverages immobilized PECs to reconcile conflicting demands of structural stability and sustained release.

Table 4.4 Mesh size estimations of the DDS formulation by rubber elasticity and equilibrium swelling theory (n=3).

Formulations	**Rubber elasticity theory**		**Equilibrium swelling theory**	
	M_c **(g mol^{-1})**	**ξ (nm)**	M_c **(g mol^{-1})**	**ξ (nm)**
HAOX	(129.2 ± 0.4) x 10^3	317 ± 13	(150 ± 0.002) x 10^3	342 ± 13
HAOX-MN	(130.2 ± 1.3) x 10^3	275 ± 8	(150 ± 0.004) x 10^3	295 ± 7
HAOX-CHELATE	(131.1 ± 0.7) x 10^3	284 ± 2	(150 ± 0.000) x 10^3	304 ± 1
HAOX_PECS	(132.9 ± 0.9) x 10^3	287 ± 4	(150 ± 0.002) x 10^3	304 ± 5
HAOX_PECOX	(93.3 ± 0.01) x 10^3	279 ± 2	(105 ± 0.079) x 10^3	299 ± 2
HAOX	(129.2 ± 0.4) x 10^3	317 ± 13	(150 ± 0.002) x 10^3	342 ± 13

Calculation of M_c and ξ revealed a trend wherein simpler formulation exhibited larger M_c and ξ values. The reduction in both parameters for HAOX_PECOX is attributed to the covalent anchoring of CSOX within the HAOX matrix, which introduces additional crosslinking sites and sulfate-mediated electrostatic interactions (Fig. 4.9).

Furthermore, the uniformity in M_c values for HAOX, HAOX-MN, HAOX-CHELATE, and HAOX_PECS under equilibrium swelling theory (~150,000 g mol^{-1}) arises from fixed parameters (χ = 0.439, V_1=18 cm^3 mol^{-1}) and constrained swelling ratios, which homogenize polymer volume fractions ($v_{2,s}$, $v_{2,r}$) in calculations. In contrast, HAOX_PECOX's covalent anchoring of CSOX introduces structural modifications, reduced M_n (209,000 vs. 300,000 g mol^{-1}), adjusted bond parameters, and additional crosslinking sites that disrupt this uniformity, validating its distinct value. While rubber elasticity theory shows slight M_c variations (129,000 – 132,000 g mol^{-1}), equilibrium swelling's reliance on fixed constants accentuates uniformity. This consistency is not coincidental but a consequence of model limitations.

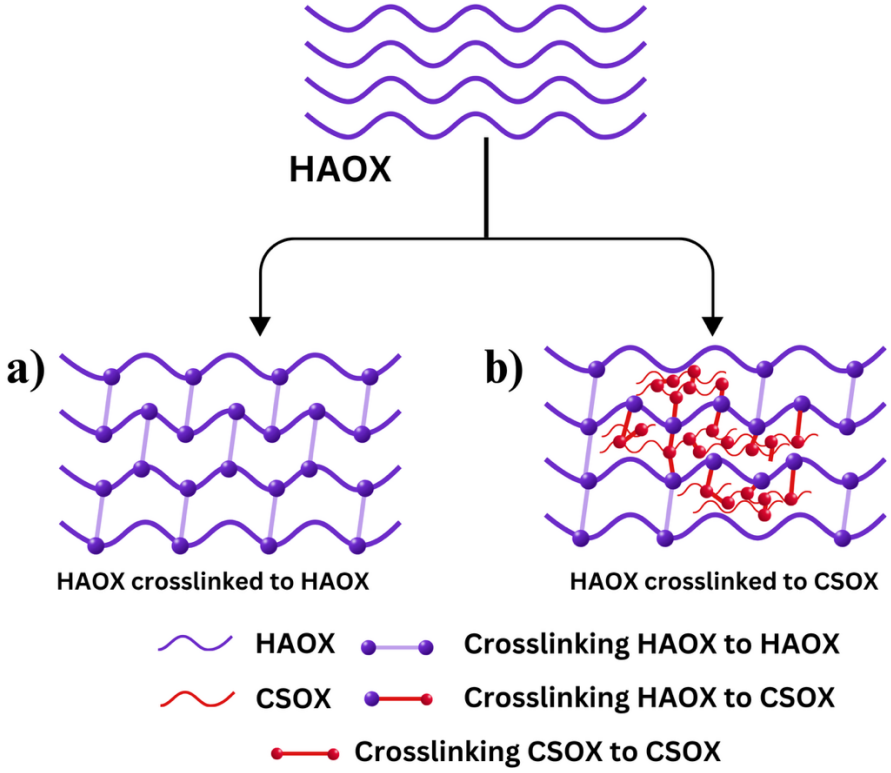

Fig. 4.9: Key structural differences in HAOX hydrogel formulations: a) HAOX-HAOX: Minimal crosslinking and larger mesh size enable fast, diffusion-driven drug release, b) HAOX-CSOX: Enhanced crosslinking density and sulfate-mediated interactions create a tighter network of HAOX-CSOX and CSOX-CSOX, slowing MN diffusion and reducing burst release.

Further validation of the calculations for M_c and ξ derived from both theories is essential for the goodness fit of the models to the formulated DDS network. Equations (3.7) and (3.17) render all calculated values as approximations, as the equations do not consider network defects. Structural defects may be present within the crosslinked network, such as entanglements, closed loops, and loose ends. These malformations do not contribute to network elasticity, which further influences the mechanical properties and moduli. Overall, this situation can

significantly affect the validity of the equations and the calculated M_c values. Currently, direct quantification of ξ under equilibrium conditions remains methodologically unfeasible; existing approaches instead derive estimations through indirect correlations with rheological parameters and swelling data.

4.1.5 Whole blood monocytes activation test (WB-MAT) for minocycline bioactivity analysis

This study evaluated the anti-inflammatory efficacy of MN released from the HAOX_PECOX hydrogel system using a whole blood monocyte activation assay. The objective was to validate whether HAOX_PECOX preserves MN's bioactivity in suppressing interleukin-6 (IL-6), a pro-inflammatory cytokine exacerbated in neuroinflammation during MS [132–134]. Whole blood monocytes isolated from three healthy donors were treated with two experimental groups: (1) release medium from MN-loaded HAOX_PECOX (5 μg mL^{-1} MN), and (2) MN-free HAOX_PECOX release medium (control). Monocytes were stimulated with lipopolysaccharide (LPS) at 1 IU mL^{-1}, a concentration optimized in preliminary dose-response experiments to induce significant IL-6 production ($p < 0.05$; Fig. 4.10a). Preliminary testing also confirmed MN's direct anti-inflammatory activity, significantly reducing LPS-induced IL-6 production (Fig. 4.10b).

Results demonstrated that LPS stimulation significantly increased IL-6 secretion in a concentration dependent manner (Fig. 4.10 a). Critically, monocytes treated with MN-loaded HAOX_PECOX exhibited a 56% reduction in IL-6 levels compared to the MN-free control ($p < 0.05$), confirming MN's retained anti-inflammatory activity post-encapsulation (Fig. 4.10 c).

This finding demonstrates that the HAOX_PECOX system maintains MN's anti-inflammatory activity despite the physical and chemical stresses inherent to hydrogel preparation and injection. Furthermore, this delivery system addresses MN's pharmacokinetic limitations by maintaining its therapeutic activity up to a 6-fold improvement over free drug formulations [78,135]. This aligns with clinical observations of MN's immunomodulatory effects but extends them through controlled delivery paradigms.

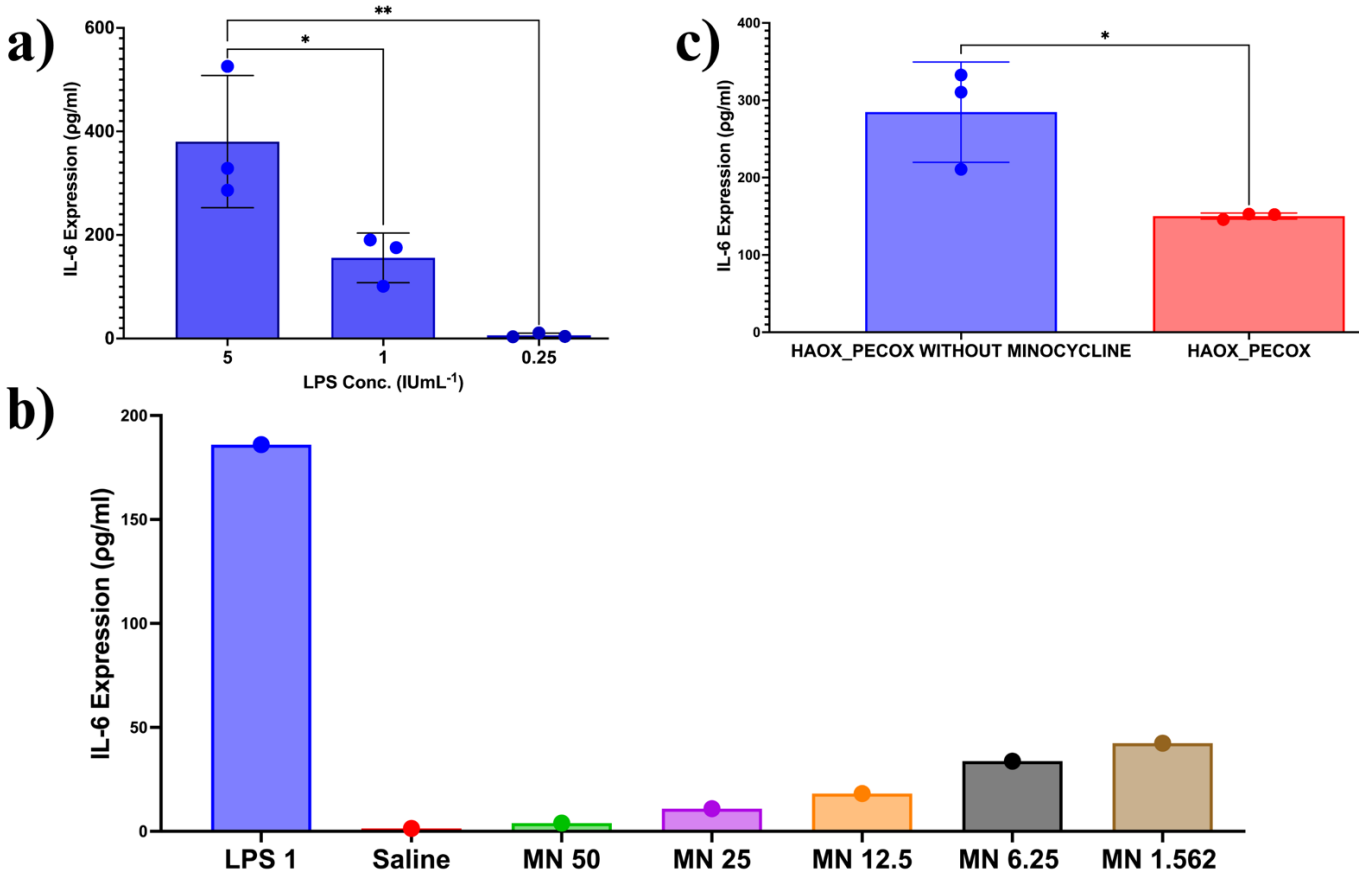

Fig. 4.10: Suppression of LPS-induced IL-6 secretion by MN released from HAOX_PECOX: a) LPS dose-response concentration to provoke substantial IL-6 release (mean ± SD; p <0.05; n = 3 donors). b) a preliminary single- replicate study of IL-6 expression following treatment with 1 IU mL⁻¹ LPS, standard MN solution (50 -1.562 □g mL⁻¹) and saline. All samples, including the saline control, were treated with LPS. Saline demonstrates baseline IL-6 levels despite the presence of LPS, as saline lacks of bioactive components necessary to activate the inflammatory receptors (TLR4/NF-κB pathways). c) Monocytes were exposed to either free MN or MN-loaded HAOX_PECOX release media, followed by stimulation with LPS (1 IU mL⁻¹). Treatment with MN-loaded HAOX_PECOX significantly decreased IL-6 production compared to MN-free HAOX_PECOX (mean ± SD; p < 0.05; n = 3 donors).

4.2 In situ forming hydrogel from aldehyde-modified hyaluronic acid and aldehyde-modified chondroitin sulfate for synthetic preimplantation factor delivery

Recent advancements highlight SPIF's therapeutic promise in addressing neuroinflammatory disease, particularly MS. Despite its potential to cross the BBB and modulate inflammation, its clinical application is hindered by challenges such as enzymatic degradation, short biological half-life, and the need for frequent systemic dosing, which can lead to poor patient adherence and suboptimal therapeutic outcomes. An improved controlled release strategy for SPIF is essential to address these limitations and enhance its therapeutic efficacy in managing chronic inflammatory diseases like MS. Current delivery methods, often reliant on systemic administration, fail to provide sustained drug levels, resulting in rapid clearance and potential toxicity. Meanwhile, MS patients increasingly Favor implantable drug reservoirs for controlled release to reduce dosing frequency and improving quality of life. However, developing such systems requires stable delivery and structural integrity. Thus, there is a critical need for a delivery system that localizes SPIF release, prolongs its therapeutic window, and simplifies administration to enhance patient outcomes.

Building on the application of immobilized PEC within HAOX hydrogel for controlled MN release, as detailed in **Chapter 4.1**, this study investigates the adaptability of the system for FITC-SPIF delivery. While the versatility of this DDS is evident, optimizing its formulation for peptides like FITC-SPIF presents unique challenges due to their charge, hydrophilicity, and susceptibility to aggregation. To address these challenges, strategies were developed to enhance FITC-SPIF retention within the HAOX-CSOX matrix to minimize burst and the rapid diffusion (Fig. 4.11). HAOX serves as the primary component, ensuring injectability and mechanical stability, while the amine residues of FITC-SPIF (presented by lysine and arginine) interact electrostatically with the sulfate groups of CSOX to form PEC. PDHA, a biocompatible crosslinker, further stabilizes the system by crosslinking HAOX and CSOX, creating immobilized PECs for sustained release.

To optimize the system, two key strategies were employed: 1) varying the preparation pH to enhance the charge density of FITC-SPIF, thereby strengthening its interaction with CSOX and achieving more controlled release, and 2) adjusting CSOX concentration to maximize sulfate group availability for improved FITC-SPIF entrapment. These strategies were systematically characterized by evaluating polymer concentration, crosslinking density, injectability, gelation time, swelling behaviour, drug release kinetics, and biocompatibility. The goal was to identify a formulation that balances therapeutic efficacy, stability, and safety. By harnessing the structural and chemical properties

of HAOX and CSOX, this approach effectively addresses the challenges of peptide delivery while enhancing the system's potential for clinical application in managing neuroinflammatory conditions such as MS.

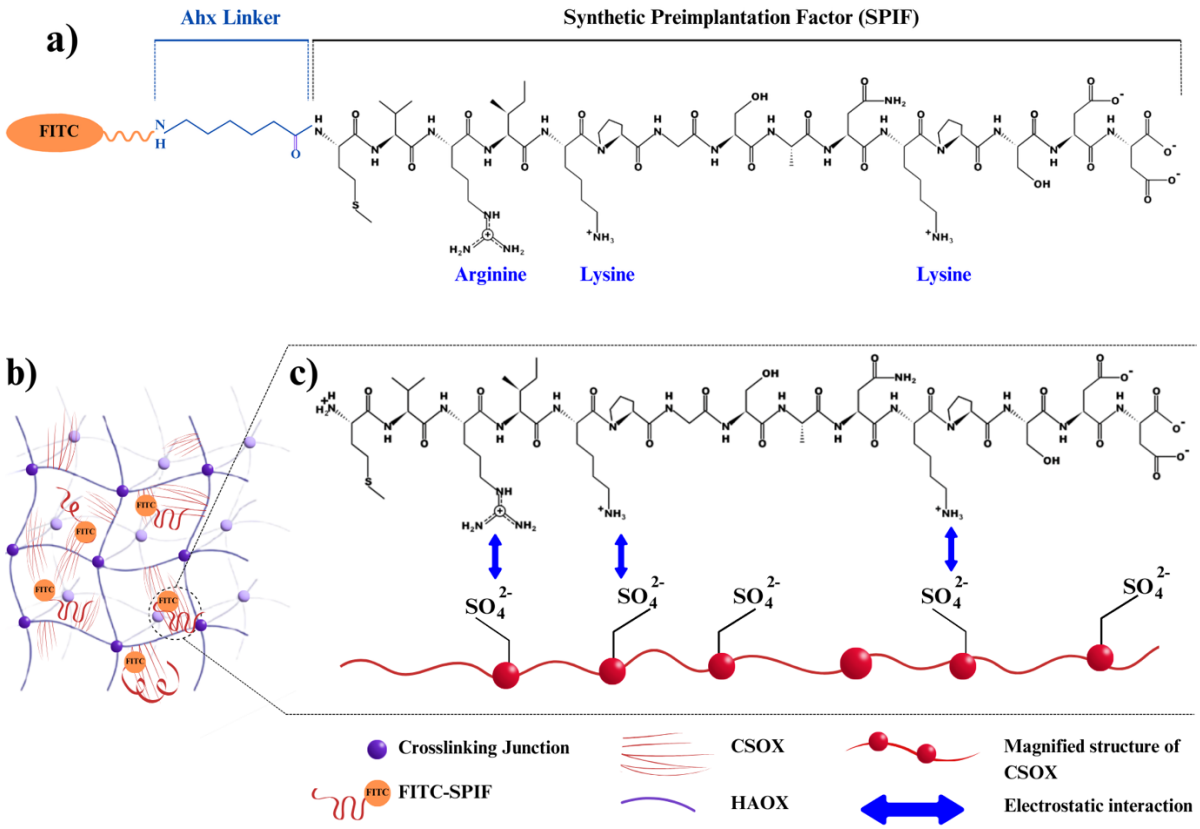

Fig. 4.11: Drug delivery strategy for FITC-SPIF:a) chemical structure of FITC-SPIF, b) DDS prepared from HAOX-CSOX leveraging electrostatic interaction between FITC-SPIF and CSOX, c) zoomed-in view showing electrostatic interactions between FITC-SPIF and the positively charged residues lysine (Lys) and arginine (Arg) as part of the polypeptide chain. The marked region in the left panel corresponds to the interaction site magnified in the right panel.

4.2.1 Gelation time of FITC-SPIF-loaded HAOX-CSOX hydrogels: balancing pH-dependent crosslinking for clinical translation

FITC-SPIF presents considerable challenges for clinical application due to its inherent instability. Unlike conventional systems where peptides often serve as structural components, in this study, FITC-SPIF functions as the therapeutic payload, requiring carriers that balance protective immobilization with bio responsive release. These requirements add complexity to the gelation design, as the system must achieve sufficient fluidity for injectability while ensuring rapid solidification to entrap the drug and prevent premature release. In this study, the gelation dynamics is further influenced by preparation pH and CSOX

concentration, which modulates FITC-SPIF's charge density and its electrostatic interactions with CSOX.

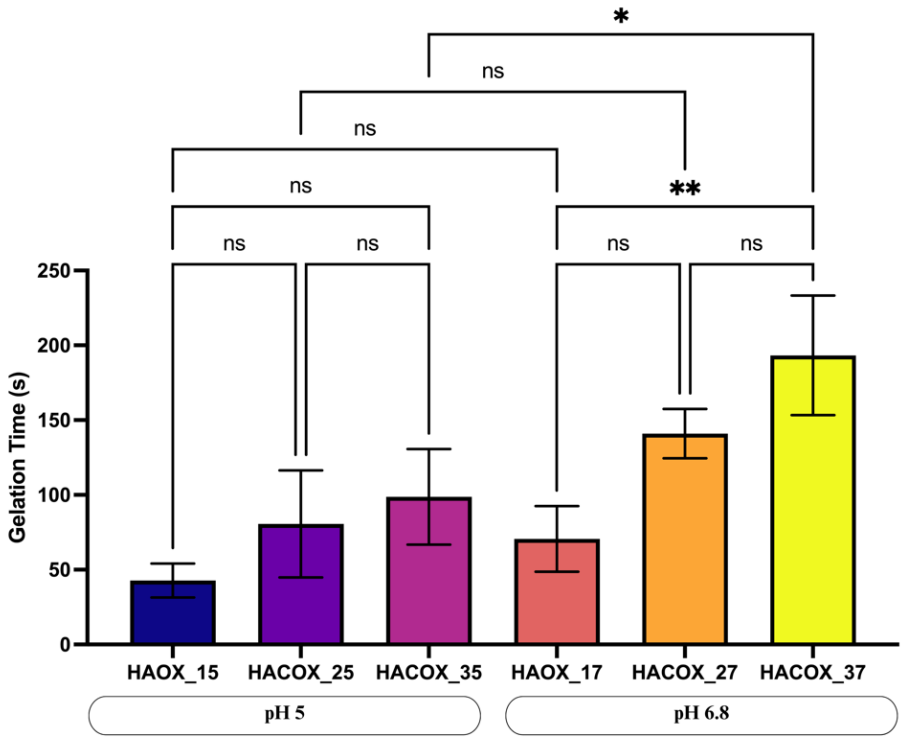

*Fig. 4.12: Gelation time of injectable hydrogels containing FITC-SPIF, measured at two preparation pH values (5.0 and 6.8). Each group includes three formulations with increasing CSOX concentrations: no CSOX (HAOX_15 at pH 5, HAOX_17 at pH 6.8), 0.5% CSOX (HACOX_25, HACOX_27), and 1% CSOX (HACOX_35, HACOX_37). Results represent mean ± SD (n = 3). Statistical significance: *p < 0.05, **p < 0.01, ***p < 0.001, ****p < 0.0001, ns = non-significant.*

The gelation behaviour of HAOX-CSOX hydrogels was profoundly influenced by preparation pH and CSOX concentration, with distinct mechanisms governing network formation under acidic (pH 5) and near-physiological (pH 6.8) conditions (Fig. 4.12). At pH 5, hydrogels exhibited rapid and uniform gelation (74 ± 3 s, $p > 0.05$ across CSOX concentrations), driven by acid-catalysed oxime bond formation between HAOX aldehydes and the crosslinker PDHA. In contrast, at pH 6.8, gelation times varied significantly, ranging from 70 s for HAOX-only formulations (HACOX_17) to 193 s for CSOX-rich systems (HACOX_37, $p < 0.01$). The accelerated gelation at pH 5 where acidic conditions enhance nucleophilic attack by hydroxylamine groups on aldehyde moieties, enabling rapid covalent crosslinking. Similar pH-dependent behaviour has been observed in Schiff base-crosslinked hydrogels, where protonation of amino groups at low pH accelerates imine bond formation [89,136,137]. However, the translational limitation of acidic formulations concerning tissue incompatibility and

inflammation risk renders pH 6.8 formulations clinically imperative, despite their slower kinetics.

Besides variety in pH preparation, the low molecular mass of CSOX (12 kDa) and its high sulfate group density introduce unique challenges and opportunities. The sulfated residues of CSOX enhance electrostatic interactions with FITC-SPIF's cationic amino acids (e.g., lysine and arginine), which can improve peptide loading and retention within the hydrogel. However, CSOX's limited chain length reduces its capacity to participate in effective crosslinking, which can slow network formation. This duality explains why increasing CSOX concentration at pH 6.8 prolonged gelation: the polymer's short chains slowed network formation despite its high charge density. However, the 193 s gelation time observed for HACOX_37 at pH 6.8 aligns with literature-reported ideals (3–5 minutes) for injectable systems concerning the balance between syringe-ability and injectability [138]. This duration accommodates multiple steps in PEC formation, including primary complex assembly, conformational changes via hydrogen bonding, and secondary complex aggregation driven by hydrophobic interactions [114], all of which are essential for optimal drug delivery performance. In contrast, the observed more rapid gelation duration at pH 5 aligns with previously reported values for HAOX-based DDS [87,88], indicating that the acidic pH environment effectively compensates for the low molecular mass of CSOX for the robust network formation.

The transition from acidic to physiological pH in this study mirrors the shift from benchtop optimization to clinical application. While pH 5 formulations demonstrate superior controllability in vitro, their translational potential is limited by the incompatibility of acidic conditions with living tissues. Conversely, the 193-second gelation time of HACOX_37 provides a clinically essential extended injectability window, significantly reducing leakage risk and ensuring spatial confinement to target tissues or implant [138–140]. This extended gelation window differs fundamentally from rapid thermosensitive systems like poloxamer 407, which gels within 10-20 s upon contact with body heat [50]. The system of HAOX-CSOX thus achieves a key clinical requirement: prolonged, tuneable injectability for precise implantation. This attribute is particularly valuable for neuroinflammatory applications, where localized delivery mitigates systemic exposure.

4.2.2 Release study of FITC-SPIF, T50 %, and Korsmeyer-Peppas parameters

The controlled release kinetics of FITC-SPIF from HAOX-CSOX hydrogels were systematically investigated to evaluate the formulation's potential for sustained peptide delivery. HA-based hydrogels have emerged as promising drug delivery platforms due to their inherent biocompatibility and tuneable mechanical properties [46,48,54]. However, their highly hydrated network structure presents

challenges for retaining small hydrophilic peptides such as FITC-SPIF. To address this limitation, PECs were formed between the cationic FITC-SPIF and anionic CSOX, which were subsequently immobilized within a 2% (w/v) HAOX-CSOX hydrogel matrix. This approach leverages electrostatic interactions to modulate drug release while maintaining the injectability essential for clinical applications.

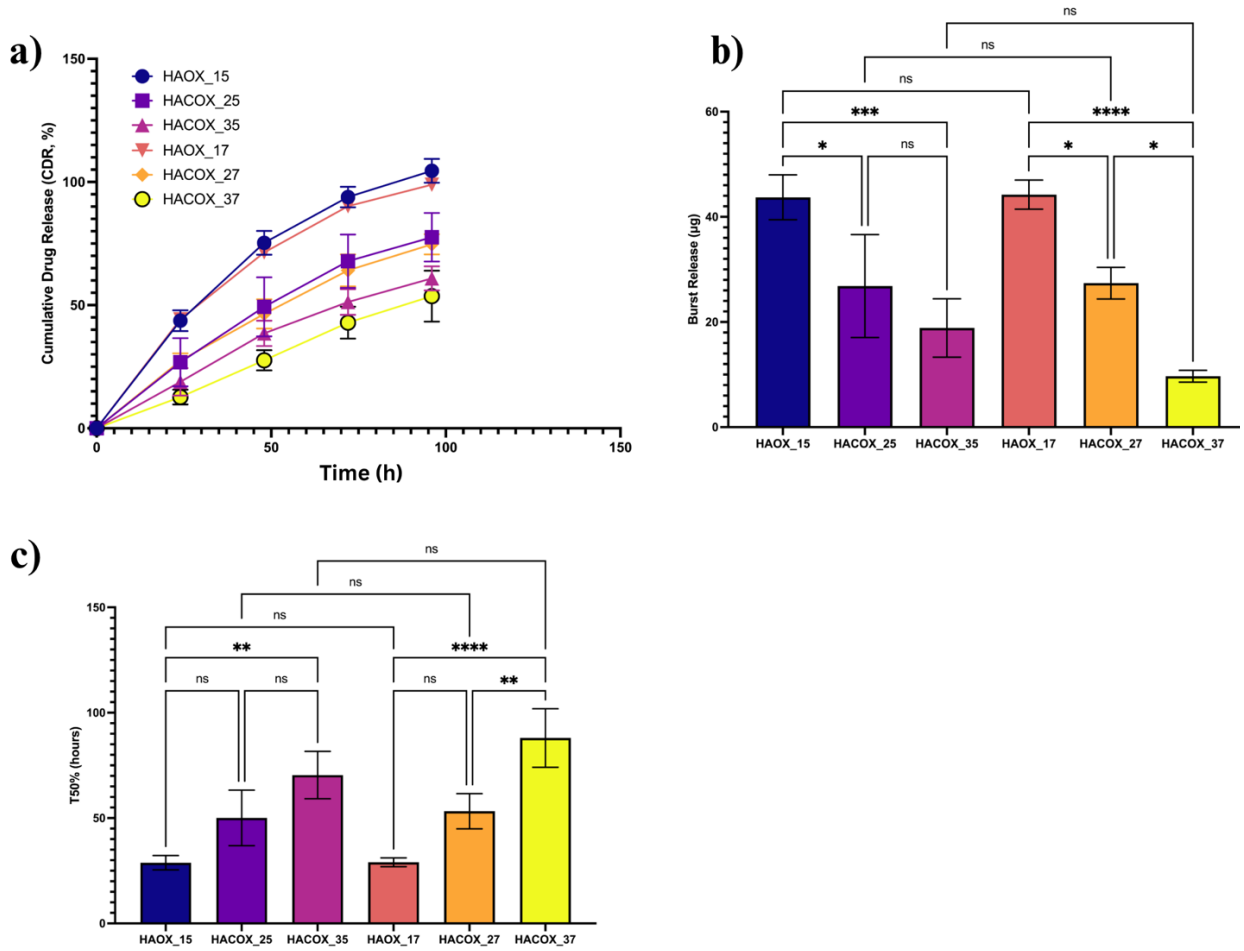

*Fig. 4.13: Drug release profile across different preparation pH and formulation, a) cumulative drug release, b) burst profile, c) T50%. Data are expressed as mean ± SD (n = 3). Significance levels: *p < 0.05, **p < 0.01, ***p < 0.001, ****p < 0.0001, ns = non-significant.*

UV-Vis analysis revealed that CSOX concentration serves as a critical determinant of burst release characteristics (Fig. 4.13). Control formulations lacking CSOX (HAOX_15 and HAOX_17) exhibited high burst, releasing 43–44 µg of FITC-SPIF during the initial 24 h, followed by sustained daily release of 18–20 µg. Incorporation of 0.5% CSOX significantly attenuated burst release: HACOX_25 showed a 40% reduction ($p < 0.05$), with subsequent sustained release of 18 µg per day, while HACOX_27 achieved comparable suppression (38% reduction) and maintained 15 µg per day. Further increasing CSOX to 1% enhanced burst suppression markedly: HACOX_35 and HACOX_37

demonstrated 58% and 78% reductions ($p < 0.001$), respectively, followed by controlled daily release of 14 µg and 13 µg. These findings provide evidence for the role of CSOX in enhancing electrostatic interactions that promote FITC-SPIF retention within the hydrogel network.

The temporal control of drug release was further quantified through determination of T50% values (Fig. 4.13c), exhibiting a distinct concentration-dependent relationship with CSOX content. Formulations without CSOX displayed a T50% of 29 h, while those containing 0.5% CSOX showed extended-release durations of 53 h. The most pronounced extension occurred with 1% CSOX, achieving T50% values of 70 to 88 h. Critically, the daily drug output derived from these release profiles aligns with established therapeutic dosing requirements, matching murine study doses (1 µg g^{-1} for a 20 g mouse) [141] and clinical administration ranges (7-70 µg per dose for 70 kg adults) [44]. This HAOX-CSOX system thus delivers clinically relevant dosing while providing enhanced controlled release relative to conventional single-dose regimens.

Table 4.5 Korsmeyer-Peppas kinetic modelling of FITC-SPIF release from DDS prepared at varied pH levels (n=3).

Formulations	k	n	R^2
HAOX_15	0.037 ± 0.01	0.783 ± 0.05	0.999
HACOX_25	0.020 ± 0.02	0.833 ± 0.16	0.999
HACOX_35	0.018 ± 0.01	0.761 ± 0.08	0.997
HAOX_17	0.050 ± 0.01	0.692 ± 0.07	1.000
HACOX_27	0.025 ± 0.01	0.764 ± 0.09	0.999
HACOX_37	0.008 ± 0.01	0.917 ± 0.08	0.997

Mechanistic analysis using the Korsmeyer-Peppas model (Table 4.5) yielded diffusional exponent values (n) between 0.692 - 0.917. These values indicate anomalous transport behaviour, where drug release is not exclusively dependent on diffusion but is also modulated by additional variables such as solubility, crosslinking density, matrix composition, and intermolecular interactions between FITC-SPIF and the polymeric matrix within the DDS. The kinetic constant (k) exhibited an inverse relationship with CSOX concentration, decreasing by up to 84% in high-CSOX formulations. This reduction correlates with enhanced electrostatic interactions between FITC-SPIF's cationic amino acid residues (lysine and arginine) and CSOX's anionic sulfate groups. These findings align with previous studies demonstrating that sulfate-rich polymers can effectively retard the release of cationic peptides through electrostatic binding [142–144]. In contrast, HAOX-only formulations demonstrated significantly higher k values, attributable to the absence of strong electrostatic retention forces and the favorable aqueous solubility of FITC-SPIF.

The optimized HAOX-CSOX hydrogel system advances peptide therapeutics by addressing two critical challenges: a 78% reduction in burst release and extended therapeutic availability (T50%= 88 h). These improvements hold relevance for MS management, where reduced dosing frequency alleviates patient burden and healthcare costs [20]. Critically, the system maintains pH-insensitive release profile across pH 5–6.8, ensuring consistent performance under physiological conditions. This is achieved by preserving the protonation of FITC-SPIF's cationic residues (lysine pKa ≈ 10.8 [145]; arginine pKa ≈ 13.8 [146]), enabling stable electrostatic interactions with CSOX's sulfate groups. These interactions form PECs acting as drug reservoirs, while the unbound peptide contributes to the burst release phase. This dynamic equilibrium is inversely related to CSOX concentration. Although prolonged gelation (193 s for HACOX_37) presents practical limitations, it ensures PEC stabilization (millisecond-scale formation [147]) and network integration, synergizing with HAOX crosslinking to minimize leakage. This harmonization of injectability with sustained release bridges controlled delivery and clinical needs, positioning it for preclinical validation and potential combination therapies.

4.2.3 Swelling profile and crosslinking density of the drug delivery system

In aqueous or physiological environments, the swelling of hydrogels is primarily governed by osmotic pressure. This force mainly arises from the interplay between polymer hydrophilicity, static charges, and counterions. The same force induces structural shifts capable of modulating drug elution kinetics, where volumetric transitions in the polymer matrix may alter diffusion pathways or interaction dynamics. This situation renders swelling as a critical parameter for optimizing hydrogel performance. Swelling can be tailored by modulating factors such as hydrogel dimension, confinement, and crosslinking density to achieve desired release kinetics. FITC-SPIF release experiments exhibited comparable release profiles at pH 5 and pH 6.8. Although pH 5 provides some insights into pH-dependent behaviour, its relevance is limited due to the lack of significant variations within the tested range. Therefore, swelling studies were conducted exclusively at pH 6.8, as this condition closely mimics the physiological environment in which the DDS is intended to operate.

Central to these findings is the demonstration that increasing CSOX concentration reduces crosslinking density (Table 4.6) while enhancing swelling capacity (Fig. 4.14). This inverse relationship arises from CSOX's hydrophilic hydroxyl (–OH) and sulfate ($–SO_3$) groups, which promote water uptake through hydrogen bonding, as well as its lower molecular weight, which disrupts HAOX chain packing. These results align with prior studies on sulfate-rich polymers like chondroitin sulfate [74,127], where hydration-driven swelling was shown to modulate drug diffusion pathways. However, unlike conventional HA hydrogels

that prioritize effective crosslinking for stability (often at the expense of drug retention), the HAOX-CSOX platform leverages CSOX's unique physicochemical properties to reconcile swelling with sustained release, addressing a key limitation in existing systems.

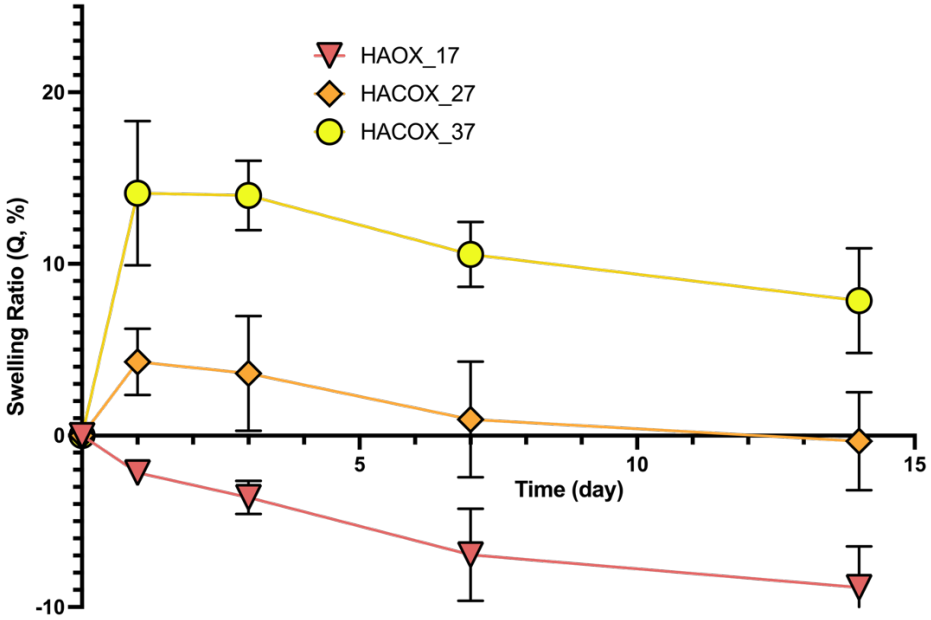

Fig. 4.14: Swelling ratio of formulation prepared at pH 6.8 (n=3).

Table 4.6 Crosslinking density for formulations prepared at pH 6.8 (n=3).

Formulation	**Crosslinking density (mol/m³)**
HAOX_17	8.193 ± 0.023
HACOX_27	6.864 ± 0.014
HACOX_37	5.297 ± 0.076

The minimal to non-swelling characteristics observed across formulations contrast significantly with traditional HA-based hydrogels. Conventional systems typically exhibit higher swelling ratios (>1000%) due to inherent polymers hydrophilicity, leading to structural disintegration and unpredictable drug release profile as reported in prior studies [93,148,149]. This discrepancy underscores the structural benefit of HAOX-CSOX system's: covalent crosslinking via PDHA stabilizes the network, while CSOX's sulfate groups fine-tune hydration without compromising mechanical resilience. For instance, HACOX_37's lower crosslinking density allows greater swelling, yet its sulfate-mediated electrostatic interactions with FITC-SPIF mitigate rapid drug release. This dual functionality

obtained by combining covalent stability with tuneable hydration, resolves the historical compromise between hydrogel swelling and drug retention.

The role of Transwell® inserts in mimicking confined physiological environments further differentiates this study from earlier work. While conventional swelling assays under free conditions often overestimate expansion [87,93,148,149], the Transwell® setup revealed how physical confinement restricts fluid penetration, creating uneven swelling gradients and retractive forces that counteract osmotic pressure [124,127,150]. This confined environment, which is analogous to an implanted reservoir, reduced overall swelling ratios and delayed equilibrium. The semi-permeable membrane of Transwell® allows only a controlled amount of fluid to diffuse into the hydrogel, thus slowing the swelling process. Furthermore, the physical confinement leads to uneven swelling and deswelling kinetics. The hydrogel experiences faster fluid penetration near the insert membrane, resulting in localized swelling, while inner regions swell more slowly due to limited fluid access. During deswelling, outer regions lose water more rapidly, creating a gradient in water content that potentially affects the structural integrity and drug release behaviour. The combination of crosslinking junctions within the hydrogel and the confinement imposed by the Transwell® insert generates retractive forces that counteract swelling [150]. The covalent bonds formed during crosslinking create a network that resists expansion. At the same time, the physical confinement adds an external force that further limits swelling, resulting in a minimal swelling ratio that can be desirable for controlled drug delivery.

The practical and translational implications of these findings are profound. HAOX_17's low swelling and high crosslinking density make it ideal for scenarios demanding rigid, rapid release, while CSOX-enriched formulations like HACOX_37 cater to applications requiring moderate hydration without sacrificing controlled release. This versatility directly addresses patient preferences for implantable DDS that minimize dosing frequency, as emphasized in surveys where 72% of MS patients prioritized reduced treatment burdens [10,11]. Moreover, the system's ability to maintain structural stability under physiological confinement mitigates risks of premature degradation, which recognised as a critical technological refinement over physically crosslinked systems, where rapid swelling often led to burst release and mechanical failure [50,100,105].

4.2.4 Drug delivery system development of HACOX_37: influence of FITC-SPIF loading levels on CDR, swelling behaviour, and Korsmeyer-Peppas parameters

The significant reduction in burst release, prolonged T50%, and physiologically relevant preparation pH in HACOX_37 collectively set a foundation for optimizing the system and improving its potential for enhanced

control release applications. While the 100-µg of FITC-SPIF loading established proof-of-concept efficacy, its clinical relevance can be improved by enhancing the dosing range. Preclinical and clinical studies of SPIF highlight dose-dependent therapeutic effects [24,44,141,151]. To bridge this gap, the hydrogel system should accommodate higher drug payloads without sacrificing controlled release. Increasing the drug concentration will allow us to investigate saturation effects while retaining its core functionality. This section examines the HACOX_37 formulation, with SPIF concentrations systematically increased to 250 µg mL^{-1} (HACOX_37_250) and 500 µg mL^{-1} (HACOX_37_500), to assess their effects on the release profile (Table 3.3).

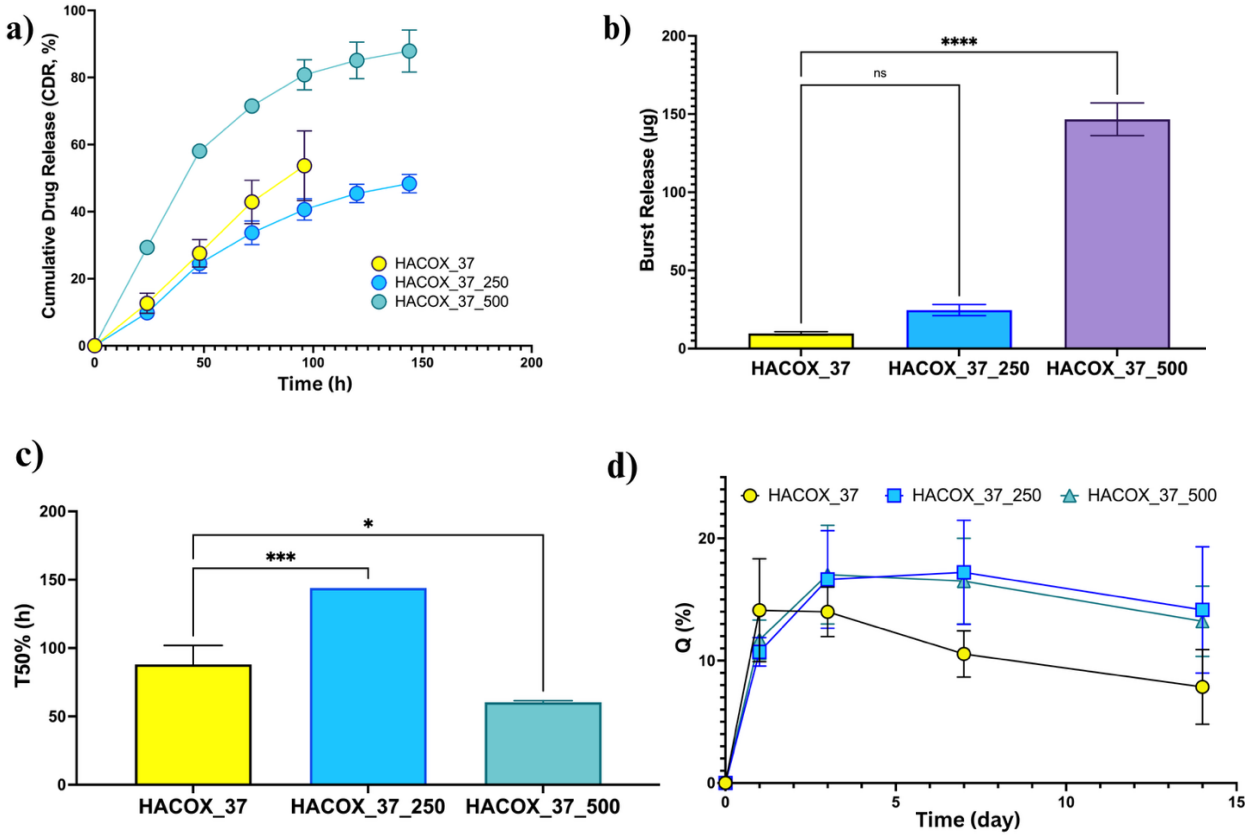

*Fig. 4.15: Influence of FITC-SPIF Loading Levels on a) CDR, b) burst release, c) T50%, and d) swelling ratio. Data are expressed as mean ± SD (n = 3). Significance levels: *p < 0.05, **p < 0.01, ***p < 0.001, ****p < 0.0001, ns = non-significant.*

Figure 4.15 indicates that optimal loading capacity and binding dynamics were achieved at a 1:1 HAOX:CSOX ratio for 100 µg (HACOX_37) and 250 µg FITC-SPIF (HACOX_37_250). No significant differences in burst and cumulative release were observed between these formulations ($p > 0.05$). However, HACOX_37_250 showed a prolonged T50% from 96 h to 144 h ($p < 0.001$), indicating that higher FITC-SPIF loading extends release duration without altering the initial release rate. In contrast, HACOX_37_500 exhibited a 200% increase in burst release, reaching 146 µg ($p < 0.0001$ compared to HACOX_37). Clinically, the 250-µg formulation aligns with Phase I trial dosing (7–70 µg per

adult dose), offering a scalable solution for chronic MS management that reduces dosing frequency while avoiding toxicity risks [44].

Table 4.7 Influence of FITC-SPIF Loading Levels on Korsmeyer-Peppas model fitting (n=3).

Formulations	k	n	R^2
HACOX_37	0.008 ± 0.01	0.917 ± 0.08	0.997
HACOX_37_250	0.021 ± 0.01	0.644 ± 0.05	0.990
HACOX_37_500	0.081 ± 0.02	0.497 ± 0.07	0.986

Table 4.7 presents the Korsmeyer-Peppas analysis of FITC-SPIF release kinetics from HACOX_37 hydrogels. The analysis revealed concentration-dependent release rates (k) as FITC-SPIF loading increased from 100 to 500 μg mL^{-1}, with k rising linearly from 0.08 (HAOX_37) to 0.021 (HACOX_37_250) and 0.081 (HACOX_37_500). Notably, the release mechanism (n) shifted from anomalous transport (non-Fickian) in HAOX_37 and HACOX_37_250 to Fickian diffusion in HACOX_37_500, indicating a transition from coupled diffusion-polymer relaxation to pure diffusion at higher SPIF concentrations. Importantly, because the swelling profiles were comparable across all formulations (Fig. 4.15 d), the observed differences in release kinetics are unlikely to be driven by variations in hydrogel swelling or mesh size. Instead, this shift highlights the role of drug-polymer interactions; at lower FITC-SPIF concentrations, electrostatic interactions between the anionic sulfate groups of CSOX and cationic amino acids of SPIF govern release, resulting in anomalous diffusion. As FITC-SPIF concentration increases (HACOX_37_500) and binding sites become saturated, excess FITC-SPIF molecules diffuse freely through the hydrogel matrix. These findings directly address the clinical imperative for dosing regimens that balance therapeutic efficacy with safety, as emphasized in preclinical studies where SPIF's dose-dependent immunomodulatory effects required precise pharmacokinetic control to avoid cytotoxicity [44,151]. Consequently, HACOX_37_500 risks burst release-induced cytotoxicity and subtherapeutic drug levels post-burst. This highlights the system's unfitness for clinical applications. The rapid initial release of high FITC-SPIF concentrations may overwhelm cellular tolerance thresholds, while the subsequent depletion of release compromises long-term therapeutic activity. These multitude limitations underscore the need for fundamental adjustment in high-load formulations as increased payload is achieved at the cost of release control, rendering such systems ineffective for chronic or acute-phase therapies requiring precise pharmacokinetic modulation.

4.2.5 Development of HACOX_37: influence of CSOX concentration on CDR, swelling behaviour, and Korsmeyer-Peppas parameters

The 250-µg loading (HACOX_37_250) maintained a controlled release similar to the optimized 100 µg formulation but with an extended T50%, making it a promising candidate for optimization. Since the released dosages from HACOX_37_250 also align with preclinical and clinical dosing requirements (e.g., 1–20 µg per day in murine models and 7–70 µg kg^{-1} in human trials), optimizing the system for this loading provides a more targeted and clinically relevant approach. By increasing CSOX concentration relative to a fixed HAOX concentration (total polymer content >2%), this section seeks to enhance the hydrogel's ability to retain and control the release of 250 µg FITC-SPIF. A series of hydrogel formulations were prepared to optimize FITC-SPIF delivery. All formulations maintained a constant HAOX concentration of 1% (w/v). Experimental formulations consisted of 1% HAOX with increasing CSOX concentrations (Table 3.4): 1% CSOX with 1% HAOX (HACOX_37_250), 2% CSOX with 1% HAOX (HACOX_47_250), and 3% CSOX with 1% HAOX (HACOX_57_250). This design allowed a systematic evaluation of CSOX's impact on FITC-SPIF release.

Figure 4.16 shows that adding 1% and 2% CSOX to the HACOX_37 formulation resulted in similar burst release profiles and did not produce a linear trend in sustained release with increasing sulfate content. Although higher CSOX concentrations theoretically offer more sulfate groups for electrostatic interactions with FITC-SPIF's amine residues, the comparable release behaviour of HACOX_37_250 (1% CSOX) and HACOX_47_250 (2% CSOX) suggests that binding site saturation occurs at lower CSOX levels. Once the accessible cationic sites on FITC-SPIF are fully occupied, further increases in CSOX do not enhance peptide retention. This explains the absence of progressive release retardation with higher sulfate content.

Notably, the accelerated release after 48 h and reduced T50% in HACOX_57_250 (3% CSOX) potentially stems from compromised hydrogel matrix integrity. CSOX's low molecular weight (12 kDa) and high sulfate density may disrupt HAOX's crosslinking network at elevated concentrations. Excess CSOX could interfere with integral oxime bond formation between HAOX and CSOX or create steric hindrance, leading to a less cohesive hydrogel structure. This instability allows faster FITC-SPIF diffusion as the matrix degrades prematurely, evidenced by HACOX_57_250 releasing ≈70% of its payload within 120 h compared to ≈50% in HACOX_37_250 and HACOX_47_250.

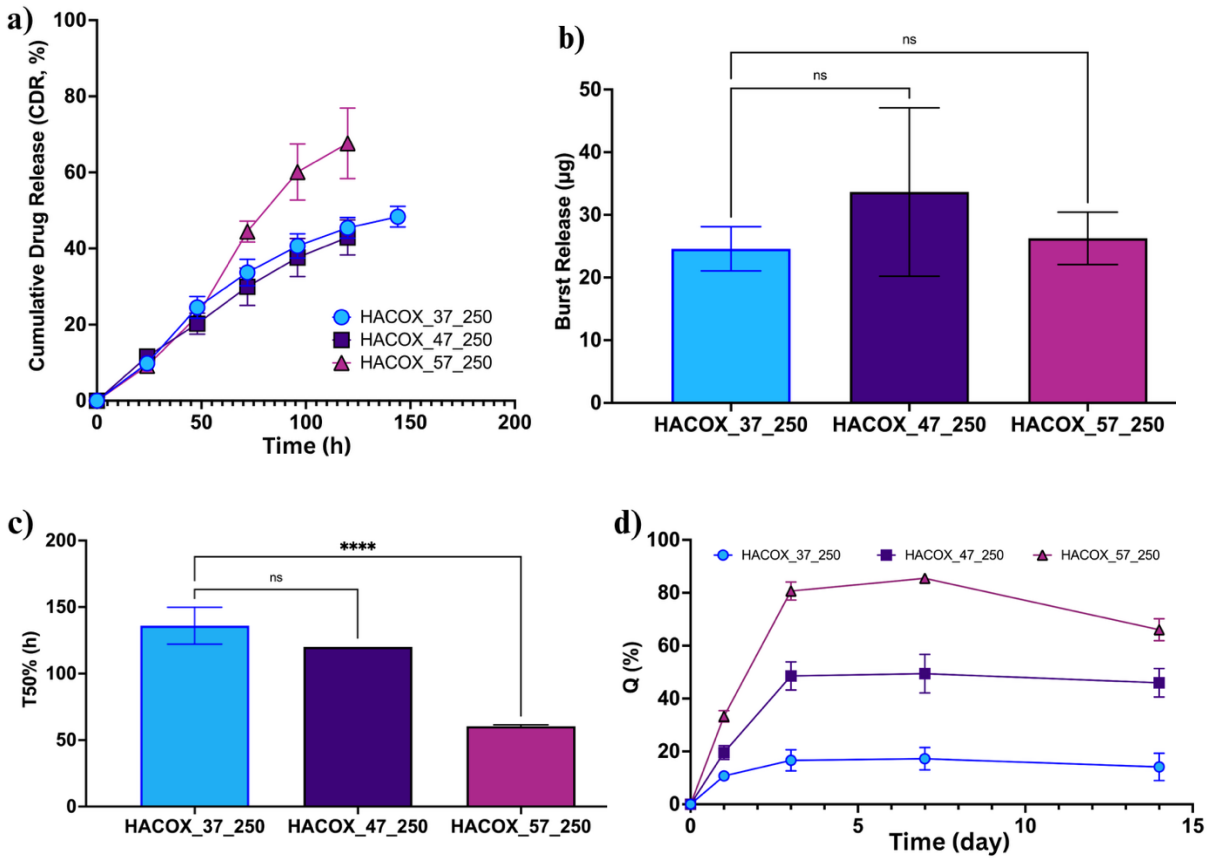

*Fig. 4.16: Influence of CSOX concentrations on a) CDR, b) burst release, c) T50%, and d) swelling ratio. Data are expressed as mean ± SD (n = 3). Significance levels: *p < 0.05, **p < 0.01, ***p < 0.001, ****p < 0.0001, ns = non-significant.*

Table 4.8 Influence of CSOX concentrations on Korsmeyer-Peppas model fitting (n=3).

Formulations	k	n	R^2
HACOX_37_250	0.021 ± 0.01	0.644 ± 0.05	0.990
HACOX_47_250	0.013 ± 0.01	0.739 ± 0.09	0.997
HACOX_57_250	0.004 ± 0.01	1.079 ± 0.11	0.991

The Korsmeyer-Peppas analysis of FITC-SPIF release kinetics (Table 4.8) reveals a concentration-dependent decrease in release rates as CSOX concentration increases from 1% to 3% (w/v), with k values declining linearly from 0.021 (HACOX_37_250) to 0.013 (HACOX_47_250) and 0.004 (HACOX_57_250). This trend is accompanied by a shift in release mechanisms, transitioning from anomalous transport (non-Fickian, $n \approx$ 0.644–0.739) in HACOX_37_250 and HACOX_47_250 to supercase transport ($n \approx$ 1.079) in HACOX_57_250. The significant increase in swelling characteristics with higher CSOX concentrations (Fig. 30 d) plays a critical role in altering release mechanisms. At 1–2% CSOX, the hydrogel maintains a balance between swelling and structural integrity, enabling anomalous transport dominated by coupled

diffusion-polymer relaxation. However, at 3% CSOX, excessive swelling gradually disrupts the matrix. This extreme form of release is characterized by severe structural modifications, where the hydrogel swells beyond its insert and disintegrates, accelerating FITC-SPIF release. The dominance of CSOX at higher concentrations (3%) compromises the structural role of DDS by reducing crosslinking efficiency and matrix durability. This instability profile is reflected in the lowest k value (0.004) and highest cumulative release in HACOX_57_250, as the matrix disintegrates faster under physiological conditions.

The seemingly contradictory observation that HACOX_57_250 exhibits the lowest release rate constant while achieving the highest cumulative FITC-SPIF release can be explained by the interplay of the hydrogel's hydrophilicity, swelling behaviour, and structural integrity. The increased CSOX concentration creates a highly hydrophilic environment within the hydrogel matrix, resulting in significantly greater water uptake compared to HACOX_37_250 and HACOX_47_250. This excessive water absorption restricts drug diffusion, as minimal water exits to facilitate exchange, causing the hydrogel to primarily absorb water rather than release the drug [66,67,152]. The subsequent inability of water removal generates localized stress, which can accelerate structural disintegration. Consequently, as the matrices degrade, the high drug concentration is released, resulting in an overall increase in drug release.

The findings in this study challenge conventional assumptions that higher polyelectrolyte concentrations invariably enhance drug retention, instead revealing a critical threshold beyond which structural compromises outweigh electrostatic benefits. This nonlinear relationship between CSOX concentration and release kinetics diverges from prior studies, where increasing polyelectrolyte content linearly improved drug retention [40,53,122,153]. The HAOX-CSOX system’s covalent crosslinking framework, which was absent in earlier physically crosslinked systems, introduces a significant constraint: excessive CSOX disrupts the PDHA-mediated network, compromising structural cohesion. It is essential to achieve a careful balance between controlled release, sustained therapeutic levels, and long-term stability for effective clinical translation in MS treatment. The HACOX_37 formulation, whether loaded with 100 µg or 250 µg FITC-SPIF, demonstrates a sufficient release profile for both preclinical and clinical applications. However, while HACOX_47_250 offers minor improvements in performance, its increased CSOX concentration adversely affects structural integrity over time. Furthermore, HACOX_57_250's significant matrix swelling and inconsistent drug delivery pose serious risks to both efficacy and safety.

4.2.6 Molecular weight between crosslinks (M_c) and mesh size (ξ) and their roles in release kinetics of FITC-SPIF-loaded drug delivery system

This study analyses the mesh size (ξ) of HAOX-CSOX hydrogels prepared at pH 6.8 with 100 µg FITC-SPIF (Formulation in Table 3.2), using rubber elasticity theory and equilibrium swelling theory. While previous research examined higher FITC-SPIF loads (250 µg) and varying CSOX concentrations (1-3% w/v), the 100 µg formulations serve as a benchmark for controlled release and structural stability, ensuring continuity and comparability across experiments. By strategically revisiting these formulations, this study allows us to isolate the effects of varying HAOX-CSOX concentrations contributing to the rational design of effective DDS by elucidating the relationship between prior release profile observations to intrinsic structural properties.

Table 4.9 Mesh size estimations of the DDS formulation by rubber elasticity and equilibrium swelling theory (n=3).

Formulations	**Rubber elasticity theory**		**Equilibrium swelling theory**	
	M_c (g mol^{-1})	**ξ (nm)**	**M_c (g mol^{-1})**	**ξ (nm)**
HAOX_17	(142 ± 0.4) x 10^3	299 ± 11	(150 ± 0.002) x 10^3	307 ± 11
HACOX_27	(136 ± 1.3) x 10^3	247 ± 4	(139 ± 0.004) x 10^3	250 ± 4
HACOX_37	(126 ± 0.7) x 10^3	201 ± 10	(127 ± 0.005) x 10^3	202 ± 10

The results in Table 4.9 reveal that Increasing CSOX concentration systematically reduces both M_c and ξ. HAOX_17 (0% CSOX) exhibits the highest M_c (142,000 g mol⁻¹) and ξ (299 nm), while HACOX_37 (1% CSOX) shows the lowest values (M_c = 126,000 g mol⁻¹, and ξ = 201 nm). This inverse relationship aligns with established polymer physics principles where low molecular weight polymers like CSOX shorten crosslink distances, tightening the network [129,154]. Crucially, despite significant variations in ξ (up to 34%), the hydrogel's restricted swelling profile minimizes the impact of ξ on diffusion pathways. This decoupling of structural changes from functional performances represents a key system characteristic: ξ variations do not proportionally influences swelling or drug release behaviour.

This deviation from expectations underscores a critical distinction between the HAOX-CSOX system and prior hydrogel designs. Traditional studies, such as those by Rehmann (2017) and Vanoli (2020), emphasize ξ as a key regulator of

diffusion, where smaller mesh sizes restrict drug mobility [65,128]. Yet, in HAOX-CSOX system, HACOX_37's smaller ξ (201 nm) exhibits higher swelling than HAOX_17 (299 nm). This counterintuitive behaviour arises from the hydrophilic nature of hydroxyl (–OH) and sulfate ($–SO_3$) by CSOX, which enhances water uptake despite the tighter network structure. The localized crosslinking behaviour of CSOX, characterized by shorter segments between crosslinks, creates a denser but less cohesive network, contributing to increased swelling. This discrepancy between ξ and swelling behaviour is consistent with previous studies [127,155,156], which report that highly hydrophilic polymers like CSOX can increase swelling even in tightly crosslinked networks. These observations underscore that ξ is not the primary factor governing hydrogel hydration or drug release.

Analysis of FITC-SPIF release kinetics via the Korsmeyer-Peppas model (Chapter 4.2.2) suggests that ξ does not play a dominant role in regulating drug release. All formulations follow anomalous transport (non-Fickian, $n \approx 0.692–0.917$), indicating that the release mechanism is influenced by a combination of factors, potentially PEC decomplexation, diffusion, and polymer relaxation. Despite significant variations in ξ, the consistency in the release mechanism across formulations suggests that ξ is not the primary driver of release kinetics. Instead, the release rate constant (k) varies inversely with CSOX concentration, highlighting the dominant role of electrostatic interactions between FITC-SPIF and CSOX sulfate groups. For example, HACOX_37, with the highest CSOX concentration (1%), exhibits the lowest k value (0.008) and the most controlled release profile, while HAOX_17, with no CSOX, shows the highest k value (0.050) and the fastest release. This inverse relationship between CSOX concentration and k values is consistent with previous studies [153,155,157], which demonstrate that sulfate-rich polymers can effectively retard the release of cationic moieties through electrostatic binding. These findings collectively demonstrate that electrostatic interactions, rather than ξ, modulate FITC-SPIF release.

The limitations of theoretical models in predicting these behaviours further emphasize the system's complexity. While rubber elasticity theory prioritizes mechanical stiffness (yielding lower M_c and ξ estimates) and equilibrium swelling theory accounts for solvent-polymer interactions (yielding higher values), neither fully captures the dynamic interplay of CSOX's hydrophilicity and network defects. CSOX's low molecular weight (12 kDa) promotes localized crosslinking, creating a dense but fragmented network that enhances water uptake while compromising cohesive elasticity, a structural malformation overlooked in idealized models. This aligns with critiques by Rehmann et al. (2017) and Richbourg (2020), who noted that traditional theories often neglect the heterogeneities inherent in natural polymer networks, leading to overestimations of ξ's influence [65,66].

Clinically, the smaller ξ and lower M_c values in HAOX-CSOX are not just structural metrics; they represent a design approach derived from a network optimized for dual functionality. The electrostatic "traps" formed by CSOX's sulfate groups retain FITC-SPIF at therapeutic levels. Simultaneously, covalent crosslinks offer the durability of implantable devices, aligning with patient preferences for autonomy and reduced treatment burden. By localizing delivery, the hydrogel potentially circumvents the hidden costs of systemic DMTs, such as hepatotoxicity monitoring for interferons or immunosuppression risks from anti-CD20 therapies, while reducing drug waste, thereby lowering annual treatment costs that now exceed $43,606 per patient [20]. For MS pathophysiology, sustained SPIF delivery directly targets neuroinflammation and BBB repair, addressing the dual neurodegenerative-inflammatory axes of the disease [2]. In conclusion, the HAOX-CSOX hydrogel transcends traditional reliance on ξ and M_c as predictors of drug release. Instead, it benefits from chemistry-driven control, covering electrostatic retention and covalent stability, to meet MS-specific needs: adherence, safety, and efficacy.

4.2.7 Viscoelastic properties and injectability of the drug delivery system

The viscoelastic properties and injectability of the HAOX-CSOX hydrogel system represent a critical advancement in addressing the dual demands of mechanical stability and patient-centric administration for MS therapy. Increasing CSOX concentration systematically reduces the G' while enhancing strain limits (Fig. 4.17), as demonstrated by HAOX_17 (0% CSOX, G' = 1083.7 Pa, strain limit = 25%) versus HACOX_37 (1% CSOX, G' = 125.7 Pa, strain limit = 245%). This inverse relationship between mechanical rigidity and deformability arises from CSOX's shorter chain length and lower molecular weight, which disrupt HAOX's covalent network, reducing crosslinking density and fostering a more flexible structure. While this compromises absolute mechanical strength, it significantly improves injectability providing a trade-off essential for clinical translation, where rigid hydrogels risk patient discomfort or device failure during administration.

These findings challenge conventional design principles for hydrogel-based DDS, which often prioritize high G' to ensure structural integrity at the expense of practical usability. The HAOX-CSOX platform reconciles these opposing demands by leveraging CSOX's physicochemical properties. Crucially, HACOX_37 achieves injectability within clinically acceptable thresholds (sustained dispensing force = 2.8 N; peak injection force = 2.9 N; Table 4.10), directly addressing MS patients' preference for minimally invasive therapies [10,11]. This contrast with conventional HA-based systems like those reported by Seong (2019) and Chandel (2024) [158,159], where dense crosslinked networks enhance mechanical stability but require high injection forces that limit clinical utility.

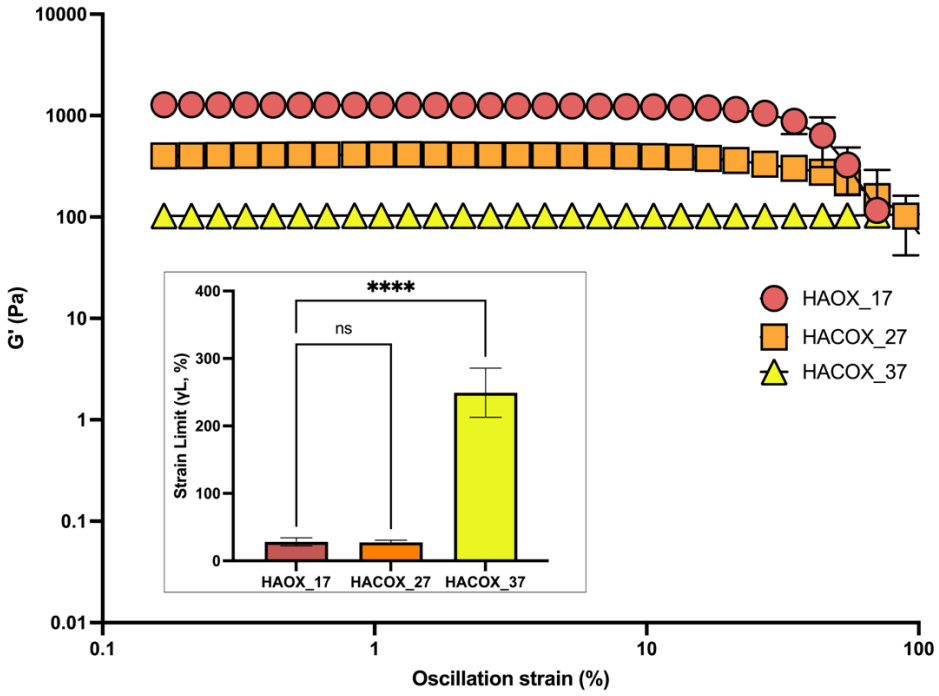

*Fig. 4.17: Rheological characterization of HAOX-CSOX hydrogels prepared at pH 6.8, assessing G' (LVE) and γL. Data derived from triplicate experiments (n=3), with significance levels: *p < 0.05, **p < 0.01, ***p < 0.001, ****p < 0.0001, ns = non-significant.*

Table 4.10 Injectability parameters of HACOX_37, evaluated through dynamic glide force (DGF) and maximum extrusion force (Fmax) (n=3).

Formulation	**Needle size (G)**	**Duration from crosslinking process (s)**	P_{max} **[kPa]**	**DGF (N)**	F_{max} **[N]**
HACOX_37	27	60	185 ± 22	2.8 ± 0.5	3.1 ± 0.3
		180	192 ± 25	2.89 ± 0.4	2.9 ± 0.4

Symbol definition:
$\boldsymbol{P_{max}}$ = Maximum fluid stress experienced by the hydrogel inside the syringe/needle.
$\boldsymbol{F_{max}}$ = Maximum mechanical load applied to the syringe plunger to initiate flow.

The HAOX-CSOX system's performance diverges further from prior systems through its time-dependent viscosity modulation. The gradual increase in P_{max} from 185 kPa (60 s post-crosslinking) to 192 kPa (180 s) reflects controlled gelation kinetics, enabling clinicians to administer the hydrogel within a practical timeframe without risking premature solidification. This balance is absent in thermosensitive or physically crosslinked hydrogels [52,100,105], where excessive flexibility led to the diffusion of structural component. This temporal control, combined with low *DGF* values, ensures smooth injection through

narrow-gauge needles (27 G), mimicking the ease of subcutaneous therapies like glatiramer acetate while avoiding their frequent dosing requirements.

Practically, the viscoelastic of HAOX-CSOX system align with MS's pathophysiological and socioeconomic realities that potentially redefines DDS design. Its ability to harmonize mechanical compliance with injectability directly addresses the clinical imperative for patient-centric therapies which focus on prolonging therapeutic coverage while minimizing intervention. This development not only bridges the gap between preclinical innovation and clinical practicality but also establishes a framework for tailoring hydrogels to the dynamic demands of chronic neurodegenerative diseases. By prioritizing functional adaptability over rigid structural metrics, this work offers a potential of interdisciplinary approaches in advancing MS care.

4.2.8 FITC-SPIF-induced macrophage polarization: an in vitro bioactivity study

MS is a neurodegenerative disease associated with aberrant immune activity that leads to demyelination and cognitive impairment. This hyperactivity of the immune system is primarily driven by the overexpression of adhesion molecules, particularly VCAM-1. VCAM-1 interacts with VLA-4 expressed on macrophages, promoting their polarization toward a pro-inflammatory phenotype and facilitating their trafficking into inflamed tissues [160–162]. As a result, therapeutic strategies targeting VCAM-1 have emerged as potential interventions to disrupt this pathogenic cascade.

Recent studies have indicated that FITC-SPIF may modulate immune responses, although its precise mechanisms are not yet fully understood [82]. This study aims to evaluate the bioactivity of FITC-SPIF by comparing the FITC-SPIF solution with the FITC-SPIF released from HACOX_37. The assessment of bioactivity will involve examining the in vitro capacity of FITC-SPIF to target THP-1 macrophages, specifically focusing on its selective induction of VCAM-1 expression following established method by [82] with modifications. The study will further investigate the influence of released FITC-SPIF on the cytokine's expression dynamics, specifically quantifying pro-inflammatory markers (CXCL8, PTGS2, TNF, IL-6, IL-1β) and anti-inflammatory regulators (IL-10, TGF-β) to assess immunomodulatory outcomes.

This study utilized THP-1 monocytes, a human leukaemia-derived cell line, which were differentiated into macrophages using PMA. Non-activated macrophages were pretreated with FITC-SPIF at concentrations ranging from 3.25 to 50 μg mL^{-1}, or with FITC-SPIF released from HACOX_37, for a duration of 48 hours. Control groups included untreated macrophages and those exposed to a blank DDS medium devoid of FITC-SPIF.

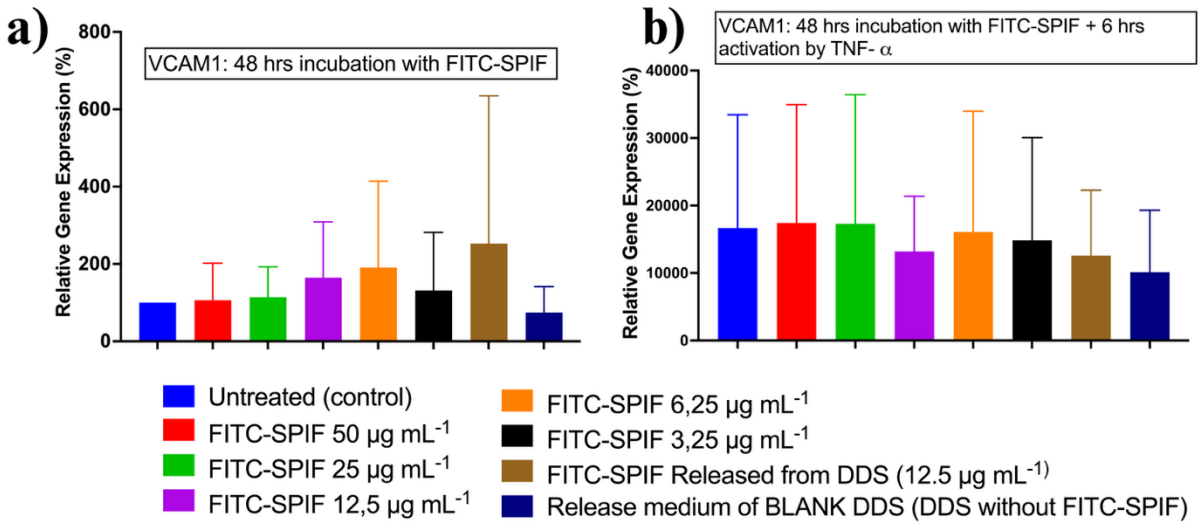

Fig. 4.18: Relative gene expression of VCAM1 from THP-1 macrophages a) before and b) after stimulation with TNF-alpha.

To mimic inflammatory conditions, the macrophages activation was induced using TNF-α at a concentration of 100 ng mL^{-1} for 6 hours. RNA was extracted at both 0- and 6-h post-TNF-α stimulation to assess the expression of pro-inflammatory markers (CXCL8, PTGS2, TNF, IL-6, IL-1β) as well as anti-inflammatory mediators (IL-10, TGF-β). The results were normalized to the housekeeping gene GAPDH to ensure accurate comparisons.

While FITC-SPIF failed to suppress VCAM-1 or pro-inflammatory cytokines (CXCL8, TNF, IL-6, IL-1β) (Fig. 4.18 and 4.19), it uniquely induced a significant increase in TGF-β expression ($p < 0.05$) (Fig. 4.20), regardless of delivery method (free peptide vs. HACOX_37-released). This selective TGF-β upregulation (absent in blank hydrogel controls) suggests a selective macrophage polarization shift toward an M2 phenotype, potentially enabling tissue repair and immunoregulation. The HAOX-CSOX hydrogel successfully preserved FITC-SPIF bioactivity, a critical outcome of its design where PDHA-mediated covalent crosslinking stabilizes against enzymatic degradation while localized delivery prevents systemic dilution. This strategy overcomes limitations of conventional DMTs [13]. However, our *in vitro* model revealed constraints: the absence of VCAM-1 inhibition and isolated suppression of PTGS2 (prostaglandin synthase) underscore the limitations of *in vitro* models in replicating SPIF's multifaceted in vivo effects (embryo protection and neuro-restoration) [24,42].

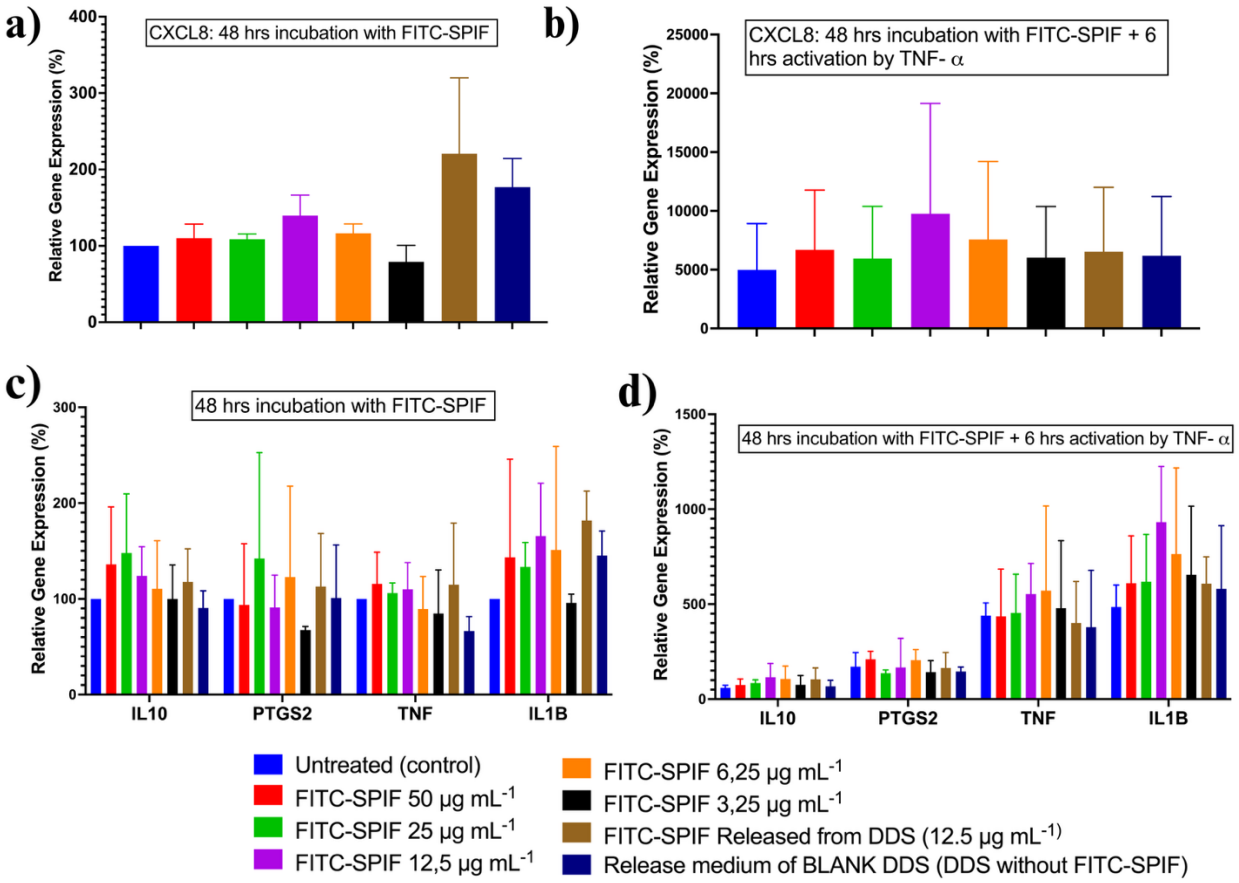

Fig. 4.19: Relative gene expression of a) CXCL8 before stimulation with TNF-alpha, b) CXCL8 after stimulation with TNF-alpha, c) IL-10. PTGS2, TNF, IL-1B before stimulation with TNF-alpha, d) IL-10. PTGS2, TNF, IL-1B after stimulation with TNF-alpha from THP-1 macrophages.

These findings contrast from prior in vivo studies where SPIF demonstrated broad anti-inflammatory effects, including reduced IL-6 and TNF-α in EAE models [41]. The discrepancy likely stems from intrinsic differences between human THP-1 macrophages and murine RAW264.7 cells, which exhibit distinct receptor expression profiles (e.g., VLA-4/VCAM-1 interactions) and cytokine responses. This cell line specificity challenges the translational validity of rodent-derived data and highlights the need for humanized models in MS therapeutic development.

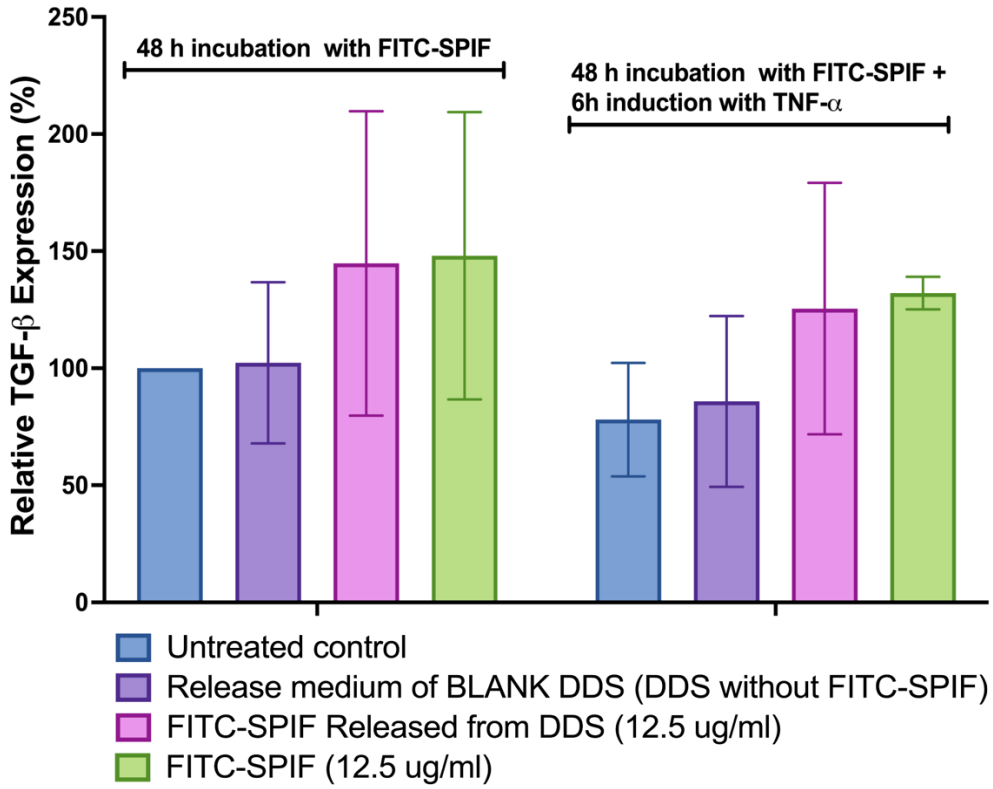

Fig. 4.20: TGF-β expression after treatment with FITC-SPIF.

5. CONCLUSIONS

Managing MS remains challenging, as current DMTs rely heavily on patient adherence despite their clinical benefits. Even with improved delivery systems like autoinjectors and oromucosal sprays, frequent dosing and cognitive demands can burden patients, especially those with fatigue or impairments. Additionally, conventional DMTs often face limitations such as poor pharmacokinetics, fluctuating plasma levels, and increased systemic side effects. An implantable DDS could address these issues by enabling sustained, localized release with minimal patient involvement, providing features strongly preferred by people with MS, according to recent surveys.

This work focuses on addressing the patient's preferences through the design of an injectable hydrogel platform combining HAOX and CSOX. The injectability characteristics of this system allow it to be administered either to implantable devices or directly to the host tissue, enhancing its practical application. The HAOX-CSOX system leverages covalent crosslinking with PDHA to immobilize PECs, creating a structurally stable network capable of entrapping both small molecules (e.g., MN) and short peptides (e.g., FITC-SPIF). By integrating electrostatic interactions, covalent bonding, and tuneable mechanical properties, the platform achieves precise control over drug release kinetics while preserving structural integrity and bioactivity, providing a balance rarely achieved in conventional DDS.

The synthesis of CSOX, a critical component of the PEC, was optimized through a one-pot reaction strategy under mild alkaline conditions. This approach enabled simultaneous oxidation and functionalization of CS, yielding a derivative with a molecular mass of 12 kDa and a 20% degree of functionalization. The preservation of CS's pyranose ring during synthesis ensured biocompatibility and mechanical robustness, while the introduction of aldehyde groups facilitate the immobilization of CSOX onto HAOX matrices via PDHA.

The immobilization of PECs within this network represented a key innovation. For MN delivery, PECs were formed through electrostatic interactions between MN's positively charged amine groups, GA, CA, and the sulfate groups of CSOX. Subsequent covalent crosslinking with PDHA to HAOX stabilized the structure, reducing burst release by 88% compared to unbound PECs and extending the half-release period (T50%) to 127 h. This prolonged release profile is attributed to the synergistic mechanism: the immobilized PEC acts as a primary reservoir responsible for tuning the release kinetic, while the HAOX matrix provides injectable and localised compartment. Importantly, the hydrogel's low swelling ratio (<20%) prevented structural deformation, ensuring consistent drug release kinetics over time. Clinically viable for patient-friendly administration, the system's viscoelastic properties and low extrusion forces facilitate smooth

injection through a 20-gauge needle. The released MN demonstrated a significant 56% suppression of LPS-stimulated IL-6 production, validating HAOX-PEC hydrogel as effective delivery platforms. This outcome underscores that encapsulated MN preserved bioactivity to modulate pro-inflammatory cytokine profiles.

For peptide delivery, the system was adapted to accommodate FITC-SPIF, a short peptide prone to enzymatic degradation. By modulating CSOX concentration, drug entrapment efficiency was maximized, and burst release was reduced from 38% to 78%. Increasing the FITC-SPIF payload from 100 μg to 250 μg further extended the T50% to 144 hours, demonstrating the platform's scalability. Crucially, released FITC-SPIF retained its bioactivity, as evidenced by its ability to induce TGF-β secretion in macrophages, a critical anti-inflammatory response in MS pathophysiology.

Furthermore, the HAOX-CSOX hydrogel distinguishes itself from existing DDS through its simplicity, reproducibility, and versatility. Unlike nanoparticle- or liposome-based systems, which often require complex synthesis steps (e.g., emulsification, solvent evaporation) or chemical modifications (e.g., PEGylation), this platform relies on straightforward polymer interactions to form PEC. The absence of organic solvents or harsh crosslinkers preserves drug integrity, a vital consideration for hindering pro-drug release.

The insights gained from this study reveal the HAOX-CSOX hydrogel platform's potential to meet essential drug delivery objectives for chronic inflammatory conditions like MS. The conducted studies have successfully established a system that achieves prolonged, controlled drug release, ensuring sustained therapeutic levels while significantly reducing the need for frequent patient involvement. By leveraging a synergistic mechanism of immobilized and maintaining structural integrity, the platform minimizes dosing frequency, directly addressing adherence challenges. Furthermore, the system enables localized delivery, confining drug activity to the target site and thereby reducing systemic toxicity, which enhances therapeutic safety. The platform's compatibility with diverse therapeutics has been demonstrated through its adaptability to both small molecules and peptides, highlighting its versatility in accommodating a wide range of drug classes without compromising efficacy. Finally, the system prioritizes minimally invasive administration, offering patient-friendly features such as smooth injectability and rapid gelation, which enhance clinical practicality and patient comfort. Synthesizing these findings propels innovation in controlled-release therapeutics while establishing a framework for bridging preclinical research and clinical applications, offering a promising pathway to enhance therapeutic efficacy in chronic inflammatory disorders.

This study demonstrates the translational potential of hydrogels for sustained drug delivery in MS, yet clinical applicability hinges on overcoming critical preclinical challenges. While *in vitro* findings validate the system's foundational feasibility, the dynamic *in vivo* milieu, marked by enzymatic activity, immune interactions, and mechanical stressors, demand rigorous evaluation of long-term biocompatibility and pharmacokinetics in biologically relevant models, such as EAE mice. Future work must prioritize targeted efficacy metrics (e.g., neuroinhibition, remyelination) and safety profiling to address risks of degradation byproduct accumulation or unintended immunogenicity. Strategically integrating these systems with existing DMTs (e.g., anti-CD20 biologics) or stimuli-responsive drug release mechanisms could further refine therapeutic precision, aligning with the evolving paradigm of personalized MS care. Ultimately, bridging the gap between engineered solutions and clinical viability will require iterative, interdisciplinary collaboration to balance innovation with patient-centred safety and practicality.

This research advances the field of drug delivery by introducing a paradigm-shifting approach to managing chronic inflammatory diseases, such as MS, through the innovative HAOX-CSOX hydrogel platform. This work addresses the critical limitations of current systems, including patient adherence challenges, systemic toxicity, and inflexibility in therapeutic compatibility. As a result, it bridges the gap between advanced material science, pharmacology, and clinical practicality. The platform's ability to deliver sustained, localized therapy while accommodating diverse drug classes underscores its potential to redefine standards in personalized medicine. Beyond its immediate application to MS, the principles of tuneable mechanics, minimally invasive administration, and bioactivity preservation established here offer a framework for addressing unmet needs in other chronic conditions, from neurodegenerative disorders to autoimmune diseases. Ultimately, this study not only contributes a cutting-edge solution but also reinforces the imperative of interdisciplinary innovation in translating laboratory findings into real-world therapeutic impact, paving the way for a future where patient-centric, precision-driven care becomes the critical component of chronic disease management.

REFERENCES

[1] Alhazzani A, Alqahtani M, Alamri N, et al. Treatment satisfaction and adherence to medications among multiple sclerosis patients in Saudi Arabia. Egyptian Journal of Neurology, Psychiatry and Neurosurgery 2019;55:1–7. https://doi.org/10.1186/s41983-019-0095-6.

[2] Sen MK, Almuslehi MSM, Shortland PJ, et al. Revisiting the Pathoetiology of Multiple Sclerosis: Has the Tail Been Wagging the Mouse? Front Immunol 2020;11:1–9. https://doi.org/10.3389/fimmu.2020.572186.

[3] Bandari D, Adamson M, Bowman M, et al. Real-world treatment preferences among health care providers in the United States in selecting disease modifying therapies for patients with multiple sclerosis: a discrete choice experiment. J Med Econ 2023;26:1507–18. https://doi.org/10.1080/13696998.2023.2279883.

[4] Kołtuniuk A, Chojdak-łukasiewicz J. Adherence to Therapy in Patients with Multiple Sclerosis—Review. Int J Environ Res Public Health 2022;19:1–9. https://doi.org/10.3390/ijerph19042203.

[5] Nicholas JA, Edwards NC, Edwards RA, et al. Real-world adherence to, and persistence with, once- and twice-daily oral disease-modifying drugs in patients with multiple sclerosis: A systematic review and meta-analysis. BMC Neurol 2020;20:1–15. https://doi.org/10.1186/s12883-020-01830-0.

[6] Poudel N, Banjara B, Kamau S, et al. Factors influencing patients' willingness-to-pay for disease-modifying therapies for multiple sclerosis. Mult Scler Relat Disord 2021;48:1–5. https://doi.org/10.1016/j.msard.2020.102720.

[7] Bauer B, Brockmeier B, Devonshire V, et al. An international discrete choice experiment assessing patients' preferences for disease-modifying therapy attributes in multiple sclerosis. Neurodegener Dis Manag 2020;10:369–82. https://doi.org/10.2217/nmt-2020-0034.

[8] EMSP. MS Barometer 2020: Assessing the gaps in care for people with multiple sclerosis across Europe. Brussels: 2021.

[9] Tabansky I, Messina MD, Bangeranye C, et al. Advancing drug delivery systems for the treatment of multiple sclerosis. Immunol Res 2015;63:58–69. https://doi.org/10.1007/s12026-015-8719-0.

[10] Visser LA, De Mul M, Redekop WK. Innovative medical technology and the treatment decision-making process in multiple sclerosis: A focus group study to examine patient perspectives. Patient Prefer Adherence 2021;15:927–37. https://doi.org/10.2147/PPA.S306132.

[11] Visser LA, Huls SPI, Uyl-de Groot CA, et al. An implantable device to treat multiple sclerosis: A discrete choice experiment on patient preferences in three European countries. J Neurol Sci 2021;428:1–11. https://doi.org/10.1016/j.jns.2021.117587.

[12] Inojosa H, Proschmann U, Akgün K, et al. The need for a strategic therapeutic approach: multiple sclerosis in check. Ther Adv Chronic Dis 2022;13:1–5. https://doi.org/10.1177/20406223211063032.

[13] Hauser SL, Cree BAC. Treatment of Multiple Sclerosis: A Review. American Journal of Medicine 2020;133:1380–90. https://doi.org/10.1016/j.amjmed.2020.05.049.

[14] Biolato M, Bianco A, Lucchini M, et al. The Disease-Modifying Therapies of Relapsing-Remitting Multiple Sclerosis and Liver Injury: A Narrative Review. CNS Drugs 2021;35:861–80. https://doi.org/10.1007/s40263-021-00842-9.

[15] Moccia M, Loperto I, Lanzillo R, et al. Persistence, adherence, healthcare resource utilisation and costs for interferon Beta in multiple sclerosis: A population-based study in the Campania region (southern Italy). BMC Health Serv Res 2020;20:1. https://doi.org/10.1186/s12913-020-05664-x.

[16] Dello Russo C, Scott KA, Pirmohamed M. Dimethyl fumarate induced lymphopenia in multiple sclerosis: A review of the literature. Pharmacol Ther 2021;219:1–18. https://doi.org/10.1016/j.pharmthera.2020.107710.

[17] Vollmer TL, Cohen JA, Alvarez E, et al. Safety results of administering ocrelizumab per a shorter infusion protocol in patients with primary progressive and relapsing multiple sclerosis. Mult Scler Relat Disord 2020;46:1–6. https://doi.org/10.1016/j.msard.2020.102454.

[18] Kang C, Blair HA. Ofatumumab: A Review in Relapsing Forms of Multiple Sclerosis. Drugs 2022;82:55–62. https://doi.org/10.1007/s40265-021-01650-7.

[19] Paz-Zulueta M, Parás-Bravo P, Cantarero-Prieto D, et al. A literature review of cost-of-illness studies on the economic burden of multiple sclerosis. Mult Scler Relat Disord 2020;43:1–9. https://doi.org/10.1016/j.msard.2020.102162.

[20] Gallehzan NA, Khosravi M, Jamebozorgi K, et al. Cost-utility and cost-effectiveness analysis of disease-modifying drugs of relapsing–remitting multiple sclerosis: a systematic review. Health Econ Rev 2024;14:1–37. https://doi.org/10.1186/s13561-024-00478-7.

[21] Vorobeychik G, Black D, Cooper P, et al. Multiple Sclerosis and Related Challenges to Young women's Health: Canadian Expert Review. Neurodegener Dis Manag 2020;10:1–13. https://doi.org/10.2217/nmt-2020-0010.

[22] De Rosa MC, Purohit R, García-Sosa AT. Drug repurposing: a nexus of innovation, science, and potential. Sci Rep 2023;13:1–3. https://doi.org/10.1038/s41598-023-44264-7.

[23] Alandijany TA, El-Daly MM, Tolah AM, et al. A multi-targeted computational drug discovery approach for repurposing tetracyclines against monkeypox virus. Sci Rep 2023;13:1–20. https://doi.org/10.1038/s41598-023-41820-z.

[24] Spinelli M, Boucard C, Nicuolo F Di, et al. Synthetic PreImplantation Factor (sPIF) reduces inflammation and prevents preterm birth. PLoS One 2020;15:1–14. https://doi.org/10.1371/journal.pone.0232493.

[25] Cheng S, Hou J, Zhang C, et al. Minocycline reduces neuroinflammation but does not ameliorate neuron loss in a mouse model of neurodegeneration. Sci Rep 2015;5:1–11. https://doi.org/10.1038/srep10535.

[26] Clarke EJ, Vodstrcil LA, Plummer EL, et al. Efficacy of Minocycline for the Treatment of Mycoplasma genitalium. Open Forum Infect Dis 2023;10:1–7. https://doi.org/10.1093/ofid/ofad427.

[27] Wang B, Lin W, Zhu H. Minocycline improves the recovery of nerve function and alleviates blood-brain barrier damage by inhibiting endoplasmic reticulum in traumatic brain injury mice model. Eur J Inflamm 2021;19:1–12. https://doi.org/10.1177/20587392211010898.

[28] Bergold PJ, Furhang R, Lawless S. Treating Traumatic Brain Injury with Minocycline. Neurotherapeutics 2023;20:1546–64. https://doi.org/10.1007/s13311-023-01426-9.

[29] Blecharz-Lang KG, Patsouris V, Nieminen-Kelhä M, et al. Minocycline Attenuates Microglia/Macrophage Phagocytic Activity and Inhibits SAH-Induced Neuronal Cell Death and Inflammation. Neurocrit Care 2022;37:410–23. https://doi.org/10.1007/s12028-022-01511-5.

[30] Yune TY, Lee JY, Jung GY, et al. Minocycline alleviates death of oligodendrocytes by inhibiting pro-nerve growth factor production in microglia after spinal cord injury. Journal of Neuroscience 2007;27:7751–61. https://doi.org/10.1523/JNEUROSCI.1661-07.2007.

[31] Garrido-Mesa N, Zarzuelo A, Gálvez J. What is behind the non-antibiotic properties of minocycline? Pharmacol Res 2013;67:18–30. https://doi.org/10.1016/j.phrs.2012.10.006.

[32] Wei C, Liu Y, Jiang A, et al. A pharmacovigilance study of the association between tetracyclines and hepatotoxicity based on Food and Drug Administration adverse event reporting system data. Int J Clin Pharm 2022;44:709–16. https://doi.org/10.1007/s11096-022-01397-5.

[33] Zhang J, Boska M, Zheng Y, et al. Minocycline attenuation of rat corpus callosum abnormality mediated by low-dose lipopolysaccharide-induced microglia activation. J Neuroinflammation 2021;18:1–11. https://doi.org/10.1186/s12974-021-02142-x.

[34] Elewa HF, Hilali R, Hess DC, et al. Minocycline for short-term neuroprotection. Pharmacotherapy 2006;26:515–21. https://doi.org/10.1592/phco.26.4.515.

[35] Metz LM, Li DKB, Traboulsee AL, et al. Trial of Minocycline in a Clinically Isolated Syndrome of Multiple Sclerosis. New England Journal of Medicine 2017;376:2122–33. https://doi.org/10.1056/nejmoa1608889.

[36] Zhang Z, Wang Z, Nong J, et al. Metal ion-assisted self-assembly of complexes for controlled and sustained release of minocycline for biomedical applications. Biofabrication 2015;7:1–11. https://doi.org/10.1088/1758-5090/7/1/015006.

[37] Holmkvist AD, Friberg A, Nilsson UJ, et al. Hydrophobic ion pairing of a minocycline/Ca2+/AOT complex for preparation of drug-loaded PLGA nanoparticles with improved sustained release. Int J Pharm 2016;499:351–7. https://doi.org/10.1016/j.ijpharm.2016.01.011.

[38] Manoharan D, Srinivasan S, Vignesh NR, et al. Tetracyclines: The Old, the New and the Improved - A Short Review. Biomedical and Pharmacology Journal 2023;16:1441–50. https://doi.org/10.13005/bpj/2722.

[39] Zbinovsky V, Chrekian GP. Minocycline. Analytical Profiles of Drug Substances and Excipients 1977;6:323–39. https://doi.org/10.1016/S0099-5428(08)60348-2.

[40] Lv H, Chen Z, Yang X, et al. Layer-by-layer self-assembly of minocycline-loaded chitosan/alginate multilayer on titanium substrates to inhibit biofilm formation. J Dent 2014;42:1464–72. https://doi.org/10.1016/j.jdent.2014.06.003.

[41] Hayrabedyan S, Shainer R, Yekhtin Z, et al. Synthetic PreImplantation Factor (sPIF) induces posttranslational protein modification and reverses paralysis in EAE mice. Sci Rep 2019;9:1–10. https://doi.org/10.1038/s41598-019-48473-x.

[42] Barnea ER, Kirk D, Ramu S, et al. PreImplantation Factor (PIF) orchestrates systemic antiinflammatory response by immune cells: Effect on peripheral blood mononuclear cells. Am J Obstet Gynecol 2012;207:1–10. https://doi.org/10.1016/j.ajog.2012.07.017.

[43] Azar Y, Shainer R, Almogi-Hazan O, et al. PreImplantation Factor Reduces Graft-versus-Host Disease by Regulating Immune Response and Lowering Oxidative Stress (Murine Model). Biology of Blood and Marrow Transplantation 2013;19:519–28. https://doi.org/10.1016/j.bbmt.2012.12.011.

[44] O'Brien CB, Barnea ER, Martin P, et al. Randomized, Double-Blind, Placebo-Controlled, Single Ascending Dose Trial of Synthetic Preimplantation Factor in Autoimmune Hepatitis. Hepatol Commun 2018;2:1235–46. https://doi.org/10.1002/hep4.1239.

[45] Hersh AM, Alomari S, Tyler BM. Crossing the Blood-Brain Barrier: Advances in Nanoparticle Technology for Drug Delivery in Neuro-Oncology. Int J Mol Sci 2022;23:1–28. https://doi.org/10.3390/ijms23084153.

[46] Casey-Power S, Ryan R, Behl G, et al. Hyaluronic Acid: Its Versatile Use in Ocular Drug Delivery with a Specific Focus on Hyaluronic Acid-Based Polyelectrolyte Complexes. Pharmaceutics 2022;14:1–40. https://doi.org/10.3390/pharmaceutics14071479.

[47] Liu B, Chen K. Advances in Hydrogel-Based Drug Delivery Systems. Gels 2024;10:1–26. https://doi.org/10.3390/gels10040262.

[48] Huang G, Huang H. Application of hyaluronic acid as carriers in drug delivery. Drug Deliv 2018;25:766–72. https://doi.org/10.1080/10717544.2018.1450910.

[49] Feng W, Wang Z. Tailoring the Swelling-Shrinkable Behavior of Hydrogels for Biomedical Applications. Advanced Science 2023;10:1–41. https://doi.org/10.1002/advs.202303326.

[50] Wang T, Ma B, Hao G, et al. Temperature-sensitive hydrogel loaded with minocycline hydrochloride complex for accelerating infected wound healing. J Drug Deliv Sci Technol 2023;88:1–13. https://doi.org/10.1016/j.jddst.2023.104961.

[51] Ngwabebhoh FA, Zandraa O, Patwa R, et al. Self-crosslinked chitosan/dialdehyde xanthan gum blended hypromellose hydrogel for the controlled delivery of ampicillin, minocycline and rifampicin. Int J Biol Macromol 2021;167:1468–78. https://doi.org/10.1016/j.ijbiomac.2020.11.100.

[52] Zhu Y, Zhou J, Hu Y, et al. Single subcutaneous injection of the minocycline nanocomposite-loaded thermosensitive hydrogel for the effective attenuation of experimental autoimmune uveitis. Int J Pharm 2022;622:1–9. https://doi.org/10.1016/j.ijpharm.2022.121836.

[53] Zhao J, Wei Y, Xiong J, et al. A multiple controlled-release hydrophilicity minocycline hydrochloride delivery system for the efficient treatment of periodontitis. Int J Pharm 2023;636:1–15. https://doi.org/10.1016/j.ijpharm.2023.122802.

[54] Sharma R, Kuche K, Thakor P, et al. Chondroitin Sulfate: Emerging biomaterial for biopharmaceutical purpose and tissue engineering. Carbohydr Polym 2022;286:1–15. https://doi.org/10.1016/j.carbpol.2022.119305.

[55] Mueller AM, Yoon BH, Sadiq SA. Inhibition of hyaluronan synthesis protects against central nervous system (CNS) autoimmunity and increases CXCL12 expression in the inflamed CNS. Journal of Biological Chemistry 2014;289:22888–99. https://doi.org/10.1074/jbc.M114.559583.

[56] Müller M. Sizing, shaping and pharmaceutical applications of polyelectrolyte complex nanoparticles. Advances in Polymer Science 2014;256:197–260. https://doi.org/10.1007/12_2012_170.

[57] Soliman GM, Choi AO, Maysinger D, et al. Minocycline block copolymer micelles and their anti-inflammatory effects on microglia. Macromol Biosci 2010;10:278–88. https://doi.org/10.1002/mabi.200900259.

[58] Kulkarni AD, Vanjari YH, Sancheti KH, et al. Polyelectrolyte complexes: mechanisms, critical experimental aspects, and applications. Artif Cells Nanomed Biotechnol 2016;44:1615–25. https://doi.org/10.3109/21691401.2015.1129624.

[59] Meka VS, Sing MKG, Pichika MR, et al. A comprehensive review on polyelectrolyte complexes. Drug Discov Today 2017;22:1697–706. https://doi.org/10.1016/j.drudis.2017.06.008.

[60] Achazi K, Haag R, Ballauff M, et al. Understanding the Interaction of Polyelectrolyte Architectures with Proteins and Biosystems. Angewandte Chemie - International Edition 2021;60:3882–904. https://doi.org/10.1002/anie.202006457.

[61] Buffa R, Šedová P, Basarabová I, et al. α,β-Unsaturated aldehyde of hyaluronan - Synthesis, analysis and applications. Carbohydr Polym 2015;134:293–9. https://doi.org/10.1016/j.carbpol.2015.07.084.

[62] Bobula T, Buffa R, Procházková P, et al. One-pot synthesis of α,β-unsaturated polyaldehyde of chondroitin sulfate. Carbohydr Polym 2016;136:1002–9. https://doi.org/10.1016/j.carbpol.2015.10.005.

[63] Šedová P, Buffa R, Kettou S, et al. Preparation of hyaluronan polyaldehyde - A precursor of biopolymer conjugates. Carbohydr Res 2013;371:8–15. https://doi.org/10.1016/j.carres.2013.01.025.

[64] Šedová P, Buffa R, Kočí T, et al. The effect of aminooxy-linkers' structure on the mechanical properties of hyaluronan-oxime hydrogels. Express Polym Lett 2022;16:265–78. https://doi.org/10.3144/EXPRESSPOLYMLETT.2022.21.

[65] Rehmann MS, Skeens KM, Kharkar PM, et al. Tuning and Predicting Mesh Size and Protein Release from Step Growth Hydrogels. Biomacromolecules 2017;18:3131–42. https://doi.org/10.1021/acs.biomac.7b00781.

[66] Richbourg NR, Peppas NA. The swollen polymer network hypothesis: Quantitative models of hydrogel swelling, stiffness, and solute transport. Prog Polym Sci 2020;105:1–14. https://doi.org/10.1016/j.progpolymsci.2020.101243.

[67] Peppas NA, Bures P, Leobandung W, et al. Hydrogels in pharmaceutical formulations. European Journal of Pharmaceutics and Biopharmaceutics 2000;50:27–46. https://doi.org/https://doi.org/10.1016/S0939-6411(00)00090-4.

[68] Korsmeyer RW, Gurny R, Doelker E, et al. Mechanisms of solute release from porous hydrophilic polymers. Int J Pharm 1983;15:25–35. https://doi.org/https://doi.org/10.1016/0378-5173(83)90064-9.

[69] Flory PJ. Network Structure and the Elastic Properties of Vulcanized Rubber. Chem Rev 1944;35:51–75. https://doi.org/https://doi.org/10.1021/cr60110a002.

[70] Treolar LRG. The Elasticity of a Network of Long- Chain Molecules - III. Transactions of the Faraday Society 1945;42:83–94. https://doi.org/https://doi.org/10.1039/TF9464200083.

[71] Flory PJ. Principle of Polymer Chemistry. Cornell University Press,USA 1953;1:432–584.

[72] Collins MN, Birkinshaw C. Investigation of the swelling behavior of crosslinked hyaluronic acid films and hydrogels produced using homogeneous reactions. J Appl Polym Sci 2008;109:923–31. https://doi.org/10.1002/app.27631.

[73] Ebube NK, William AM. Methods for Increasing Bulk Density of Chondroitin. US20020173486A1, 2002.

[74] Bryant SJ, Davis-Arehart KA, Luo N, et al. Synthesis and characterization of photopolymerized multifunctional hydrogels: Water-soluble poly(vinyl alcohol) and chondroitin sulfate macromers for chondrocyte encapsulation. Macromolecules 2004;37:6726–33. https://doi.org/10.1021/ma0499324.

[75] Martini M, Hegger PS, Schädel N, et al. Charged triazole cross-linkers for hyaluronan-based hybrid hydrogels. Materials 2016;9:1–11. https://doi.org/10.3390/ma9100810.

[76] Tanaka K. Physicochemical Properties of Chondroitin Sulfate. J Biochem 1978;83:647–53. https://doi.org/https://doi.org/10.1093/oxfordjournals.jbchem.a131955.

[77] Campbell JH, Burdo TH, Autissier P, et al. Minocycline inhibition of monocyte activation correlates with neuronal protection in SIV NeuroAIDS. PLoS One 2011;6:1–11. https://doi.org/10.1371/journal.pone.0018688.

[78] Pang T, Wang J, Benicky J, et al. Minocycline ameliorates LPS-induced inflammation in human monocytes by novel mechanisms including LOX-1, Nur77 and LITAF inhibition. Biochim Biophys Acta Gen Subj 2012;1820:503–10. https://doi.org/10.1016/j.bbagen.2012.01.011.

[79] Saadati N, Abdullah MP, Zakaria Z, et al. Limit of detection and limit of quantification development procedures for organochlorine pesticides analysis in water and sediment matrices. Chem Cent J 2013;7:1–10. https://doi.org/10.1186/1752-153X-7-63.

[80] Shrivastava A, Gupta V. Methods for the determination of limit of detection and limit of quantitation of the analytical methods. Chronicles of Young Scientists 2011;2:21–5. https://doi.org/10.4103/2229-5186.79345.

[81] Shuker Mahmood H, Zayad Al-Sarraj T, Sh Mahmood H, et al. Two Novel Spectrophotometric Methods for Determination of Naproxen via a Modulation to Hydroxy Analog. Curr Appl Sci Technol 2020;20:295–309. https://doi.org/10.14456/cast.2020.17.

[82] Chen YC, Rivera J, Fitzgerald M, et al. Preimplantation factor prevents atherosclerosis via its immunomodulatory effects without affecting serum lipids. Thromb Haemost 2016;115:1010–24. https://doi.org/10.1160/TH15-08-0640.

[83] Verdoliva V, Bedini E, De Luca S. Sustainable Chemical Modification of Natural Polysaccharides: Mechanochemical, Solvent-Free Conjugation of Pectins and Hyaluronic Acid Promoted by Microwave Radiations. Biomacromolecules 2024:6217–28. https://doi.org/10.1021/acs.biomac.4c00844.

[84] Chen Z, Xiao G. Total Synthesis of Nona-decasaccharide Motif from Ganoderma sinense Polysaccharide Enabled by Modular and One-Pot Stereoselective Glycosylation Strategy. J Am Chem Soc 2024;146:17446–55. https://doi.org/10.1021/jacs.4c05188.

[85] Gregory GL, Lopez-Vidal EM, Buchard A. Polymers from sugars: cyclic monomer synthesis, ring-opening polymerisation, material properties and applications. Chemical Communications 2017;53:2198–217. https://doi.org/10.1039/c6cc09578j.

[86] Gody G, Maschmeyer T, Zetterlund PB, et al. Rapid and quantitative one-pot synthesis of sequence-controlled polymers by radical polymerization. Nat Commun 2013;4:1–9. https://doi.org/10.1038/ncomms3505.

[87] Toropitsyn E, Ščigalková I, Pravda M, et al. Injectable Hyaluronic Acid Hydrogel Containing Platelet Derivatives for Synovial Fluid Viscosupplementation and Growth Factors Delivery. Macromol Biosci 2023;23:1–14. https://doi.org/10.1002/mabi.202200516.

[88] Toropitsyn E, Ščigalková I, Pravda M, et al. Enzymatically cross-linked hyaluronic acid hydrogels as in situ forming carriers of platelet-rich plasma: Mechanical properties and bioactivity levels evaluation. J Mech Behav Biomed Mater 2023;143:1–12. https://doi.org/10.1016/j.jmbbm.2023.105916.

[89] Dirksen A, Hackeng TM, Dawson PE. Nucleophilic catalysis of oxime ligation. Angewandte Chemie - International Edition 2006;45:7581–4. https://doi.org/10.1002/anie.200602877.

[90] Collins J, Xiao Z, Müllner M, et al. The Emergence of Oxime Click Chemistry and its Utility in Polymer Science. Polym Chem 2016;7:3812–26. https://doi.org/https://doi.org/10.1039/c6py00635c.

[91] Moeinzadeh S, Jabbari E. Gelation characteristics, physico-mechanical properties and degradation kinetics of micellar hydrogels. Eur Polym J 2015;72:566–76. https://doi.org/10.1016/j.eurpolymj.2015.04.028.

[92] Ji W, Chang B, Yu H, et al. Effect of Polymer and Crosslinker Concentration on Static and Dynamic Gelation Behavior of Phenolic Resin Hydrogel. Gels 2024;10:1–14. https://doi.org/10.3390/gels10050325.

[93] Zhang F, Zhang S, Lin R, et al. Injectable multifunctional carboxymethyl chitosan/hyaluronic acid hydrogel for drug delivery systems. Int J Biol Macromol 2023;249:1–14. https://doi.org/10.1016/j.ijbiomac.2023.125801.

[94] Zhang B, Jayalath IM, Ke J, et al. Chemically fueled covalent crosslinking of polymer materials. Chemical Communications 2019;55:2086–9. https://doi.org/10.1039/c8cc09823a.

[95] Sun Y, Nan D, Jin H, et al. Recent advances of injectable hydrogels for drug delivery and tissue engineering applications. Polym Test 2020;81:1–13. https://doi.org/10.1016/j.polymertesting.2019.106283.

[96] Alonso JM, Del Olmo JA, Gonzalez RP, et al. Injectable hydrogels: From laboratory to industrialization. Polymers (Basel) 2021;13:1–24. https://doi.org/10.3390/polym13040650.

[97] Del Olmo JA, Pérez-álvarez L, Martínez VS, et al. Drug Delivery from Hyaluronic Acid–BDDE Injectable Hydrogels for Antibacterial and Anti-Inflammatory Applications. Gels 2022;8. https://doi.org/10.3390/gels8040223.

[98] Ma X, Xu T, Chen W, et al. Injectable hydrogels based on the hyaluronic acid and poly (γ-glutamic acid) for controlled protein delivery. Carbohydr Polym 2018;179:100–9. https://doi.org/10.1016/j.carbpol.2017.09.071.

[99] Ewoldt RH, Johnston MT, Caretta LM. Experimental Challenges of Shear Rheology: How to Avoid Bad Data, 2015, p. 207–41. https://doi.org/10.1007/978-1-4939-2065-5_6.

[100] Jo SH, Roh S, Shim J, et al. Modulating the Thermoresponsive Characteristics of PLGA-PEG-PLGA Hydrogels via Manipulation of PLGA Monomer Sequences. Biomacromolecules 2024;25:5374–86. https://doi.org/10.1021/acs.biomac.4c00817.

[101] Li Y, Chen S, Zhang M, et al. Novel Injectable, Self-Healing, Long-Effective Bacteriostatic, and Healed-Promoting Hydrogel Wound Dressing and Controlled Drug Delivery Mechanisms. ACS Appl Mater Interfaces 2024;16:2140–53. https://doi.org/10.1021/acsami.3c15705.

[102] Rumon MMH, Rahman MS, Akib AA, et al. Progress in hydrogel toughening: addressing structural and crosslinking challenges for biomedical applications. Discov Mater 2025;5:1–29. https://doi.org/10.1007/s43939-025-00178-x.

[103] Wu L, Li H, Wang Y, et al. Advancing injection force modeling and viscosity-dependent injectability evaluation for prefilled syringes. European Journal of Pharmaceutics and Biopharmaceutics 2024;197:1–9. https://doi.org/10.1016/j.ejpb.2024.114221.

[104] Guvendiren M, Lu HD, Burdick JA. Shear-thinning hydrogels for biomedical applications. Soft Matter 2012;8:260–72. https://doi.org/10.1039/c1sm06513k.

[105] Gu J, Cai X, Raza F, et al. Preparation of a minocycline polymer micelle thermosensitive gel and its application in spinal cord injury. Nanoscale Adv 2024. https://doi.org/10.1039/d4na00625a.

[106] Kang NW, Yoon SY, Kim S, et al. Subcutaneously injectable hyaluronic acid hydrogel for sustained release of donepezil with reduced initial burst release: Effect of hybridization of microstructured lipid carriers and albumin. Pharmaceutics 2021;13. https://doi.org/10.3390/pharmaceutics13060864.

[107] Bayer IS. Hyaluronic acid and controlled release: A review. Molecules 2020;25. https://doi.org/10.3390/molecules25112649.

[108] Samantray S, Olubiyi OO, Strodel B. The influences of sulphation, salt type, and salt concentration on the structural heterogeneity of glycosaminoglycans. Int J Mol Sci 2021;22:1–20. https://doi.org/10.3390/ijms222111529.

[109] Tao Y, Ai L, Bai H, et al. Synthesis of pH-responsive photocrosslinked hyaluronic acid-based hydrogels for drug delivery. J Polym Sci A Polym Chem 2012;50:3507–16. https://doi.org/10.1002/pola.26159.

[110] Novoskol'tseva OA, Rogacheva VB, Zezin AB, et al. Formation and transformations of polyelectrolyte gel-ampholyte dendrimer-surfactant ternary complexes. Polymer Science - Series A 2009;51:598–605. https://doi.org/10.1134/S0965545X09060030.

[111] Abidin IZ, Murphy EJ, Fehrenbach GW, et al. Chitosan-(poly)acrylic acid polyelectrolyte complexes: Enhanced mucoadhesion and sustained drug release in vaginal tablets. Carbohydrate Polymer Technologies and Applications 2024;7. https://doi.org/10.1016/j.carpta.2024.100480.

[112] Carvalho SG, dos Santos AM, Silvestre ALP, et al. New insights into physicochemical aspects involved in the formation of polyelectrolyte complexes based on chitosan and dextran sulfate. Carbohydr Polym 2021;271. https://doi.org/10.1016/j.carbpol.2021.118436.

[113] Gibson I, Momeni A, Filiaggi M. Minocycline-loaded calcium polyphosphate glass microspheres as a potential drug-delivery agent for the treatment of periodontitis. J Appl Biomater Funct Mater 2019;17. https://doi.org/10.1177/2280800019863637.

[114] Mikulík J, Vinklárek Z, Vondruška M. Formation of Polyelectrolyte Complexes. Collect Czech Chem Commun 1993;58:713–47. https://doi.org/https://doi.org/10.1135/cccc19930713.

[115] Ishaq W, Afzal A, Farooq M, et al. Design and Evaluation of Inorganic/Organic Hybrid Bio-composite for Site-Specific Oral Delivery of Darifenacin. AAPS PharmSciTech 2024;25. https://doi.org/10.1208/s12249-024-02916-5.

[116] Bhardwaj N, Kundu SC. Silk fibroin protein and chitosan polyelectrolyte complex porous scaffolds for tissue engineering applications. Carbohydr Polym 2011;85:325–33. https://doi.org/10.1016/j.carbpol.2011.02.027.

[117] Gummel J, Cousin F, Boué F. Counterions release from electrostatic complexes of polyelectrolytes and proteins of opposite charge: A direct measurement. J Am Chem Soc 2007;129:5806–7. https://doi.org/10.1021/ja070414t.

[118] Ristroph KD, Prud'homme RK. Hydrophobic ion pairing: Encapsulating small molecules, peptides, and proteins into nanocarriers. Nanoscale Adv 2019;1:4207–37. https://doi.org/10.1039/c9na00308h.

[119] Zhao Y, Gu X, Gao S, et al. Adsorption of tetracycline (TC) onto montmorillonite: Cations and humic acid effects. Geoderma 2012;183–184:12–8. https://doi.org/10.1016/j.geoderma.2012.03.004.

[120] Zhao Y, Geng J, Wang X, et al. Tetracycline adsorption on kaolinite: PH, metal cations and humic acid effects. Ecotoxicology 2011;20:1141–7. https://doi.org/10.1007/s10646-011-0665-6.

[121] Guerra W, Silva-Caldeira PP, Terenzi H, et al. Impact of metal coordination on the antibiotic and non-antibiotic activities of tetracycline-based drugs. Coord Chem Rev 2016;327–328:188–99. https://doi.org/10.1016/j.ccr.2016.04.009.

[122] Zhang Z, Nix CA, Ercan UK, et al. Calcium binding-mediated sustained release of minocycline from hydrophilic multilayer coatings targeting infection and inflammation. PLoS One 2014;9. https://doi.org/10.1371/journal.pone.0084360.

[123] Xue Y, Chen H, Xu C, et al. Synthesis of hyaluronic acid hydrogels by crosslinking the mixture of high-molecular-weight hyaluronic acid and low-molecular-weight hyaluronic acid with 1,4-butanediol diglycidyl ether. RSC Adv 2020;10:7206–13. https://doi.org/10.1039/c9ra09271d.

[124] Lin G, Chang S, Kuo CH, et al. Free swelling and confined smart hydrogels for applications in chemomechanical sensors for physiological monitoring. Sens Actuators B Chem 2009;136:186–95. https://doi.org/10.1016/j.snb.2008.11.001.

[125] Shimojo AAM, Pires AMB, Lichy R, et al. The crosslinking degree controls the mechanical, rheological, and swelling properties of hyaluronic acid microparticles. J Biomed Mater Res A 2015;103:730–7. https://doi.org/10.1002/jbm.a.35225.

[126] Dulong V, Lack S, Le Cerf D, et al. Hyaluronan-based hydrogels particles prepared by crosslinking with trisodium trimetaphosphate. Synthesis and characterization. Carbohydr Polym 2004;57:1–6. https://doi.org/10.1016/j.carbpol.2003.12.006.

[127] Mihajlovic M, Rikkers M, Mihajlovic M, et al. Viscoelastic Chondroitin Sulfate and Hyaluronic Acid Double-Network Hydrogels with Reversible Cross-Links. Biomacromolecules 2022;23:1350–65. https://doi.org/10.1021/acs.biomac.1c01583.

[128] Vanoli V, Delleani S, Casalegno M, et al. Hyaluronic acid-based hydrogels: Drug diffusion investigated by HR-MAS NMR and release kinetics. Carbohydr Polym 2023;301. https://doi.org/10.1016/j.carbpol.2022.120309.

[129] Huang J, Sheridan GS, Chen C, et al. Reversible Reactions, Mesh Size, and Segmental Dynamics Control Penetrant Diffusion in Ethylene Vitrimers. ACS Macro Lett 2023;12:901–7. https://doi.org/10.1021/acsmacrolett.3c00244.

[130] Kirchhof S, Abrami M, Messmann V, et al. Diels-Alder Hydrogels for Controlled Antibody Release: Correlation between Mesh Size and Release Rate. Mol Pharm 2015;12:3358–68. https://doi.org/10.1021/acs.molpharmaceut.5b00375.

[131] Li J, Mooney DJ. Designing hydrogels for controlled drug delivery. Nat Rev Mater 2016;1:1–17. https://doi.org/10.1038/natrevmats.2016.71.

[132] Stampanoni Bassi M, Iezzi E, Drulovic J, et al. IL-6 in the Cerebrospinal Fluid Signals Disease Activity in Multiple Sclerosis. Front Cell Neurosci 2020;14. https://doi.org/10.3389/fncel.2020.00120.

[133] Petković F, Castellano B. The role of interleukin-6 in central nervous system demyelination. Neural Regen Res 2016;11:1922–3. https://doi.org/10.4103/1673-5374.195273.

[134] Eslami M, Mirabi AM, Baghbanian M, et al. Interleukin 6 but not Interleukin 8 Might be an Indicator of Multiple Sclerosis Progression from Relapse Remitting to Secondary Progressive Status. Research in Molecular Medicine 2020:1–8. https://doi.org/10.32598/rmm.8.1.1.

[135] Camara-Lemarroy C, Metz L, Kuhle J, et al. Minocycline treatment in clinically isolated syndrome and serum NfL, GFAP, and metalloproteinase levels. Multiple Sclerosis Journal 2022;28:2081–9. https://doi.org/10.1177/13524585221109761.

[136] Zhou J, Wang H, Chen H, et al. pH-responsive nanocomposite hydrogel for simultaneous prevention of postoperative adhesion and tumor recurrence. Acta Biomater 2023;158:228–38. https://doi.org/10.1016/j.actbio.2022.12.025.

[137] Grover GN, Lam J, Nguyen TH, et al. Biocompatible hydrogels by oxime click chemistry. Biomacromolecules 2012;13:3013–7. https://doi.org/10.1021/bm301346e.

[138] Niemczyk B, Sajkiewicz P, Kolbuk D. Injectable hydrogels as novel materials for central nervous system regeneration. J Neural Eng 2018;15:1–15. https://doi.org/10.1088/1741-2552/aacbab.

[139] Tseng TC, Tao L, Hsieh FY, et al. An injectable, self-healing hydrogel to repair the central nervous system. Advanced Materials 2015;27:3518–24. https://doi.org/10.1002/adma.201500762.

[140] Zhuo F, Liu X, Gao Q, et al. Injectable hyaluronan-methylcellulose composite hydrogel crosslinked by polyethylene glycol for central nervous system tissue engineering. Materials Science and Engineering C 2017;81:1–7. https://doi.org/10.1016/j.msec.2017.07.029.

[141] Simone N Di, Nicuolo F Di, Marana R, et al. Synthetic PreImplantation Factor (PIF) prevents fetal loss by modulating LPS induced inflammatory response. PLoS One 2017;12:1–16. https://doi.org/10.1371/journal.pone.0180642.

[142] Blachman A, Birocco AM, Curcio S, et al. Dermatan Sulfate/Chitosan Nanoparticles Loaded with an Anti-Inflammatory Peptide Increase the Response of Human Colorectal Cancer Cells to 5-Fluorouracil. Macromol Biosci 2023;23. https://doi.org/10.1002/mabi.202300193.

[143] Antropenko A, Caruso F, Fernandez-Trillo P. Stimuli-Responsive Delivery of Antimicrobial Peptides Using Polyelectrolyte Complexes. Macromol Biosci 2023;23. https://doi.org/10.1002/mabi.202300123.

[144] Bonaccorso A, Carbone C, Tomasello B, et al. Optimization of dextran sulfate/poly-L-lysine based nanogels polyelectrolyte complex for intranasal ovalbumin delivery. J Drug Deliv Sci Technol 2021;65. https://doi.org/10.1016/j.jddst.2021.102678.

[145] Marciel AB, Chung EJ, Brettmann BK, et al. Bulk and nanoscale polypeptide based polyelectrolyte complexes. Adv Colloid Interface Sci 2017;239:187–98. https://doi.org/10.1016/j.cis.2016.06.012.

[146] Fitch CA, Platzer G, Okon M, et al. Arginine: Its pKa value revisited. Protein Science 2015;24:752–61. https://doi.org/10.1002/pro.2647.

[147] Schatz C, Domard A, Viton C, et al. Versatile and Efficient Formation of Colloids of Biopolymer-Based Polyelectrolyte Complexes. Biomacromolecules 2004;5:1882–92. https://doi.org/10.1021/bm049786.

[148] Ijaz U, Sohail M, Minhas MU, et al. Biofunctional Hyaluronic Acid/κ-Carrageenan Injectable Hydrogels for Improved Drug Delivery and Wound Healing. Polymers (Basel) 2022;14. https://doi.org/10.3390/polym14030376.

[149] Hu M, Yang J, Xu J. Structural and biological investigation of chitosan/hyaluronic acid with silanized-hydroxypropyl methylcellulose as an injectable reinforced interpenetrating network hydrogel for cartilage tissue engineering. Drug Deliv 2021;28:607–19. https://doi.org/10.1080/10717544.2021.1895906.

[150] Plummer A, Adkins C, Louf JF, et al. Obstructed swelling and fracture of hydrogels. Soft Matter 2024;20:1425–37. https://doi.org/10.1039/d3sm01470c.

[151] Weiss L, Or R, Jones RC, et al. Preimplantation Factor (PIF*) reverses neuroinflammation while promoting neural repair in EAE model. J Neurol Sci 2012;312:146–57. https://doi.org/10.1016/j.jns.2011.07.050.

[152] Colombo P. Swelling-controlled release in hydrogel matrices for oral route. vol. 11. 1993.

[153] Souza PR, Vilsinski BH, de Oliveira AC, et al. Chitosan/heparin blends in ionic liquid produce polyelectrolyte complexes that quickly adsorb citrate-capped silver nanoparticles, forming bactericidal composites. J Mol Liq 2021;330. https://doi.org/10.1016/j.molliq.2021.115548.

[154] Ben Ammar NE, Saied T, Barbouche M, et al. A comparative study between three different methods of hydrogel network characterization: effect of composition on the crosslinking properties using sol–gel, rheological and mechanical analyses. Polymer Bulletin 2018;75:3825–41. https://doi.org/10.1007/s00289-017-2239-0.

[155] Wang SC, Chen BH, Wang LF, et al. Characterization of chondroitin sulfate and its interpenetrating polymer network hydrogels for sustained-drug release. Int J Pharm 2007;329:103–9. https://doi.org/10.1016/j.ijpharm.2006.08.041.

[156] Fajardo AR, Silva MB, Lopes LC, et al. Hydrogel based on an alginate-Ca2+/chondroitin sulfate matrix as a potential colon-specific drug delivery system. RSC Adv 2012;2:11095–103. https://doi.org/10.1039/c2ra20785k.

[157] Gwon K, Kim E, Tae G. Heparin-hyaluronic acid hydrogel in support of cellular activities of 3D encapsulated adipose derived stem cells. Acta Biomater 2017;49:284–95. https://doi.org/10.1016/j.actbio.2016.12.001.

[158] Seong YJ, Lin G, Kim BJ, et al. Hyaluronic Acid-Based Hybrid Hydrogel Microspheres with Enhanced Structural Stability and High Injectability. ACS Omega 2019;4:13834–44. https://doi.org/10.1021/acsomega.9b01475.

[159] Chandel AKS, Sreedevi Madhavikutty A, Okada S, et al. Injectable, shear-thinning, photocrosslinkable, and tissue-adhesive hydrogels composed of diazirine-modified hyaluronan and dendritic polyethyleneimine. Biomater Sci 2024;12:1454–64. https://doi.org/10.1039/d3bm01279d.

[160] Larochelle C, Alvarez JI, Prat A. How do immune cells overcome the blood-brain barrier in multiple sclerosis? FEBS Lett 2011;585:3770–80. https://doi.org/10.1016/j.febslet.2011.04.066.

[161] Deng W, Yi C, Pan W, et al. Vascular Cell Adhesion Molecule-1 (VCAM-1) contributes to macular fibrosis in neovascular age-related macular degeneration through modulating macrophage functions. Immunity and Ageing 2023;20. https://doi.org/10.1186/s12979-023-00389-x.

[162] Jurberg AD, Chaves B, Pinho LG, et al. VLA-4 as a Central Target for Modulating Neuroinflammatory Disorders. Neuroimmunomodulation 2021;28:213–21. https://doi.org/10.1159/000518721.

LIST OF FIGURES

FIG. 1.1: INTERDEPENDENT PATHOBIOLOGICAL AXES OF MS. 14

FIG. 1.2: RISK OF SYSTEMIC ADMINISTRATION ROUTE OF THE DISEASE MODIFYING THERAPIES. 17

FIG. 1.3: SOCIOECONOMIC BURDEN OF MS AND DRUG REPURPOSING AS ONE OF FEASIBLE STRATEGIES TO OVERCOME THE IMPACTS. 19

FIG. 1.4: MINOCYCLINE STRUCTURE: A) METAL ION CHELATION SITES, B) CHELATION STRUCTURE OF MN WITH CALCIUM [36,37] 21

FIG. 1.5: STRUCTURE OF SYNTHETIC PREIMPLANTATION (SPIF). 22

FIG. 1.6: SEVERAL FACTORS INFLUENCING THE KINETICS OF DRUG RELEASE FROM HYDROGELS. FASTER DRUG RELEASE ARISES FROM SMALLER PARTICLES (HIGHER SURFACE AREA) AND LOW-MW POLYMERS. CONVERSELY, SUSTAINED

RELEASE IS ACHIEVED WITH LARGER PARTICLES (LIMITED SURFACE EXPOSURE) AND HIGH-MW POLYMERS (DENSE MATRICES). MATRICES FLEXIBILITY DEFINED BY CROSSLINKING TYPES (COVALENT, PHYSICAL) AND THE DENSITY FURTHER REFINES CONTROL, ENABLING CUSTOMIZED THERAPEUTIC DELIVERY..... 26

FIG. 1.7: POLYELECTROLYTE COMPLEX OFFERS STRAIGHTFORWARD DRUG ENTRAPMENT PROCESS VERSUS CONVENTIONAL NANOPARTICULATE FABRICATION. PANEL A) CONVENTIONAL NANOPARTICLE FABRICATION INVOLVES MULTIPLE STEPS SUCH AS SOLVENT SELECTION, MIXING, AND POLYMERIZATION. B) IN CONTRAST, POLYELECTROLYTE-BASED SELF-ASSEMBLY ENABLES SIMPLE, SOLVENT-FREE DRUG LOADING WITH TUNEABLE NANOPARTICLE PROPERTIES, OFFERING A SCALABLE ALTERNATIVE TO COMPLEX MULTI-STEP METHODS. 27

FIG. 1.8: HAOX-CSOX VERSATILITY AS A DRUG DELIVERY PLATFORM. THE SYSTEM ENABLES A PATIENT-CENTRIC PLATFORM, OFFERING TUNEABLE MECHANICAL PROPERTIES (GELATION TIME, ELASTIC MODULUS), FINE-NEEDLE INJECTABILITY, AND DURABLE OXIME-MEDIATED CROSSLINKING. ELECTROSTATIC INTERACTIONS BETWEEN CSOX SULFATE GROUPS AND CATIONIC DRUGS FACILITATE EFFICIENT PHYSICAL ENTRAPMENT..... 30

FIG. 2.1: OVERVIEW OF THE THESIS OBJECTIVES. STEP 1) MATERIALS SELECTION AND ENTRAPMENT STRATEGY FOR DELIVERING REPURPOSED DMTS. THE PURPLE SPHERE REPRESENTS THE CONVENTIONAL NANOPARTICLE-BASED DRUG ENTRAPMENT APPROACH, WHILE THE ORANGE SPHERE ILLUSTRATES THE PROPOSED METHOD, WHERE THE DRUG IS ENCAPSULATED IN A PEC IMMOBILIZED WITHING THE HAOX-CSOX HYDROGEL STRUCTURE. STEP 2) CHARACTERIZATION OF DDS. STEP 3) IN VITRO BIOACTIVITY TESTING TO EVALUATE THE COMPATIBILITY OF THE DDS WITH THE ENCAPSULATED DMTS. 33

FIG. 3.1: ONE-POT REACTION SCHEME FOR THE PREPARATION OF ALDEHYDE-MODIFIED CHONDROITIN SULPHATE (CSOX)..... 36

FIG. 3.2: SCHEMATIC OF A PAIR-SYRINGE SYSTEM CONNECTED BY A LUER LOCK ADAPTER OR MIXING PORT USED IN THE CROSSLINKING PROCESS OF HAOX AND HAOX-CSOX HYDROGEL. 40

FIG. 3.3: CHEMICAL REACTION FOR DDS FORMATION WITH 1:1 RATIO OF THE CROSS-LINKABLE GROUPS OF ALDEHYDES FROM HAOX AND HYDROXYLAMINE FROM PDHA. 41

FIG. 3.4: ILLUSTRATION OF TRANSWELL® SYSTEM. A POROUS MEMBRANE SEPARATES TWO CHAMBERS, WITH DMTS-LOADED DDS INTRODUCED IN THE UPPER COMPARTMENT AND DRUG RELEASE IS QUANTIFIED IN THE LOWER COMPARTMENT. 43

FIG. 3.5: ILLUSTRATION OF MESH SIZE AND MOLECULAR MASS BETWEEN CROSSLINKS. 46

FIG. 3.6: SCHEMATIC REPRESENTATION OF A DUAL-SYRINGE CONFIGURATION CONNECTED BY LUER LOCK OR MIXING PORT FOR CROSSLINKING PROCESS OF HAOX-CSOX HYDROGEL..... 52

FIG. 4.1: FORMULATION TESTED AS THE DRUG DELIVERY SYSTEM FOR MN CONTROL RELEASE. 56

FIG. 4.2: ^{1}H NMR OF ALDEHYDE MODIFIED CHONDROITIN SULFATE. 57

FIG. 4.3: COMPARATIVE ASSESSMENT OF GELATION PROFILE FOR HYDROGELS BASED ON CSOX, HAOX, AND PEC (UNBOUND AND IMMOBILIZED). RESULT FROM TRIPLICATE TRIALS (N =3) SHOW **** P < 0.0001 FOR CSOX-MN VERSUS PURE HAOX). 59

FIG. 4.4: COMPARATIVE ANALYSIS OF HYDROGEL VISCOELASTICITY (N=3) ACROSS HAOX-BASED FORMULATIONS. MAIN PLOT: G' AVERAGED ACROSS THE LVE REGION (MEAN ± SD). INSET: STRAIN LIMIT (ΓL), DEFINED AS THE STRAIN AMPLITUDE WHERE G'DEVIATES >5% FROM THE PLATEAU VALUE. VALUES REPRESENT MEAN ΓL (%) PER FORMULATION. SIGNIFICANT DIFFERENCES BETWEEN HAOX_PECS AND PURE HAOX INDICATED (**P ≤ 0.01). 60

FIG. 4.5: CORRELATION BETWEEN DGF AND SYRINGE-NEEDLE GEOMETRY (40 MM NEEDLE LENGTH). THE X-AXIS DENOTES NEEDLE GAUGE (G), WITH CORRESPONDING INNER DIAMETERS PROVIDED IN TABLE 4.1..... 62

FIG. 4.6: SUSTAINED AND BURST-RELEASE PATTERNS OF MINOCYCLINE FROM DDS: SUBFIGURE (A) ILLUSTRATES TIME-DEPENDENT CDR FOR HAOX-CSOX HYDROGELS; SUBFIGURE (B) QUANTIFIES BURST-RELEASE. STATISTICAL ANALYSIS (N=3): ** P < 0.01, *** P < 0.001, NS IS NON-SIGNIFICANT. 63

FIG. 4.7: COMPARATIVE ASSESSMENT OF THE TIME TO 50% DRUG RELEASE (T50%) ACROSS DDS FORMULATION (N =3, ** P < 0.01, *** P < 0.001, NS IS NON-SIGNIFICANT). 64

FIG. 4.8:HYDROGEL SWELLING ASSESSMENT. A) QUANTITATIVE SWELLING PROFILE OF DDS FORMULATIONS (SWELLING RATIO VS. TIME; N=3). B) QUALITATIVE

STRUCTURAL EVALUATION: HAOX-MN, HAOX_PECOX, AND CSOX-MN STRUCTURAL MORPHOLOGY FOLLOWING 7 DAYS IN CONTACT WITH THE RELEASE MEDIUM. 66

FIG. 4.9: KEY STRUCTURAL DIFFERENCES IN HAOX HYDROGEL FORMULATIONS: A) HAOX-HAOX: MINIMAL CROSSLINKING AND LARGER MESH SIZE ENABLE FAST, DIFFUSION-DRIVEN DRUG RELEASE, B) HAOX-CSOX: ENHANCED CROSSLINKING DENSITY AND SULFATE-MEDIATED INTERACTIONS CREATE A TIGHTER NETWORK OF HAOX-CSOX AND CSOX-CSOX, SLOWING MN DIFFUSION AND REDUCING BURST RELEASE. 69

FIG. 4.10: SUPPRESSION OF LPS-INDUCED IL-6 SECRETION BY MN RELEASED FROM HAOX_PECOX: A) LPS DOSE-RESPONSE CONCENTRATION TO PROVOKE SUBSTANTIAL IL-6 RELEASE (MEAN ± SD; $P < 0.05$; $N = 3$ DONORS). B) A PRELIMINARY SINGLE- REPLICATE STUDY OF IL-6 EXPRESSION FOLLOWING TREATMENT WITH 1 IU mL^{-1} LPS, STANDARD MN SOLUTION (50 -1.562 □G mL^{-1}) AND SALINE. ALL SAMPLES, INCLUDING THE SALINE CONTROL, WERE TREATED WITH LPS. SALINE DEMONSTRATES BASELINE IL-6 LEVELS DESPITE THE PRESENCE OF LPS, AS SALINE LACKS OF BIOACTIVE COMPONENTS NECESSARY TO ACTIVATE THE INFLAMMATORY RECEPTORS (TLR4/NF-κB PATHWAYS). C) MONOCYTES WERE EXPOSED TO EITHER FREE MN OR MN-LOADED HAOX_PECOX RELEASE MEDIA, FOLLOWED BY STIMULATION WITH LPS (1 IU mL^{-1}). TREATMENT WITH MN-LOADED HAOX_PECOX SIGNIFICANTLY DECREASED IL-6 PRODUCTION COMPARED TO MN-FREE HAOX_PECOX (MEAN ± SD; $P < 0.05$; $N = 3$ DONORS). 71

FIG. 4.11: DRUG DELIVERY STRATEGY FOR FITC-SPIF:A) CHEMICAL STRUCTURE OF FITC-SPIF, B) DDS PREPARED FROM HAOX-CSOX LEVERAGING ELECTROSTATIC INTERACTION BETWEEN FITC-SPIF AND CSOX, C) ZOOMED-IN VIEW SHOWING ELECTROSTATIC INTERACTIONS BETWEEN FITC-SPIF AND THE POSITIVELY CHARGED RESIDUES LYSINE (LYS) AND ARGININE (ARG) AS PART OF THE POLYPEPTIDE CHAIN. THE MARKED REGION IN THE LEFT PANEL CORRESPONDS TO THE INTERACTION SITE MAGNIFIED IN THE RIGHT PANEL. .. 73

FIG. 4.12: GELATION TIME OF INJECTABLE HYDROGELS CONTAINING FITC-SPIF, MEASURED AT TWO PREPARATION PH VALUES (5.0 AND 6.8). EACH GROUP INCLUDES THREE FORMULATIONS WITH INCREASING CSOX CONCENTRATIONS: NO CSOX (HAOX_15 AT PH 5, HAOX_17 AT PH 6.8), 0.5% CSOX (HACOX_25, HACOX_27), AND 1% CSOX (HACOX_35, HACOX_37).

RESULTS REPRESENT MEAN ± SD (N = 3). STATISTICAL SIGNIFICANCE: *P < 0.05, **P < 0.01, ***P < 0.001, ****P < 0.0001, NS = NON-SIGNIFICANT. 74

FIG. 4.13: DRUG RELEASE PROFILE ACROSS DIFFERENT PREPARATION PH AND FORMULATION, A) CUMULATIVE DRUG RELEASE, B) BURST PROFILE, C) T50%. DATA ARE EXPRESSED AS MEAN ± SD (N = 3). SIGNIFICANCE LEVELS: *P < 0.05, **P < 0.01, ***P < 0.001, ****P < 0.0001, NS = NON-SIGNIFICANT. 76

FIG. 4.14: SWELLING RATIO OF FORMULATION PREPARED AT PH 6.8 (N=3). 79

FIG. 4.15: INFLUENCE OF FITC-SPIF LOADING LEVELS ON A) CDR, B) BURST RELEASE, C) T50%, AND D) SWELLING RATIO. DATA ARE EXPRESSED AS MEAN ± SD (N = 3). SIGNIFICANCE LEVELS: *P < 0.05, **P < 0.01, ***P < 0.001, ****P < 0.0001, NS = NON-SIGNIFICANT. 81

FIG. 4.16: INFLUENCE OF CSOX CONCENTRATIONS ON A) CDR, B) BURST RELEASE, C) T50%, AND D) SWELLING RATIO. DATA ARE EXPRESSED AS MEAN ± SD (N = 3). SIGNIFICANCE LEVELS: *P < 0.05, **P < 0.01, ***P < 0.001, ****P < 0.0001, NS = NON-SIGNIFICANT. 84

FIG. 4.17: RHEOLOGICAL CHARACTERIZATION OF HAOX-CSOX HYDROGELS PREPARED AT PH 6.8, ASSESSING G' (LVE) AND ΓL. DATA DERIVED FROM TRIPLICATE EXPERIMENTS (N=3), WITH SIGNIFICANCE LEVELS: *P < 0.05, **P < 0.01, ***P < 0.001, ****P < 0.0001, NS = NON-SIGNIFICANT. 89

FIG. 4.18: RELATIVE GENE EXPRESSION OF VCAM1 FROM THP-1 MACROPHAGES A) BEFORE AND B) AFTER STIMULATION WITH TNF-ALPHA. 91

FIG. 4.19: RELATIVE GENE EXPRESSION OF A) CXCL8 BEFORE STIMULATION WITH TNF-ALPHA, B) CXCL8 AFTER STIMULATION WITH TNF-ALPHA, C) IL-10. PTGS2, TNF, IL-1B BEFORE STIMULATION WITH TNF-ALPHA, D) IL-10. PTGS2, TNF, IL-1B AFTER STIMULATION WITH TNF-ALPHA FROM THP-1 MACROPHAGES. 92

FIG. 4.20: TGF-β EXPRESSION AFTER TREATMENT WITH FITC-SPIF. 93

LIST OF TABLES

TABLE 1.1 FDA APPROVED DISEASE MODIFYING THERAPIES [3,6–8]. 15

TABLE 3.1 SERIES OF STUDIED FORMULATIONS FOR MN-DDS. 39

TABLE 3.2 FORMULATIONS FOR DESIGNING A SUITABLE DELIVERY SYSTEM FOR SPIF. 50

TABLE 3.3 DEVELOPMENT OF HACOX_37: INFLUENCE OF FITC-SPIF LOADING LEVELS ON CDR, SWELLING BEHAVIOUR, AND KORSMEYER-PEPPAS MODELLING. 51

TABLE 3.4 DEVELOPMENT OF HACOX_37: INFLUENCE OF CSOX CONCENTRATION ON CDR, SWELLING BEHAVIOUR, AND KORSMEYER-PEPPAS MODELLING. 51

TABLE 4.1 INJECTABILITY ASSESSMENT OF HAOX_PECOX FORMULATION USING DYNAMIC GLIDE FORCE (DGF) AND MAXIMUM FORCE (FMAX) METRICS (N=3). 61

TABLE 4.2 KORSMEYER-PEPPAS RELEASE FITTING ACROSS FORMULATIONS. 65

TABLE 4.3 CROSSLINKING DENSITY ACROSS DIFFERENT FORMULATIONS (N=3)... 67

TABLE 4.4 MESH SIZE ESTIMATIONS OF THE DDS FORMULATION BY RUBBER ELASTICITY AND EQUILIBRIUM SWELLING THEORY (N=3). 68

TABLE 4.5 KORSMEYER-PEPPAS KINETIC MODELLING OF FITC-SPIF RELEASE FROM DDS PREPARED AT VARIED PH LEVELS (N=3). 77

TABLE 4.6 CROSSLINKING DENSITY FOR FORMULATIONS PREPARED AT PH 6.8 (N=3). 79

TABLE 4.7 INFLUENCE OF FITC-SPIF LOADING LEVELS ON KORSMEYER-PEPPAS MODEL FITTING (N=3). 82

TABLE 4.8 INFLUENCE OF CSOX CONCENTRATIONS ON KORSMEYER-PEPPAS MODEL FITTING (N=3). 84

TABLE 4.9 MESH SIZE ESTIMATIONS OF THE DDS FORMULATION BY RUBBER ELASTICITY AND EQUILIBRIUM SWELLING THEORY (N=3). 86

TABLE 4.10 INJECTABILITY PARAMETERS OF HACOX_37, EVALUATED THROUGH DYNAMIC GLIDE FORCE (DGF) AND MAXIMUM EXTRUSION FORCE (FMAX) (N=3). 89

LIST OF ABBREVIATIONS

BBB	Blood-Brain Barrier
CA	Calcium Chloride
CDR	Cumulative Drug Release
CIS	Clinically Isolated Syndrome
CNS	Central Nervous System
CS	Chondroitin Sulfate
CSF	Cerebrospinal Fluid
CSOX	Aldehyde-modified chondroitin sulfate
CXCL	C-X-C motif chemokine ligand
DDS	Drug Delivery Systems
DF	Degree of Functionalization
DGF	Dynamic Glide Force
DMT	Disease-Modifying Therapies
DNA	Deoxyribonucleic Acid
EAE	Experimental Autoimmune Encephalomyelitis
ELISA	Enzyme-Linked Immunosorbent Assay
FDA	Food and Drug Administration
FITC-SPIF	Fluorescein isothiocyanate–modified Synthetic Preimplantation Factor
GA	Gelatine type A
GalNAc	N-acetylgalactosamine
HA	Hyaluronic acid
HAOX	Aldehyde-modified hyaluronic acid

IFN-	Interferon
IL-	Interleukin
LbL	Layer-by-Layer
LoD	Limit of Detection
LoQ	Limit of Quantification
LPS	Lipopolysaccharide
MN	Minocycline
MS	Multiple sclerosis
PDHA	Propanediylbishydroxylamine Dihydrochloride
PDLLA-PEG-PDLLA	Poly(D,L-lactide)-block-poly(ethylene glycol)-block-poly(D,L-lactide)
PECs	Polyelectrolyte Complexes
PKA	cAMP-dependent Protein Kinase
PKC	Protein Kinase C
PLGA	Poly Lactic-co-Glycolic Acid
PMA	Phorbol 12-yristate 13-acetate
PPMS	Primary Progressive Multiple Sclerosis
PTSG2	Prostaglandin-endoperoxide synthase 2
qRT-PCR	quantitative Reverse Transcription Polymerase Chain Reaction
RRMS	Relapsing-Remitting Multiple Sclerosis
SEC-MALLS	Size-exclusion chromatography and multi-angle laser light scattering
SPIF	Synthetic Preimplantation Factor
SPMS	Secondary Progressive Multiple Sclerosis
TGF-	Transforming growth factor

Th1-to-Th2	T-helper cell
TNF-	Tumor Necrosis Factor
U.S.	United States
WB-MAT	Whole Blood Monocytes Activation Test
ZO-1	Zonula Occludens

CURRICULUM VITAE

Personal Information

Name	Tutut Ummul Habibah
Address	Dukelska 546/604, Ustí nad Orlici, Czech Rep.
Telephone	+420 773 032 919
Email	habibah@utb.cz / habibahtutut@gmail.com
Nationality	Indonesian
Date of birth	09. 08. 1992

Education and Training

Dates	2021 – present
Title of qualification	Doctoral study – expected defence 2025
Principal Branch	Technology of Macromolecular Substances
School	Faculty of Technology – Tomas Bata University in Zlin

Dates	2015 – 2016
Title of qualification	M.Sc.
Principal Branch	Biomaterials Science
School	School of Materials – The University of Manchester, UK

Dates	2011 – 2015
Title of qualification	B.Eng.
Principal Branch	Technology of Materials and Metallurgy
School	Materials and Metallurgy – Sepuluh Nopember Institute of Technology, Indonesia

LIST OF PUBLICATION

1. **T. Habibah**, J. Matonohová, J. Kulhánek, U. Fitzgerald, M. Ingr, M. Pravda, A. Pandit, V. Velebný, In situ formed aldehyde-modified hyaluronic acid hydrogel with polyelectrolyte complexes of aldehyde-modified chondroitin sulfate and gelatin: An approach for minocycline delivery, Carbohydr Polym 343 (2024). https://doi.org/10.1016/j.carbpol.2024.122455.

2. **T. Habibah**, A. Exnerová, K. Nešporová, U. FitzGerald, A. Pandit, M. Ingr, M. Pravda, V. Velebný, In situ delivery of synthetic preimplantation factor using aldehyde-modified hyaluronic acid hydrogel with immobilized complexes of chondroitin sulfate derivatives, Carbohydrate Polymer Technologies and Applications 9 (2025). https://doi.org/10.1016/j.carpta.2025.100689.

OVERVIEW OF OTHER ACTIVITIES

Conference:

T. Habibah, M. Ingr, M. Pravda. (2023), Polyelectrolyte Complex-loaded Hyaluronic Acid Hydrogel for Minocycline Release. DGM FEMS EUROMAT 2023 (Materials Science and Technology in Europe), Frankfurt am Main.

Studies abroad:

One month secondment program for viability study on the influence of release products from the drug-containing hydrogel and drug-containing particles on human oligodendroglial and neuronal cells at Universitätsklinikum Münster, Institut für Neuropathologie, Arbeitsgruppe Prof. Tanja Kuhlmann, WWU MÜNSTER (Germany), October 2022.

Summer schools:

- **In Vitro Model Systems for the Study of Neurodegenerative Disease**, May 25–27, 2021 (Online, South Denmark University)
- **Animal Models in MS Research, Scientific Integrity**, Intellectual Property, and Practical MRI Skills, May 30 – June 3, 2022 (University of Antwerp, Belgium)
- **Hyaluronan Hydrogel and Its Technological Transfer**, November 22–24, 2022 (Contipro a.s., Czech Republic).

.

Vývoj a charakterizace multimodálního hydrogelu kyseliny hyaluronové s řízeným uvolňováním protizánětlivých léčiv k léčbě roztroušené sklerózy

Development and Evaluation of a Multi-Modal Hyaluronic Acid Hydrogel for Anti-Inflammatory Drug Delivery for Multiple Sclerosis Therapy

Doctoral Thesis

Published by: Tomas Bata University in Zlín

nám. T. G. Masaryka 5555, 760 01 Zlín.

Edition: Doctoral Thesis

Typesetting by: Tutut Ummul Habibah

This publication has not undergone any proofreading or editorial review.

Publication year: 2025